Studies on Catalysis of Metal Complexes and Nanoparticle on Inorganic Supports

（無機担体に担持した金属錯体および
金属ナノ粒子の触媒作用に関する研究）

Nobuhiro Ishito
石戸　信広

Hokkaido University
北海道大学

2017

Contents

Chapter 1. General Introduction

1.1. General background

Chemical industry in the 20th century enriched our lives through supplying us with energy and essential chemicals such as plastics, synthetic fibers, medicines, and pesticides. In particularly, large-scale production of ammonia was established by German researchers using atmospheric N_2 and petroleum-derived H_2 with a heterogeneous catalyst, which is one of the key technologies in modern chemistry to enable steady production and supply for essential fertilizers and chemicals.[1,2] This process, called Haber–Bosch process, impacted particularly on agriculture and food industry, caused high population growth, and thus literally changed the world. On the other hand, rapid development of chemical industry accompanied serious problems such as air pollution, global warming, waste and depletion of fossil fuel resources. Hence, the concept of green chemistry was initiated worldwide involving the uses of raw materials efficiently, elimination of toxic or hazardous substrates and by-products, and minimization of energy consumption.[3,4] Catalytic process satisfied these criteria because catalysts can accelerate reactions at low temperatures and pressures by orders of magnitude to change reaction route to equilibrium, and to give desired products selectively. The use of renewable and abundant

raw material (lignocellulosic biomass[5,6] and CO_2[7,8], for example) and energy (H_2 produced by water splitting with sunlight[9,10]) is required to realize sustainable chemical production in the upcoming years. In this regard, the author has made great efforts to develop new catalysts and reactions targeting on the activation of less reactive compounds (CO_2 and alkanes) in this thesis.

1.2. Bridge between homogeneous and heterogeneous catalyst

Catalysis is simply categorized into three types: homogeneous catalysis working in the same phase of reactants, heterogeneous catalysis where solid catalysts react with reactants in gas or liquid phase, and biocatalysis using enzymes. These three kinds of catalysis have their own advantages and are used in an appropriate manner. For example, heterogeneous catalysis played a key role in the development of environmentally benign processes in petroleum industry. Synthesis of ε-caprolactam, an important intermediate for the production of Nylon 6 fibers, was renovated with heterogeneous catalysts[11] (Scheme 1.1). Industrial production of ε-caprolactam relied on oximation and subsequent Beckmann rearrangement with H_2SO_4, which produced a large amount of ammonium sulfate as an acid waste. On the contrary, heterogeneous catalytic system using TS-1 zeolite and high silica MFI zeolite drastically reduced environmental loads by the

elimination of H_2SO_4-derived by-product, ammonium sulfate.

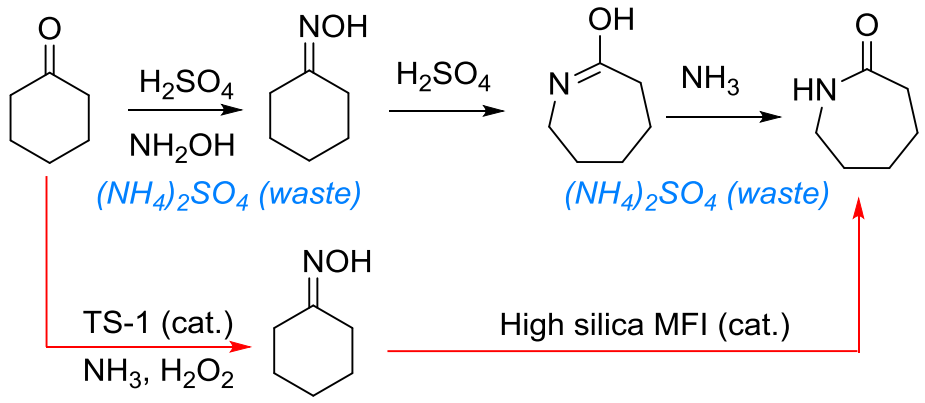

Scheme 1.1. Industrial process of ε-caprolactam synthesis. A conventional method with H_2SO_4 (black allows) and new method with solid catalysts (red allows).

Homogeneous metal complexes have attractive properties such as high activity, chemoselectivity, regioselectivity, and enantioselectivity, compared with heterogeneous catalysts. Despite these advantages, commercialized processes using these homogeneous catalysts were limited to a few applications: one-step synthesis of acetic acid from methanol and carbon monoxide by a rhodium complex, hydroformylation of alkenes by a Co carbonyl catalyst, coordination polymerization of ethylene by Ziegler-Natta catalyst, asymmetric reaction by metal complexes with chiral ligands.[12,13] Many homogeneous catalysts are not used in chemical industry because of economic and environmental disadvantages such as low durability and large energy consumption for separation of

products and catalysts from reaction mixtures.[14,15] In order to overcome these problems, several techniques have been proposed for the development of heterogeneous counterparts with similar functionality to homogeneous catalysts (Figure 1.1). Several polymers[16] and metal oxides[17] have been widely used as solid supports for immobilization of homogeneous metal complexes. Among these materials, polystyrene (Figure 1.1(a)) and silica (Figure 1.1(b)) are recognized as versatile supports, because a variety of organic functionality can be introduced by post-synthetic modification of phenylene moiety in polystylene with organic reactions (Figure 1.1(a)) and silanol moiety on silica surface with silane coupling reagents (Figure 1.1(b)). Another approach, named ship-in-bottle method, for the stabilization of metal complexes within zeolite nanocages is shown in Figure 1.1(c),[18,19] Reaction of metal ion with four *o*-dicyanobenzene molecules produces phthalocyanine in the supercage of Y-type zeolite. Large metal complexes can be successfully encapsulated within zeolite framework and readily available as catalytically active sites without change in their original functionality.

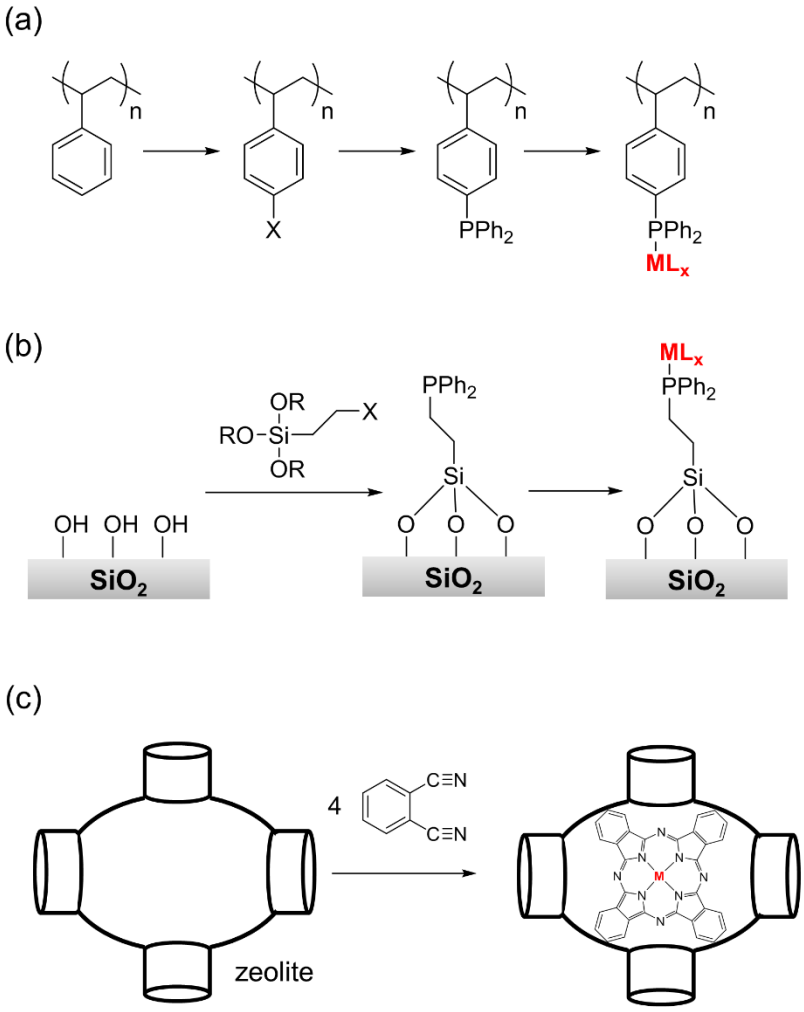

Figure 1.1. Examples of immobilization of metal complexes on (a) polystyrene, (b) silica, and (c) in zeolite cages.

Two representative examples were briefly described for immobilization of metal complexes on polymer supports (Figure 1.2). Figure 1.2(a) shows a novel procedure to encapsulate homogeneous metal complexes with polystyrene network where metal complexes are stabilized with phenylene moiety through strong interaction of π

electrons.[20,21] The resulting polystyrene beads contain large amounts of metal complexes. $Sc(OTf)_3$, OsO_4 and $Pd(PPh_3)$ immobilized in polystyrene shell showed high catalytic activities in C-C bond forming reactions such as the aldol condensation, the Diels-Alder reaction, and the Friedel-Crafts acylation, dihydroxylation of olefins to the corresponding vicinal diols, substitution reaction of allyl compounds, the Suzuki-Miyaura coupling reaction, and olefin metathesis. This solid catalyst can be recovered and reused several times without loss of its original activity and leaching of metal complexes. Despite high activities, these catalysts cannot be used in the organic solution that is able to dissolve polystyrene. To address this issue, large amounts of cross-linkages were formed in polystyrene after encapsulation of metal complexes, producing a robust and insoluble polymer shell (Figure 1.2(b)).[21-23]

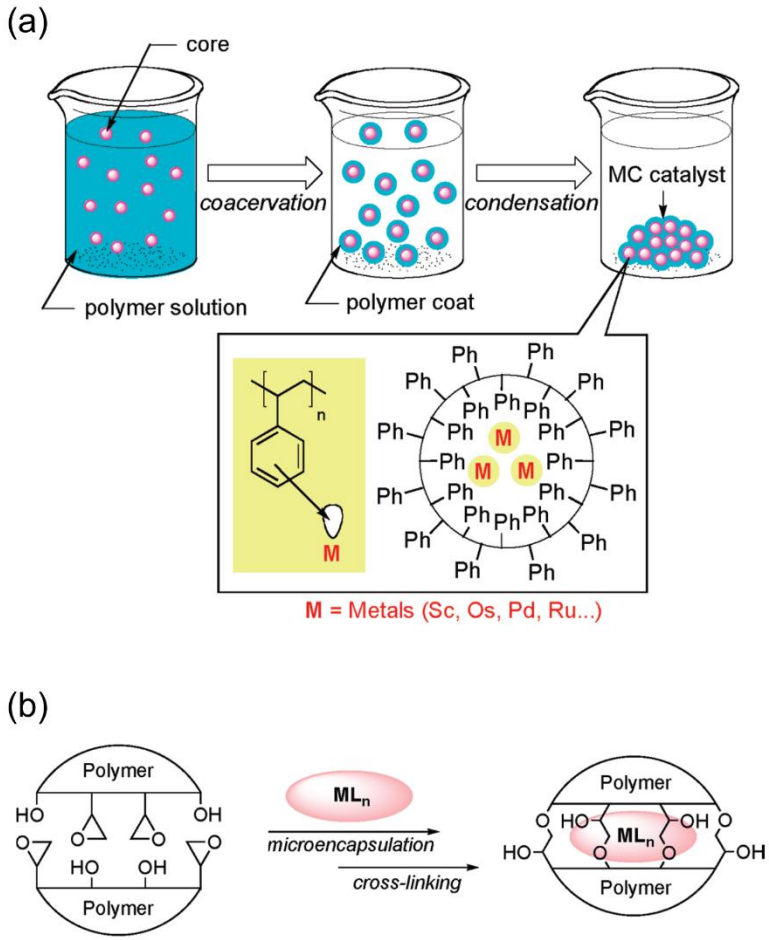

Figure 1.2. Encapsulation of homogeneous metal complexes with a stable and rigid polystyrene network: (a) simple microencapsulation and (b) microencapsulation-crosslinking techniques.

1.3. Periodic mesoporous organosilicas (PMOs): application for heterogeneous catalysis

Because of intrinsic properties such as chemical inertness and large surface area, porous silica is an ideal support for organic functional groups, metal complexes, and metal nanoparticles to develop supported catalysts.[24] According to the IUPAC definition, porous materials are divided into three classes; microporous (poresize < 2nm), mesoporous (2–50nm), and macroporous (>50nm) materials.[25] Zeolites are crystalline aluminosilicate compounds with micropores in the molecular dimension. Isomorphous substitution of Si in the framework with several metals including Al, Ti, Ga, and Fe results in the formation of catalytically active sites.[26] While metallosilicate zeolites are conventionally used as solid catalysts in chemical industry, small-sized micropores sometime limits their applications for large-sized reactants and products, due to severe mass transfer limitation.[27] Mesoporous silicas have large-sized pores exceeding 2 nm in diameter. Mesopores enable smooth incorporation and diffusion of bulk reactants and products in comparison with microporous solids.[28-30] Amorphous nature of the framework, however, makes them difficult to functionalize acid-base or redox properties by a simple introduction of transition metal sites with an impregnation technique.[31]

Periodic mesoporous organosilica (PMO) is a series of ordered mesoporous silica with

organic functional groups integrated through covalent Si-C bonds within silicate framework and can be synthesized from a bridged alkoxysliane precursor ($(RO)_3Si\text{-}R'\text{-}Si(OR)_3$) in the presence of a structure-directing agent.[32] PMOs with ethylene (**1**),[33] ethenylene (**2**),[34] 1,4-phenylene (**3**),[35] 4,4'-biphenylene (**4**)[36] are typical examples in the early stage of this research. Ethenylene-bridged PMO (**1**) has a great potential to introduce a variety of functional groups at ethenylene moieties of the surface with chemical modification such as bromination,[37] epoxidation,[38] and Diels-Alder reactions.[39] Phenylene (**3**) and biphenylene bridged PMOs (**4**) have an ordered mesoporous structure and a crystal-like arrangement of aromatic rings though $\pi-\pi$ interaction inside silica wall. Heteroatom-containing organic functionality such as azo group (**5**),[40] thiophene group (**6**),[41] 2-phenylpyridine group (**7**),[42] and bipyridine group (**8**)[43] can be directly introduced from corresponding bridged-type precursors. Because 2-phenylpyridine and bipyridine are recognized as typical chelating groups that can coordinate with various metals, metal complexes working as catalytically active sites could be densely accumulated on the surface of these PMOs. A metal complex (**9)** is also directly incorporated into PMO with maintaining its original structure and functionality.[44] A Pd-carbene complex can be formed on PMO surface after post-synthetic treatment of imidazolium-containing PMO (**10**) with $Pd(OAc)_2$. The resulting

Pd immobilized PMO can work as a heterogeneous carbene catalyst for the Mizoroki-Heck reaction. [45,46]

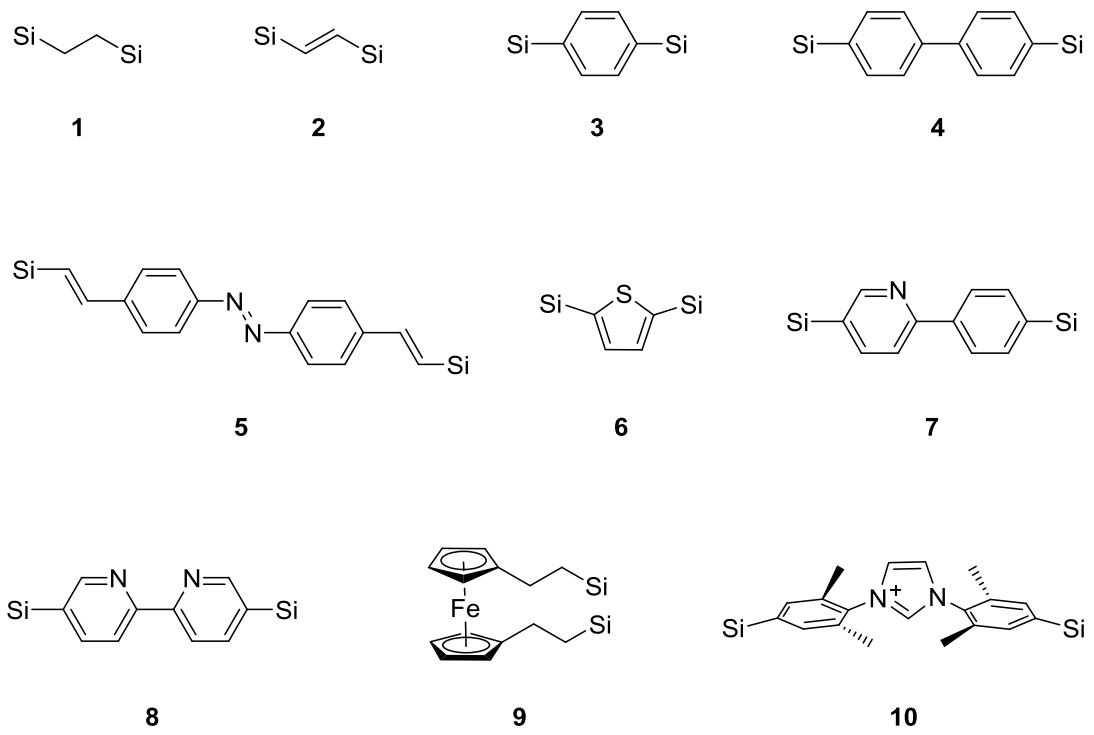

Figure 1.3. Organic moieties in a variety of PMOs.

Table 1.2 summarizes several examples of PMOs as heterogeneous catalysts in liquid-phase reactions. Sulfonic acid functionalized phenylene-PMO showed an excellent activity as a solid acid catalyst in the Friedel-Crafts acylation of anisole with acetic anhydride (Entry 1, yield 88%, selectivity 97%).[47] Sulfonated PMOs were also applicable to the hydrolysis of sugars,[48] the Friedel-Crafts alkylation,[49] and various

rearrangement reactions.[50] Formation of metal complexes on PMO surface by post-synthetic treatment results in the development of a novel supported catalyst. PMO with a palladium complex was successfully synthesized by co-condensation of the palladium-containing organosilane precursor and $Si(OC_2H_5)_4$ and applied to the Suzuki-Miyaura cross-coupling reaction (Entry 2).[51] Despite high catalytic performance, leaching of Pd complex and collapse of mesoporous structure taking place during the reaction are serious problem of this system. Coordination of $RhCl_3$ with PPh_3 groups on PMO surface produced a rhodium complex that effectively catalyzed alkanes oxidation.[52] This catalyst also showed high yield (94%) and selectivity (95%) of the desired product in the Miyaura-Michael reaction (Entry 3). Note that no significant loss of rhodium species was observed in solution after the reaction.[53] High stability and reusability of this system is beneficial for the development of other transition-metal complexes (Pd and Ru) for catalytic applications. Catalytic oxidation have also been demonstrated by Fe porphyrin-incorporated PMO catalyst.[54,55] Fe porphyrin based cytochrome P450 is a monooxygenase that catalyzes a variety of oxidation reactions such as alkene epoxidation and alkane hydroxylation with molecular oxygen.[56] Regardless of its large molecular size, Fe porphyrin can be immobilized on PMO surface and used in selective epoxidation of alkanes[54] and the Baeyer-Villiger oxidation of ketones,[55] as shown in Entry 4. PMO

with a chiral ligand, 2,20-bis(diphenylphosphino)-1,10-binaphthyl (BINAP), was utilized as host material to immobilize a Ru complex $[RuCl_2(benzene)]_2$.[57] The resulting PMO afforded high catalytic performance in the asymmetric hydrogenation of β-keto esters with 99% ee (Entry 5). Recently, PMO with incorporated 2,2'-bipyridyl groups exhibited excellent property as a solid chelating ligand for the immobilization of metal complexes.[43] Ir complexes, Ir(cod)(OMe), immobilized on 2,2'-bipyridyl-PMO catalyzed the borylation of C–H bonds in substituted benzene compounds to afford desired products (Entry 6). Interestingly, the activity of the solid catalyst was higher than that of a corresponding homogeneous catalyst.

Table 1.2. Catalytic systems using metal complex immobilized-PMOs.

Entry	Catalyst	Reaction	Ref.
1	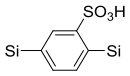	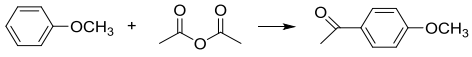	[47]
2	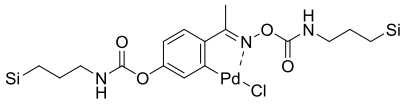	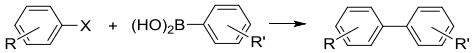	[51]
3	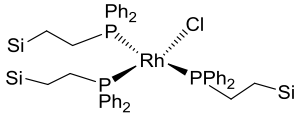	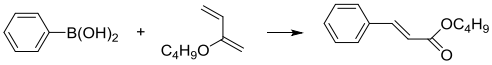	[53]
4	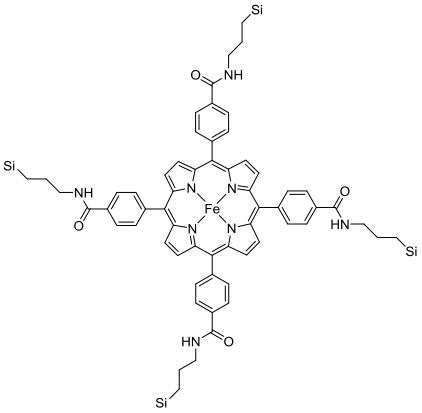	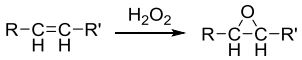	[54]
		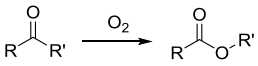	[55]
5	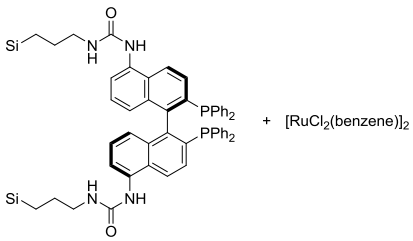	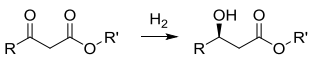	[57]
6	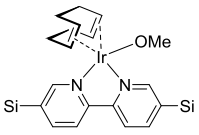	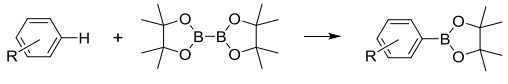	[43]

A coumarin-encapsulated biphenyl-PMO exhibited unique UV light absorption and subsequent fluorescence by a light-harvesting effect; the photoexcitation of biphenyl moieties by UV light adsorption induces energy transfer to coumarin dye immobilized within mesopores, which results in highly efficient fluorescence.[58] This light-harvesting effect is expected to be useful for the development of efficient photocatalytic systems by combination with reaction centers. Electron-accepting viologen groups were covalently attached onto the framework of biphenyl-bridged PMO (Figure 1.3, **4**) to form charge transfer (CT) complexes. After loading Pt nanoparticles, the Pt-supported biphenyl-bridged PMO with viologen groups was reported to be promising for photocatalytic hydrogen evolution from water.[59] Photoexcitation induced electron transfer from biphenyl to viologen to yield long lived radical cations and hydrogen evolution was promoted by the platinum catalyst in the presence of reduced nicotinamide adenine dinucleotide (NADH) as a sacrificial agent (Figure 1.4).

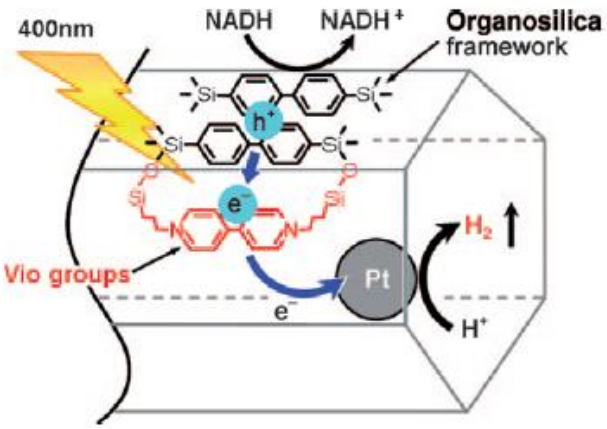

Figure 1.4. Photocatalytic hydrogen evolution by combination of viologen, Pt nanoparticles, and biphenyl PMO.

A photocatalytic CO_2 reduction system was developed with a Re complex immobilized onto biphenyl-incorporated PMO.[60] Biphenyl chromophores in the framework funneled the light energy into the Re complex (Figure 1.5). Consequently, light-harvesting system of biphenyl-PMO with the Re complex enhanced photocatalytic CO evolution from CO_2 by a factor of 4.4 compared with direct photoexcitation of the Re complex.

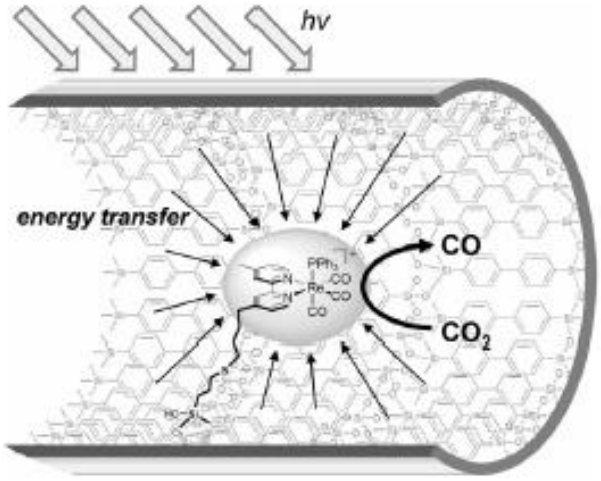

Figure 1.5. Photocatalytic reduction of CO_2 with a Re complex onto biphenyl-incorporated PMO.

1.4. Metal nanoparticles-supported catalyst using silicas

Metal-supported catalyst is one of the important heterogeneous catalysts used widely in many industrial processes[61,62] as summarized in Table 1.3. A lot of metal supported catalysts were synthesized by impregnation of metal ions on organic and inorganic supports and subsequent thermal or chemical reductions. Because catalytic reactions take place only on external surface of metal catalyst, nanoparticle formation contributes largely to increase of effective surface area and minimization of metal usage to reduce inaccessible sites inside the metal particle.

Table 1.3. Conventional chemical processes based on metal-supported heterogeneous catalysts.

Reaction	Catalyst
Ammonia synthesis ($N_2 + 3H_2 \rightarrow 2NH_3$)	Fe-K_2O-Al_2O_3
Steam reforming of methane ($CH_4 + H_2O \rightarrow CO + 3H_2$)	Ni-Al_2O_3
Water-gas shift reaction ($CO + H_2O \rightarrow CO_2 + H_2$)	Cu-ZnO
Methanol synthesis ($CO + 2H_2 \rightarrow CH_3OH$)	Cu-ZnO-Al_2O_3
Reforming of naphtha	Pt, Pt-Re-zeolite
Hydrodesulfurization ($R_2S + H_2 \rightarrow 2RH + H_2S$)	Co-Mo-Al_2O_3
Ethylene epoxidation to ethylene oxide	Ag-Al_2O_3
Oxidation of CO and hydrocarbons, Reduction of NO_x	Pt, Pd, Rh-CeO_2-Al_2O_3

Catalytic activities of supported metal catalyst strongly depend on shape, size, and distribution of metal nanoparticles. Precise control of these parameters has been studied [63-66] to accomplish the formation of stable and highly active metal nanoparticles for catalytic reactions.[67-72] Several strategies have been reported to control the size and distribution of Pt nanoparticles: simple impregnation-thermal reduction, electrochemical reduction of immobilized Pt ions,[73] , chemical vapor deposition of Pt metal,[74] and immobilization of preformed Pt nanoparticles with a stabilizing agent such

as poly-*N*-vinyl-2-pyrrolidone (PVP).[75] Mesoporous silica is an effective support for the immobilization of metal nanoparticles,[76] because of its high surface area and tunable mesoporous structure. Pt nanoparticles can be formed on mesoporous silica, SBA-15, by various strategies as shown in Figure 1.6. SBA-15 was synthesized from $Si(OC_2H_5)_4$ in the presence of an amphiphilic triblock copolymer, P123 ($HO\text{-}(CH_2CH_2O)_{20}\text{-}(CH_2CH(CH_3)O)_{70}(CH_2CH_2O)_{20}\text{-}H$) as a structure-directing agent.[30] Colloidal Pt nanoparticles coated with surfactant molecules was successfully deposited on SBA-15 by capillary inclusion with the assistance of ultrasonication treatment and subsequent removal of the surfactant (Figure 1.6(a)).[77] Inclusion of colloidal Pt nanoparticles into micelle during in situ growth of SBA-15 (Figure 1.6(b)) is also an another approach for the preparation of Pt-loaded SBA-15.[78] Encapsulation of Pt nanoparticle inside the micelle of SBA-15 enabled high dispersion inside mesopores in the resulting SBA-15. Figure 1.6(c) shows a typical immobilization-thermal reduction technique for the preparation of Pt nanoparticles. H_2PtCl_6 was conventionally used as a metal precursor dissolved in water. Deposition of water-soluble Pt ions and thermal reduction with H_2 result in the formation of Pt nanoparticle on SBA-15.[79] Due to its simplicity , this method should be successful for the large scale production of supported Pt catalysts. Recently, Pt nanoparticles on mesoporous silica exhibited high activity in ethylene oxidation at low

temperature, and this catalyst was installed in a refrigerator to keep vegetables fresh.[80]

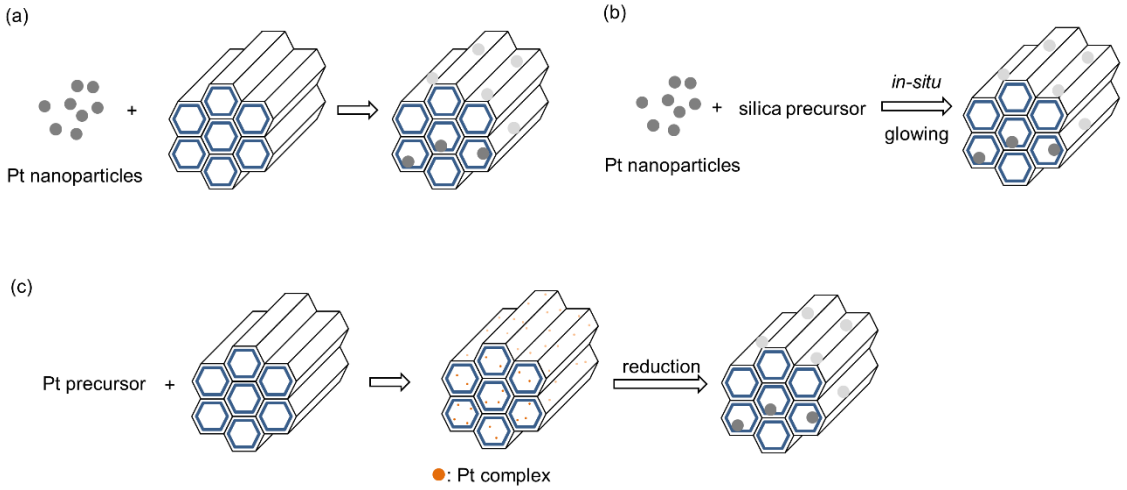

Figure 1.6. Deposition of Pt nanoparticles on mesoporous silica by (a) inclusion, (b) encapsulation, and (c) impregnation techniques.

Catalytic activity and selectivity of metal nanoparticles can be manipulated by size, shape, and composition. One representative example is Au catalyst. Bulk Au metal has no functionality for catalysis, but gold particles in nanometer scale shows high catalytic activity in the oxidation of CO at low temperature.[81,82] Catalytic performance of gold nanoparticles is controlled by its particle size.[83] Figure 1.7 shows sharp increase in catalytic activity of gold nanoparticle with decrease in diameter below 4 nm.[84] The total number of surface atoms changes when the average particle size is getting small. Along with the increase in the fraction of corner atoms, catalytic activity of Au nanoparticle

increases in CO oxidation.

Supported Au catalysts were also applied for oxidation of organic compounds such as alcohols and hydrocarbons,[85-87] and hydrogenation of alkanes and nitro compounds.[87,88] A gold nanoparticle consisting of 55 Au atoms on boron nitride exhibited excellent performance in the partial oxidation of styrene to benzaldehyde using O_2.[89] Size-controlled gold nanoparticles (10, 18, 25, 39, 85 atoms) were examined in the selective oxidation of cyclohexane.[90] Au nanoparticle with 39 Au atoms was found to be most active catalyst for the aerobic oxidation of cyclohexane.

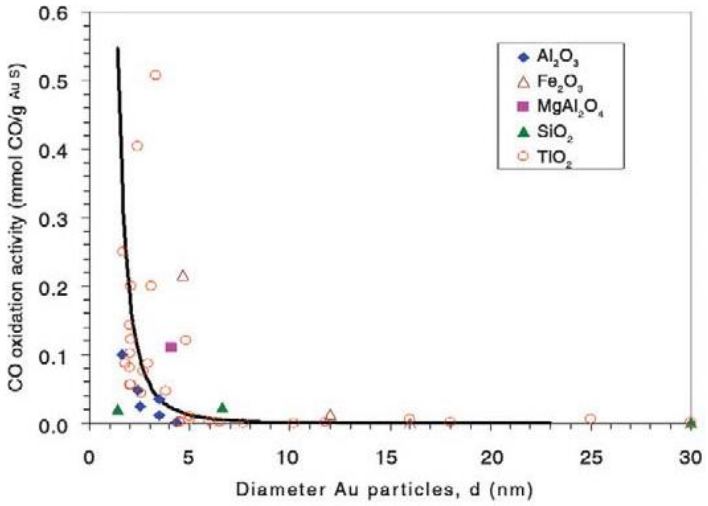

Figure 1.7. CO oxidation activity over gold supported on various metal oxides as function of the mean diameter of gold nanoparticles.

1.5. C1 chemical processes

Although many useful heterogeneous catalysts have been developed from the view point of green chemistry, current processes in the chemical industry should be renovated to realize sustainable chemical production. Syngas (Synthesis gas, $CO+H_2$) production is one of the most important reactions in C1 chemistry because this can be utilized as feedstock for the production of essential chemicals such as methanol, formaldehyde, methyl formate, acetic acid, formic acid, dimethyl ether, and hydrocarbons (Scheme 1.2).[91-96] To date, syngas has been synthesized by the gasification of coal, partial oxidation of hydrocarbons in oil, and steam reforming of methane in natural gas. In addition, CO_2 has been recognized as an abundant and inexpensive carbon resource for chemical industry, [97-100] and can be converted to syngas by reverse water-gas shift reaction (RWGS, equation 1.1) without any purification process.

$$CO_2 + H_2 \rightleftarrows CO + H_2O \qquad (1.1)$$

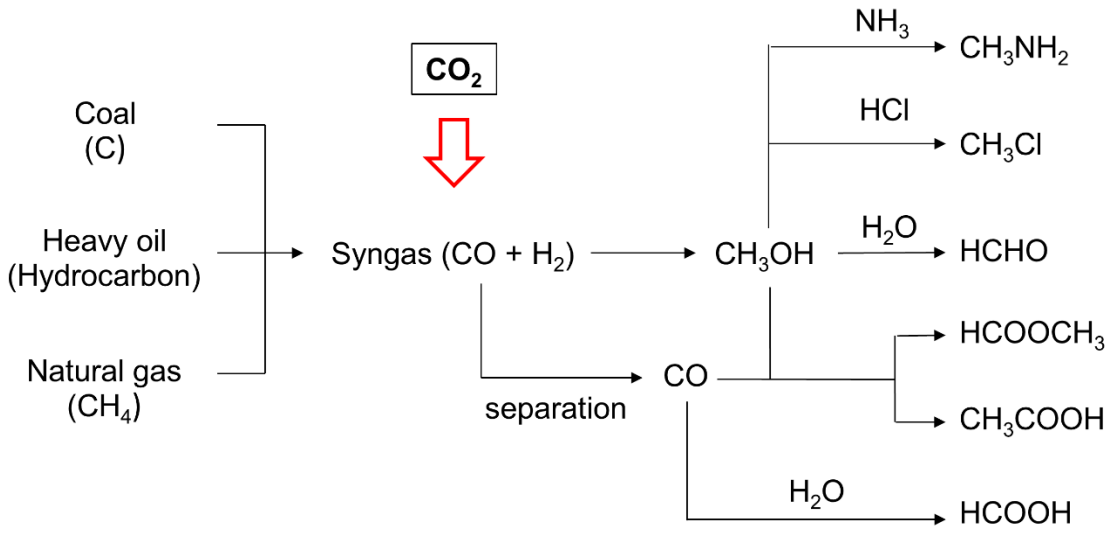

Scheme 1.2. Routes to basic industrial chemicals in C1 chemistry

RWGS reaction is an endothermic reaction ($\Delta H_{298\ K}$ = 41.2 kJ mol^{-1}), so that high temperature facilitates CO formation. It is essential to use a thermally stable inorganic metal oxide as a support to withstand the reaction at high temperature (Table 1.3). Because catalysts used in the water gas shift (WGS) reaction are also active in RWGS, a typical catalyst, Cu-ZnO, shows high activity at 250 ˚C under 1 atm (Entry 1).[101] However, this catalyst is favorable to produce methanol because Cu-ZnO also has activity in methanol synthesis from syngas. Some transition metals such as Fe or Co promote the formation of hydrocarbons in CO_2 hydrogenation. Al_2O_3 supported Fe catalyst converted CO_2 to CO in low selectivity (Entry 2).[95] In contrast, supported noble metal catalysts such as Pt, Ru, Pd and Rh typically have high ability toward H_2 dissociation, and can be used as efficient

catalysts for CO_2 hydrogenation. Supported Rh catalyst afforded CO in high selectivity of 87 %.[102] TiO_2 supported Au nanoparticles catalyst showed highly selective conversion of CO_2 to CO (93% selectivity, Entry 4).[103]

Table 1.4. Catalytic CO_2 conversion to CO by hydrogenation.

Entry	Catalyst	Conditions	Performance	[Ref.]
1	Cu/ZnO	250 ˚C, 1 atm	Conv. 21 %, Sel. 50 %	[101]
2	$Mn/Fe/Al_2O_3$	290 ˚C, 14 atm	Conv. 26 %, Sel. 16 %	[95]
3	Li/Rh-Y-zeolite	250 ˚C, 30 atm	Conv. 16 %, Sel. 87 %	[102]
4	Au/TiO_2	250 ˚C, 8 atm	Conv. 13 %, Sel. 93 %	[103]

1.6. Objectives of this work

Heterogeneous catalyst showing extremely high activity and selectivity is inevitable to realize sustainable society. In this regard, the author focuses special attention on periodic mesoporous organosilica (PMO) as a versatile support that has a well-defined mesoporous structure and crystal-like arrangement of organic moiety inside the silica wall. Because bi-pyridine functions as a coordination site for metals, bi-pyridine-containing PMO (BPy-PMO) can be utilized as a solid ligand for various homogeneous complexes

with unique catalysis. In this work, the author attempted to prepare BPy-PMO-based catalysts. In addition, the author also studied Al_2O_3-loaded Au catalyst for selective reduction of carbon dioxide to carbon monoxide via the formation of formic acid as an intermediate, which is an important process in chemical industry.

1.7. Constitution of the thesis

Chapter 1. General Introduction

The methods for immobilization of organic functional groups, homogeneous complexes, and novel metal nanoparticles on solid supports were summarized and discussed to develop heterogeneous catalysts with high activity and reusability. Then, objectives of this research are described.

Chapter 2. Synthesis, characterization, and catalysis of Ru-immobilized BPy-PMO

A Ru complex, $[RuCl_2(CO)_3]_2$, was successfully immobilized onto 2,2'-bipyridine (BPy) units of PMO to form a single site catalyst, which has been confirmed by various physicochemical analyses. The Ru-immobilized BPy-PMO selectively oxidizes the tertiary C−H bonds and showed reusability.

Chapter 3. Synthesis and characterization of various metal immobilized on BPy-PMO

Silica-supported gold nanoparticles were synthesized with BPy-PMO as an inorganic support. Reaction of a bipyridine group in BPy-PMO with $HAuCl_4$ forms $AuCl_2$-based complexes, and thermal reduction of the complex in H_2 results in the formation of small gold nanoparticles with an average size of ca. 3.8 nm.

Chapter 4. Selective reduction of carbon dioxide to carbon monoxide on alumina-supported gold catalyst

The objective in this chapter is to develop highly selective catalysts for reduction of carbon dioxide to carbon monoxide. Thermal decomposition of formic acid on γ-Al_2O_3 was studied by *in-situ* infrared spectroscopy measurement as an elementary step of reverse water-gas shit reaction (RWGS) over supported Au catalysts. Consequently, the supported Au catalyst gave CO with high selectivity over 99% from CO_2 and H_2.

Chapter 5. General conclusions

This chapter summarizes and integrates all of the study.

References

[1] F. Haber, *The synthesis of Ammonia from its Elements* **1920**, Nobel lecture.

[2] *Nature geoscience* **2008**, *1*, 637–639.

[3] R. A. Sheldon, *Pure Appl. Chem.* **2000**, *72*, 1233.

[4] P. T. Anatas, M. M. Kirchhoff, *Acc. Chem. Res.* **2002**, *35*, 686.

[5] A. Fukuoka, P. L. Dhepe, *Angew. Chem. In. Ed.* **2006**, *45*, 5161−5163.

[6] G. W. Huber, S. Iborra, A. Corma, *Chem. Rev.* **2006**, *106*, 4044−4098.

[7] D. J. Darensbourg, *Chem. Rev.* **2007**, *107*, 2388−2410.

[8] G. A. Olah, A. Goeppert, G. K. S. Prakash, *J. Org. Chem.* **2009**, *74*, 487–498.

[9] K. Maeda, K. Teramura, D. Lu, T. Takata, N. Saito, Y. Inoue, K. Domen, *Nature* **2006**, *440*, 295–295.

[10] K. Maeda, M. Higashi, D. Lu, R. Abe, K. Domen, *J. Am. Chem. Soc.* **2010**, *132*, 5858–5868.

[11] H. Ichihashi, M. Kitamura, *Catal. Today* **2002**, *73*, 23–28.

[12] G. Rothenberg, *Catalysis: Concepts and Green Applications* **2007**, VCH, Weinheim.

[13] B. Cornils, W. A. Herrmann, *J. Catal*. **2003**, *216*, 23–31.

[14] D. J. C.-Hamilton, *Science* **2003**, *299*, 1702–1706.

[15] P. W. N. M. van Leeuwen, *Appl. Catal. A*, 212 (2001) 61–81.

[16] J. Lu, P. H. Toy, *Chem. Rev.* **2009**, *109*, 108, 815–838.

[17] S. Hübner, J. G. Vries, V. Farina, *Adv. Synth. Catal.* **2016**, *358*, 3–25.

[18] B. V. Romanovsky, A. G. Gabrielov, *J. Mol. Catal.* **1992**, *74*, 293–303.

[19] N. Herron, G. D. Stucky, C. A. Tolman, *J. Chem. Soc., Chem. Commun.* **1986**, 1521–1522.

[20] S. Kobayashi, R. Akiyama, *Chem. Commun.* **2003**, 449–460.

[21] R. Akiyama, S. Kobayashi, *Chem. Rev.* **2009**, *109*, 594–642.

[22] R. Akiyama, S. Kobayashi, *J. Am. Chem. Soc.* **2003**, *125*, 3412–3413.

[23] D. J. Cram, *Science* **1983**, *219*, 1177–1183.

[24] L. Yin, J. Liebscher, *Chem. Rev.* **2007**, *107*, 133−173.

[25] K. S. W. Sing, D. H. Everett, R. A. W. Haul, L. Moscou, R. A. Pierotti, J. Rouquerol, T. Siemieniewska, *Pure Appl. Chem.* **1985**, *57*, 603–619.

[26] C. T-W. Chu, C. D. Chang, *J. Phys. Chem.* **1985**, *89*, 1569–1571.

[27] R. Krishna, J. A. Wesselingh, *Chem. Eng. Sci.* **1997**, *52*, 861–911.

[28] S. Inagaki, A. Koiwai, N. Suzuki, Y. Fukushima, K. Kuroda, *Bull. Chem. Soc. Japan* **1996**, *69*, 1449–1457.

[29] C. T. Kresge, M. E. Leonowicz, W. J. Roth, J. C. Vartuli, J. S. Beck, *Nature* **1992**,

359, 710–712.

[30] D. Zhao, J. Feng, Q. Huo, N. Melosh, G. H. Fredrickson, B. F. Chmelka, G. D. Stucky, *Science* **1998**, *279*, 548–552.

[31] A. Taguchi, F. Schüth, *Microporous Mesoporous Mater.* **2005**, *77*, 1–45.

[32] N. Mizoshita, T. Tani, S. Inagaki, *Chem. Soc. Rev.* **2011**, *40*, 789–800.

[33] S. Inagaki, S. Guan, Y. Fukushima, T. Ohsuna, O. Terasaki, *J. Am. Chem. Soc.* **1999**, *121*, 9611–9614.

[34] B. J. Melde, B. T. Holland, C. F. Blanford, A. Stein, *Chem. Mater.* **1999**, *11*, 3302–3308.

[35] S. Inagaki, S. Guan, T. Ohsuna, O. Terasaki, *Nature* **2002**, *416*, 304–307.

[36] M. P. Kapoor, Q. H. Yang, S. Inagaki, *J. Am. Chem. Soc.* **2002**, *124*, 15176–15177.

[37] K. Nakai, Y. Oumi, H. Horie, T. Sano, H. Yoshitake, *Microporous Mesoporous Mater.* **2007**, *100*, 328–339.

[38] M. Sasidharan, S. Fujita, M. Ohashi, Y. Goto, K. Nakashima, S. Inagaki, *Chem. Commun.* **2011**, *47*, 10422–10424.

[39] K. Nakajima, I. Tomita, M. Hara, S. Hayashi, K. Domen, J. N. Kondo, *Adv. Mater.* **2005**, *17*, 1839–1842.

[40] M. Cornelius, F. Hoffmann, B. Ufer, P. Behrens, M. Fröba, *J. Mater. Chem*. **2008**, *18*, 2587–2592.

[41] A. Sayari, S. Hamoudi, Y. Yang, I. L. Moudrakovski, J. R. Ripmeester, *Chem. Mater.* **2000**, *12*, 3857–3863.

[42] M. Waki, N. Mizoshita, T. Ohsuna, T. Tani, S. Inagaki, *Chem. Commun.* **2010**, *46*, 8163–8165.

[43] M. Waki, Y. Maegawa, K. Hara, Y. Goto, S. Shirai, Y. Yamada, N. Mizoshita, T. Tani, W.-J. Chun, S. Muratsugu, M. Tada, A. Fukuoka, S. Inagaki, *J. Am. Chem. Soc.* **2014**, *136*, 4003−4011.

[44] T. M. Zhang, C. G. Gao, H. Q. Yang, Y. X. Zhao, *J. Porous Mater.* **2010**, *17*, 643–649.

[45] T. P. Nguyen, P. Hesemann, P. Gaveaub, J. J. E. Moreau, *J. Mater. Chem.* **2009**, *19*, 4164–4171.

[46] T. P. Nguyen, P. Hesemann, J. J. E. Moreau, *Microporous Mesoporous Mater.* **2011**, *142*, 292–300.

[47] M. P. Kapoor, Y. Kasama, M. Yanagi, T. Yokoyama, S. Inagaki, T. Shimada, H. Nanbu, L. R. Juneja, *Microporous Mesoporous Mater.* **2007**, *101*, 231–239.

[48] P. L. Dhepe, M. Ohashi, S. Inagaki, M. Ichikawa, A. Fukuoka, *Catal. Lett.* **2005**,

102, 163–169.

[49] B. Rác, P. Hegyes, P. Forgo, Á. Molnár, *Appl. Catal. A: General* **2006**, *299*, 193–201.

[50] K. Nakajima, I. Tomita, M. Hara, S. Hayashi, K. Domen, J. N. Kondo, *Catal. Today* **2006**, *116*, 151–156.

[51] A. Corma, D. Das, H. Garcia, A. Leyva, *J. Catal.* **2005**, *229*, 322–331.

[52] V. Dufaud, F. Beauchesne, L. Bonneviot, *Angew. Chem., Int. Ed.* **2005**, *44*, 3475–3477.

[53] F. Zhang, C. M. Kang, Y. Y. Wei, H. X. Li, *Adv. Funct. Mater.* **2011**, *21*, 3189–3197.

[54] E. Y. Jeong, A. Burri, S. Y. Lee, S. E. Park, *J. Mater. Chem.* **2010**, *20*, 10869–10875.

[55] E. Y. Jeong, M. B. Ansari, S. E. Park, *ACS Catal.* **2011**, *1*, 855–863.

[56] P. E. Ellis, J. E. Lyons, *Coord. Chem. Rev.* **1990**, *105*, 181–193.

[57] P. Y. Wang, X. Liu, J. Yang, Y. Yang, L. Zhang, Q. H. Yang, C. Li, *J. Mater. Chem.* **2009**, *19*, 8009–8014.

[58] S. Inagaki, O. Ohtani, Y. Goto, K. Okamoto, M. Ikai, K. Yamanaka, T. Tani, T. Okada, *Angew. Chem. Int. Ed.* **2009**, *48*, 4042–4046.

[59] M. Ohashi, M. Aoki, K. Yamanaka, K. Nakajima, T. Ohsuna, T. Tani, S. Inagaki, *Chem. Eur. J.* **2009**, *15*, 13041–13046.

[60] H. Takeda, M. Ohashi, T. Tani, O. Ishitani, S. Inagaki, *Inorg. Chem.* **2010**, *49*, 4554–4559.

[61] I. Chorkendorff, J. W. Niemantsverdriet, *Concepts of Modern Catalysis and Kinetics*, *Second Edition* **1997**, VCH, Weinheim.

[62] J. M. Thomas, W. J. Thomas, *Principles and Practice of Heterogeneous Catalysis* **1997**, VCH, Weinheim.

[63] G. A. Somorjai, K. McCrea, *Appl. Catal. A: General* **2012**, *222*, 3–18.

[64] G. Ertl, D. Prigge, *J. Catal* **1983**, *79*, 359–377.

[65] J. Yang, V. Tschamber, D. Habermacher, F. Garin, P. Gilot, *Appl. Catal. B: Environmental* **2008**, *83*, 229–239.

[66] G. A. Somorjai, R. M. Rioux, *Catal. Today* **2005**, *100*, 201–215.

[67] C. J. Jia, F. Schuth, *Phys. Chem. Chem. Phys.* **2011**, *13*, 2457–2487.

[68] H. Duan, D. Wang, Y. Li, *Chem. Soc. Rev.* **2015**, *44*, 5778–5792.

[69] D. Astruc, F. Lu, J. R. Aranzaes, *Angew. Chem. Int. Ed.* **2005**, *44*, 7852–7872.

[70] B. R. Cuenya, *Thin Solid Films* **2010**, *518*, 3127–3150.

[71] A. Taleb, C. Petit, M. P. Pileni, *Chem. Mater.* **1997**, *9*, 950–959.

[72] R. M. Crooks, M. Zhao, L. Sun, V. Chechik, L. K. Yeung, *Acc. Chem. Res.* **2001**, *34*, 181–190.

[73] S. D.-Dominguez, J. A. Pardilla, A. B.-Murcia, E. Morallon, D. C. Amoros, *J. Appl. Electrochem.* **2008**, *38*, 259–268.

[74] P. Serp, P. Kalck, R. Feurer, *Chem. Rev.* **2002**, *102*, 3085–3128.

[75] C. K. Tsung, J. N. Kuhn, W. Z. Huang, C. Aliaga, L. I. Hung, G. A. Somorjai and P. D. Yang, *J. Am. Chem. Soc.* **2009**, *131*, 5816–5822.

[76] R. J. White, R. Luque, V. L. Budarin, J. H. Clark, D. J. Macquarrie, *Chem. Soc. Rev.* **2009**, *38*, 481–494.

[77] R. M. Rioux, H. Song, J. D. Hoefelmeyer, P. Yang, G. A. Somorjai, *J. Phys. Chem. B* **2005**, *109*, 2192–2202.

[78] H. Song, R. M. Rioux, J. D. Hoefelmeyer, R. Komor, K. Niesz, M. Grass, P. Yang, G. A. Somorjai, *J. Am. Chem. Soc.* **2006**, *128*, 3027–3037.

[79] A. Fukuoka, J. Kimura, T. Oshio, Y. Sakamoto, M. Ichikawa, *J. Am. Chem. Soc.* **2007**, *129*, 10120–10125.

[80] C. Jiang, K. Hara, A. Fukuoka, *Angew. Chem., Int. Ed.* **2013**, *52*, 6265–6268.

[81] M. Haruta, T. Kobayashi, H. Sano, N. Yamada, *Chem. Lett.* **1987**, 405–406.

[82] S. Panigrahi, S. Basu, S. Praharaj, S. Pande, S. Jana, A. Pal, S. K. Ghosh, T. Pal,

J. Phys. Chem. C **2007**, *111*, 4596–4605.

[83] M. Haruta, S. Tsubota, T. Kobayashi, H. Kageyama, M. J. Genet, B. Delmon, *J. Catal.* **1993**, *144*, 175–192.

[84] B. Hvolbæk, T. V. W. Janssens, B. S. Clausen, H. Falsig, C. H. Christensen, J. K. Nørskov, *nanotoday* **2007**, *2*, 14–18.

[85] D. I. Enache, J. K. Edwards, P. Landon, B. S.-Espriu, A. F. Carley, A. A. Herzing, M. Watanabe, C. J. Kiely, D. W. Knight, G. J. Hutchings, *Science* **2006**, *311*, 362–365.

[86] M. D. Hughes, Y.–J. Xu, P. Jenkins, P. McMorn, P. Landon, D. I. Enache, A. F. Carley, G. A. Attard, G. J. Hutchings, F. King, E. H. Stitt, P. Johnston, K. Griffin, C. J. Kiely, *Nature* **2005**, *437*, 1132–1135.

[87] A. Corma, H. Garcia, *Chem. Soc. Rev.* **2008**, *37*, 2096–2126.

[88] A. Corma, P. Serna, *Science* **2006**, *313*, 332–334.

[89] M. Turner, V. B. Golovko, O. P. H. Vaughan, P. Abdulkin, A. B.-Murcia, M. S. Tikhov, B. F. G. Johnson, R. M. Lambert, *Nature* **2008**, *454*, 981–983.

[90] Y. Liu, H. Tsunoyama, T. Akita, S. Xie, T. Tsukuda, *ACS Catal.* **2011**, *1*, 2–6.

[91] L. G. Fierro, Catal. Lett. **1993**, *22*, 67–91.

[92] W. Wang, S. Wan, X. Ma, J. Gong, *Chem. Soc. Rev.* **2011**, *40*, 3703–3727.

[93] R. Tanaka, M. Yamashita, K. Nozaki, *J. Am. Chem. Soc.* **2009**, *131*, 14168–14169.

[94] J. Sloczynski, R. Grabowski, A. Kozlowka, P. Olszewski, J. Stoch, J. Skrzypek, M. Lachowska, *Appl. Catal. A* **2004**, *278*, 11–23.

[95] R. W. Dorner, D. R. Hardy, F. W. Williams, H. D. Willauer, *Appl. Catal. A* **2010**, *373*, 112–121.

[96] O. S. Joo, K. D. Jung, I. Moon, A.Y. Rozovskii, G.I. Lin, S. H. Han, S. J. Uhm, *Ind. Eng. Chem. Res.* **1999**, *38*, 1808–1812.

[97] G. Centi, S. Perathoner, *Catal. Today* **2009**, *148*, 191–205.

[98] T. Schaub, R. A. Paciello, *Angew. Chem. Int. Ed.* **2011**, *50*, 7278–7282.

[99] S. Fukuoka, M. Kawamura, K. Komiya, M. Tojo, H. Hachiya, K. Hasegawa, M. Aminaka, H. Okamoto, I. Fukawa, S. Konno, *Green Chem.* **2003**, *5*, 497–507.

[100] G. W. Coates, D. R. Moore, *Angew. Chem. Int. Ed.* **2004**, *43*, 6618–6639.

[101] K. -W. Jun, W. -J. Shen, K. S. R. Rao, K. -W. Lee, *Appl. Catal. A* 1998, *174*, 231–238.

[102] H. Kusama, K. K. Bando, K. Okabe and H. Arakawa, *Appl. Catal. A*, **2001**, *205*, 285–294.

[103] H. Sakurai, S. Tsubota, M. Haruta, *Appl. Catal. A* **1993**, *102*, 125–136.

Chapter 2. Synthesis, characterization, and catalysis of Ru-immobilized BPy-PMO

Abstract

Periodic mesoporous organosilica (PMO) is a unique material that has a crystal-like wall structure with coordination sites for metal complexes. A Ru complex, $[RuCl_2(CO)_3]_2$, is successfully immobilized onto 2,2'-bipyridine (BPy) units of PMO to form a single site catalyst, which has been confirmed by various physicochemical analyses. Using NaClO as an oxidant, the Ru-immobilized PMO oxidizes the tertiary C−H bonds of adamantane to the corresponding alcohols at 57 times faster than the secondary C−H bonds, thereby exhibiting remarkably high regioselectivity. Moreover, the catalyst converts *cis*-decalin to *cis*-9-decalol in 63% yield with complete retention of the substrate stereochemistry. The Ru catalyst can be separated by simple filtration and reused without loss of the original activity and selectivity for the oxidation reactions.

2.1. Introduction

Periodic mesoporous organosilicas (PMOs) are unique materials that possess uniform mesopores (2-30 nm) consisting of crystal-like ordered arrays of organic moieties bridged by siloxane bonds.[1,2] Various chemical and physical properties can be introduced into the PMO materials by varying the organic groups. Ethylene-bridged PMO provides a highly hydrophobic environment inside the restricted mesopores that can stabilize protein molecules.[3] A coumarin-doped biphenyl-PMO system exhibits unique UV light absorption and subsequent fluorescence by a light-harvesting effect; the photoexcitation of biphenyl moieties by UV light adsorption induces energy transfer to coumarin dye immobilized within mesopores, which results in highly efficient fluorescence.[4] A photocatalytic CO_2 reduction system was constructed by anchoring a Re complex onto biphenyl-incorporated PMO.[5] Recently, a PMO with incorporated 2,2'-bipyridyl (BPy) groups, BPy-PMO, was successfully synthesized and exhibited high performance as a solid chelating ligand for the immobilization of metal complexes to produce new types of single-site heterogeneous catalysts. An Ir-immobilized BPy-PMO catalyzed the borylation of C–H bonds in substituted benzenes to afford desired products.[6] and the activity of the solid catalyst was higher than that of a corresponding homogeneous catalyst. Immobilization of a Ru complex on BPy-PMO was also reported to be promising for solar

energy conversion systems.[6] After loading Pt nanoparticles, the Ru-supported BPy-PMO continuously reduced protons in water into hydrogen in the presence of a sacrificial reagent (ethylenediaminetetraacetic acid; EDTA) under visible-light irradiation. Direct injection of photoexcited electrons from the Ru complex to Pt nanoparticles enabled efficient hydrogen production, even in the absence of a typical electron mediator such as methyl viologen.

The author attempts to utilize PMO-based catalysts in the partial oxidation of hydrocarbons, which is a significant challenge in catalysis.[7-10] The oxidation of hydrocarbons using metal complex catalysts is subject to oxidation of the ligands by their own active oxygen species.[11] To avoid this problem, oxidation enzymes, as typified by cytochrome P-450, rigidly fix the active center (iron protoporphyrin-IX) in an isolated state on the pore wall of a protein.[12] It is thus expected that the immobilization of isolated active sites directly on the pore walls of PMOs will suppress self-oxidation, which is in sharp contrast to conventional catalysts[13] with mobile active centers grafted through linkers.

Herein, the author reports a new and reusable Ru-immobilized BPy-PMO catalyst that achieves selective oxidation of alkanes. The catalyst was synthesized from $[RuCl_2(CO)_3]_2$ and BPy-PMO; various physicochemical analyses verified the formation of a uniform

chemical structure with the Ru complex on PMO. The Ru catalyst oxidizes adamantane and *cis*-decalin to the corresponding tertiary alcohols with excellent regio- and stereoselectivity using a practical oxidant (NaClO). No solid catalyst has achieved high selectivity or durability in the oxidation of these alkanes. Although several homogeneous metal complexes have already shown high selectivity, these are single-use catalysts.[10,14] In contrast, the immobilization of the Ru complex on BPy-PMO realizes both high selectivity and reusability for the oxidation of alkanes. Tertiary alcohols of adamantane are precursors to photoresists for ArF lithography, engineering plastics, and medicines.[15,16] The selective oxidation of decalin is a model reaction for the synthesis of steroids and terpene based anti-tumor medicines.[10,17] The Ru-immobilized PMO catalyst developed in this study will contribute to practical industrial applications of fine chemical synthesis.

2.2. Experimental

2.2.1. Reagents

$[RuCl_2(CO)_3]_2$ was purchased from Sigma-Aldrich, and dehydrated tetrahydrofuran (THF) was obtained from Kanto Chemical Co. Other reagents were of the highest grade and were used without purification.

2.2.2. Synthesis of BPy-PMO

BPy-PMO was synthesized according to the literature method, using 5,5'-bis(triisopropoxysilyl)-2,2'-bipyridine as a monomer and octadecyltrimethylammonium chloride as a surfactant.[6] The bipyridine precursor, 5,5'-bis(triisopropoxysilyl)-2,2'-bipyridine, was prepared in two steps as shown in Scheme 2.1.

First, triisopropoxysilane was synthesized under an argon atmosphere. Trichlorosilane (50 g, 0.37 mol) diluted with CH_2Cl_2 (50 mL) was slowly added to a mixture of isopropanol (88 mL, 1.2 mol), pyridine (92 mL, 1.2 mol) and CH_2Cl_2 (500 mL) at 0 ºC. The mixture was stirred at room temperature for 6 h. After evaporation of the solvent, extraction of the product with hexane, and purification by silica gel column chromatography (eluent: hexane), triisopropoxysilane (70 g, 95%) was obtained as a transparent oil. ^{1}H NMR (400 MHz, $CDCl_3$, Me_4Si, ppm): δ 1.23 (d, J = 5.9 Hz, 18H), δ

4.26 (sept, J = 5.9 Hz, 3H), δ 4.34 (s, 1H).

Triisopropoxysilane (11 g, 53 mmol) was added to a solution containing DMF (100 mL), Et_3N (30 mL, 210 mmol), 2-bromo-5-iodopyridine (10 g, 35 mmol), $[RhCl(cod)]_2$ (0.17 g, 0.35 mmol), Bu_4NI (16 g, 42 mmol) at 0 ºC under an argon atmosphere. After addition of all triisopropoxysilane, the reaction mixture was stirred at 100 ºC for 24 h. After cooling to room temperature, the solvent was removed from the reaction mixture by vacuum evaporation. Crude product obtained by solvent extraction with Et_2O and pentane, suction filtration, and evaporation was purified by distillation to give 2-bromo-5-(trimethoxysilyl)pyridine (7.0 g, 55%) as a pale yellow oil. ^{1}H NMR (400 MHz, $CDCl_3$, Me_4Si, ppm): δ 1.20 (d, J = 6.0 Hz, 18H), δ 4.26 (sept, J = 6.4 Hz, 3H), δ 7.47 (d, J = 7.6 Hz, 1H), δ 7.78 (dd, J = 7.6 Hz, 1.6 Hz, 1H), δ 8.56 (d, J = 1.6 Hz, 1H).

2-Bromo-5-(trimethoxysilyl)pyridine (8.0 g, 23 mmol), bis(tributyltin) (6.5 g, 11 mmol), $Pd(PPh_3)_4$ (0.52 g, 0.45 mmol) was added to *m*-xylene (200 ml) under an argon atmosphere. The mixture was stirred at 130 ºC for 40 h. After cooling to room temperature, evaporation treatment, the residue was purified by silica gel column chromatography (eluent: CH_2Cl_2 and AcOEt/hexane = 1:10) to afford 5,5'-bis(triisopropoxysilyl)-2,2'-bipyridine (4.0 g, 75 %). ^{1}H NMR (400 MHz, $CDCl_3$, Me_4Si, ppm): δ 1.20 (d, J = 6.4 Hz, 36H), δ 4.31 (sept, J = 6.4 Hz, 6H), δ 8.08 (dd, J = 7.8 Hz, 1.6 Hz, 2H), δ 8.39 (d, J = 7.8

Hz, 2H), δ 8.92 (s, 2H).

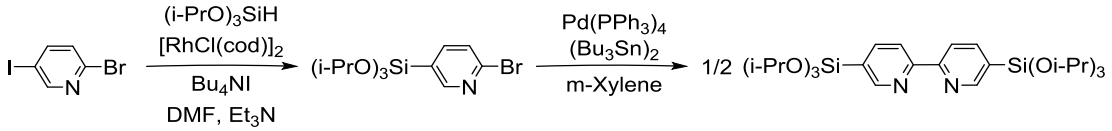

Scheme 2.1. Synthesis of 5,5'-Bis(triisopropoxysilyl)-2,2'-bipyridine.

The resulting bridged alkoxysilane was used as a precursor for the preparation of BPy-PMO. 5,5'-bis(triisopropoxysilyl)-2,2'-bipyridine (4.6 g)/EtOH (10 mL) solution was slowly dropped to an aueous solution containing H_2O (200 mL), sodium hydroxide (6N, 1.2 mL), and octadecyltrimethylammonium chloride (C18TMACl, 3.8 g) under vigorous stirring at 50 ºC for 2 h. After stirring the suspension for 3 days and subsequent aging for additional 3 days at 50 ºC, the resulted precipitate was filtered and washed with distilled water, affording as-made BPy-PMO. The as-made sample was added to an aqueous surfactant solution and heated at 95 ºC for 24 h to improve arrangement of uniform mesopores. After filtration and washing with H_2O and EtOH, the surfactant was removed by solvent extraction with 0.05 M HCl/EtOH solution at room temperature for 18 h. Filtration and water washing several times produce BPy-PMO (1.0 g, 40%) as a white powder.

2.2.3. Immobilization of ruhenium complexes

A Ru-immobilized BPy-PMO, denoted **1**, was prepared from BPy-PMO and $[RuCl_2(CO)_3]_2$ as follows. BPy-PMO (100 mg) was added to a THF solution (30 mL) of $[RuCl_2(CO)_3]_2$ (100 mg, 0.50 mmol) under Ar, and the mixture was magnetically stirred under reflux conditions for 3 h. The resulting solid was filtered, washed with THF, and dried at 298 K *in vacuo*, to afford **1** (110 mg) as a brownish powder. A model complex for **1**, $RuCl_2(bpy)(CO)_2$, was synthesized according to a procedure in the literature,[18] and purified by recrystallization. Immobilization of Ru complexes on BPy-PMO was also conducted using other Ru precursors, $RuCl_3 \cdot xH_2O$ and $RuCl_2(bpy)_2 \cdot 2H_2O$, to obtain the Ru-immobilized BPy-PMOs, denoted **2** and **3**, respectively (Figure 2.1).

2.2.4. Characterization of metal complexes immobilized materials

The synthesized materials were analyzed and characterized using ultraviolet-visible diffuse reflectance spectroscopy (UV-vis DRS; Jasco, V-650), Fourier transform infrared spectroscopy (FT-IR; Perkin-Elmer, Spectrum 100, transmission mode, triglycine sulfate (TGS) detector with a 1 cm^{-1} resolution, 16 times integration), X-ray absorption fine structure (XAFS; at the BL14B2 of SPring-8), energy dispersive X-ray spectroscopy (EDX; Shimadzu EDX-720), nitrogen adsorption (BEL, Belsorp-mini II), and X-ray

diffraction (XRD; Rigaku, Ultima IV, Cu Kα).

2.2.5. Oxidation reaction

The substrate (230 μmol), catalyst (10 mg), ethylacetate (2.4 mL), acetate buffer (0.39 mL, pH 4.4, 2.0 M), and a magnetic stirrer were placed into a Pyrex vial (10 mL) equipped with a screw cap. The reaction was performed at 323 K for a designated time with an aqueous solution of NaClO (19 mM) supplied at a rate of 27 μL h^{-1} using a microfeeder (YMC, YSP-201) through a stainless steel needle (0.15 mm diameter) that penetrated the cap. Evolved gas was removed through another needle (0.1 mm diameter). After the addition of NaClO, the mixture was further stirred for 3 h to completely consume the oxidant. Unreacted substrate and products were extracted five times with ethylacetate and hexane and undecane was added into the extract as an external standard. The solution was analyzed using gas chromatography (GC; Shimadzu GC-14B, flame ionization detector) with an HR-1 (0.25 mm diameter, 25 m long) column and an HR-20M (0.25 mm diameter, 30 m long) column. Products were identified by gas chromatography-mass spectrometry (GC-MS; Shimadzu GC2010/PARVUM2, electron ionization) and nuclear magnetic resonance (NMR; Jeol, ECP-400, ^{1}H 400 MHz) spectroscopy.

2.3. Results and discussion

2.3.1. Characterization of Ru-immobilized PMO

PMO-based catalyst **1** was synthesized using BPy-PMO and $[RuCl_2(CO)_3]_2$ (Scheme 2.2) and characterized in detail. Immobilization of Ru complexes on BPy-PMO was also conducted using other Ru precursors, $RuCl_3 \cdot xH_2O$ and $RuCl_2(bpy)_2 \cdot 2H_2O$, to obtain the Ru-immobilized BPy-PMOs, denoted as **2** and **3**, respectively (Figure 2.1).

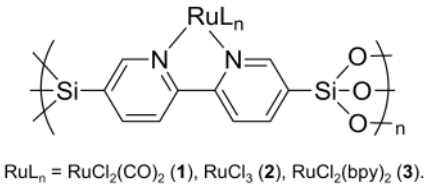

Figure 2.1. Plausible structures of **1**, **2** and **3**.

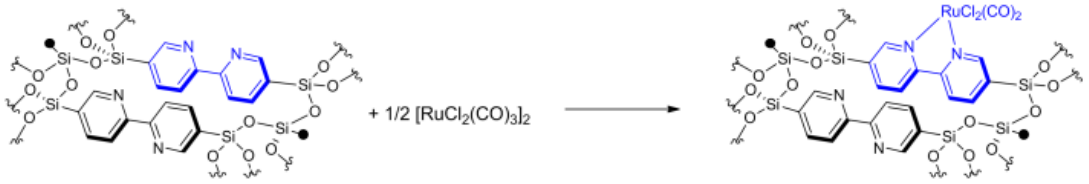

Scheme 2.2. Synthesis of Ru-immobilized BPy-PMO.

Nitrogen adsorption experiments of BPy-PMO and **1** both provided type-IV isotherms with no hysteresis, which indicates uniform mesopores (Figure 2.2(a)). Non-linear density functional theory (NLDFT) analysis of the isotherms indicated that the pore

diameter decreases from 4.6 to 4.0 nm after Ru loading (Figure 2.2(b)). The Brunauer-Emmett-Teller (BET) specific surface area was also slightly decreased from 690 to 530 $m^2\ g^{-1}$ by impregnation of Ru complexes onto BPy-PMO. The amount of surface BPy units in BPy-PMO was estimated to be 2.2 mmol g^{-1}, which was obtained by dividing the BET surface area (690 $m^2\ g^{-1}$) by the cross-sectional area of a PMO unit (310 $m^2\ mmol^{-1}$ for Si-BPy-Si-O_3; Figure 2.1). XRD measurements of BPy-PMO and **1** represented similar diffraction lines at 2θ = 1.8° (100) (Figure 2.3). These results clearly show that the ordered mesoporous structure of BPy-PMO is preserved after formation of the Ru complex.

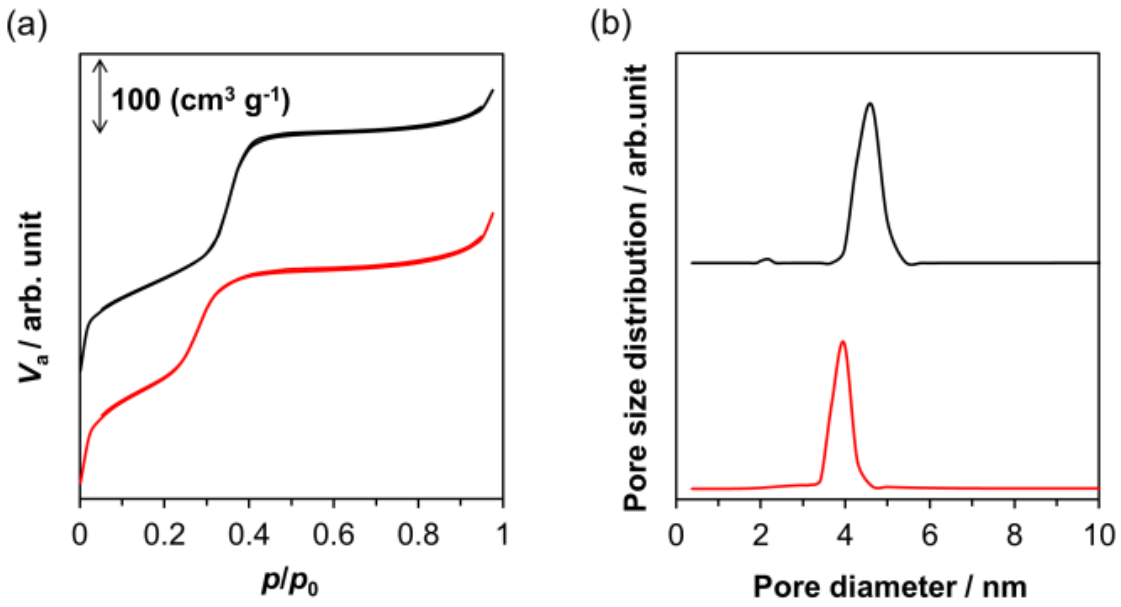

Figure 2.2. (a) N_2 adsorption isotherms and (b) NLDFT pore diameter distributions for BPy-PMO (black) and 1 (red) at 77 K.cheme 1. Synthesis of Ru-immobilized BPy-PMO.

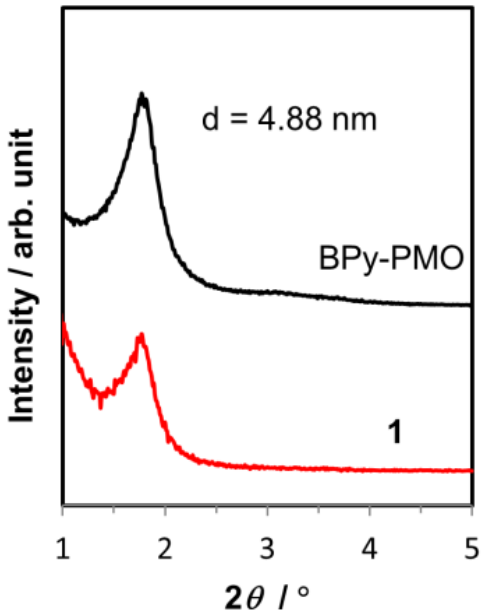

Figure 2.3. XRD patterns for **1** (red line) and BPy-PMO (black line).

EDX analysis indicated that the amount of Ru in **1** is 0.30 mmol g^{-1} (3.0 wt%), which corresponds to 15% of the total BPy units on the surface. This ratio of Ru/BPy is more than double the ratio previously reported for **3** (7.1%).[6] In a control experiment, it was verified that no Ru complex is immobilized on a mesoporous silica without BPy ligands.

Figure 2.4 shows UV-vis DRS spectra of BPy-PMO, **1**, the precursor $[RuCl_2(CO)_3]_2$, and $RuCl_2(bpy)(CO)_2$ as a model of **1**. BPy-PMO gave a broad peak at 300 nm derived from π–π* transition for BPy units within the silica framework.[19] A new peak was observed at 410 nm after the immobilization of Ru, which is ascribed to a metal-ligand charge transfer (MLCT) from Ru to BPy.[20] It was confirmed that $RuCl_2(bpy)(CO)_2$ has

the same MLCT band at 410 nm, where $[RuCl_2(CO)_3]_2$ provides no absorption band, which indicates the complexation between BPy units of BPy-PMO and Ru for **1**.

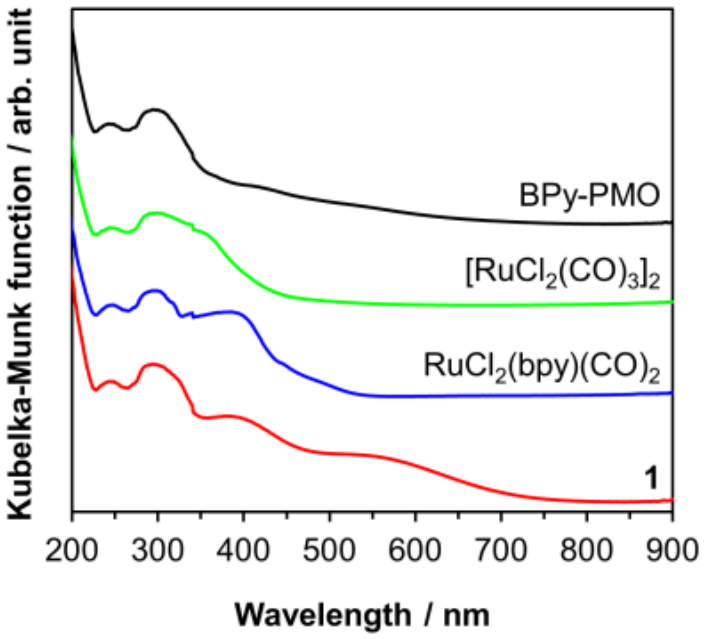

Figure 2.4. UV-vis DRS spectra for BPy-PMO (black), $[RuCl_2(CO)_3]_2$ (green), $RuCl_2(bpy)(CO)_2$ (blue), and **1** (red).

IR was employed to characterize the carbonyl groups on the same materials as shown in Figure 2.5. BPy-PMO showed no peaks derived from C–O stretching vibrations. The precursor to **1**, $[RuCl_2(CO)_3]_2$, showed two peaks at 2110 and 2160 cm^{-1}, which are assigned to symmetric and asymmetric C–O stretching vibrations.[21] **1** exhibited two strong peaks at 2075 and 2012 cm^{-1} for CO ligands of the immobilized Ru complex. This red-shift is due to an increase of the back-donation from Ru to CO by reducing the number

of CO ligands from three to two (see Scheme 2.2) and coordination of an electron-donating ligand, BPy.

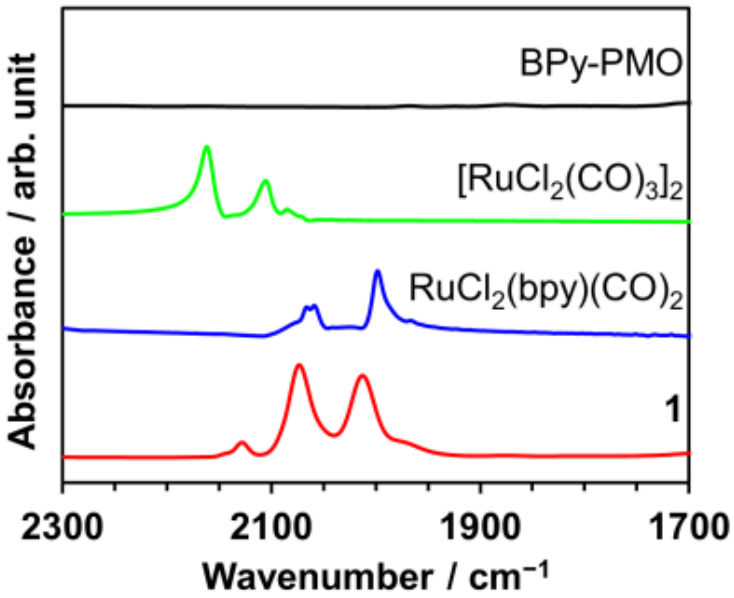

Figure 2.5. IR spectra of BPy-PMO (black), $[RuCl_2(CO)_3]_2$ (green), $RuCl_2(bpy)(CO)_2$ (blue), and **1** (red).

Ru K-edge XAFS measurements were conducted to reveal the electronic state and structure of the Ru center on **1**. In the X-ray absorption near-edge structure (XANES; Figure 2.6(a)), the edge energy of Ru immobilized on BPy-PMO (22119 eV) was in the divalent region and the spectrum was almost identical with that of $RuCl_2(bpy)(CO)_2$. This result indicates that the electronic structures of Ru atoms in **1** are similar to $RuCl_2(bpy)(CO)_2$. With respect to the extended X-ray absorption fine structure (EXAFS;

Figure 2.6(b)), EXAFS oscillation (Figure 2.6(c)), and its Fourier transforms (Figure 2.6(d)), **1** and $RuCl_2(bpy)(CO)_2$ yielded almost the same spectra; therefore, the coordination structure of **1** was analyzed based on the crystallographic data for $RuCl_2(bpy)(CO)_2$.[18] Curve fitting for **1** indicated the presence of Ru–C 1.7±0.3 C atoms at 1.82 Å, Ru–N 1.9±0.4 N atoms at 2.18 Å, and Ru–Cl 1.8±0.2 Cl atoms at 2.42 Å. These results suggest that a similar structure to the corresponding homogeneous complex, $RuCl_2(bpy)(CO)_2$, is successfully formed on the surface of BPy-PMO. It should be noted that no peak corresponding to Ru–Ru was observed around 4 Å in Figure 2.6(b), which means that the Ru centers are isolated on BPy-PMO.

Based on these characterization data, the author proposes the structure of **1** in Figure 2.7, in which $RuCl_2(CO)_2$ is immobilized on BPy units of BPy-PMO. The well-defined and isolated Ru species on the pore walls are applicable for selective catalytic reactions.

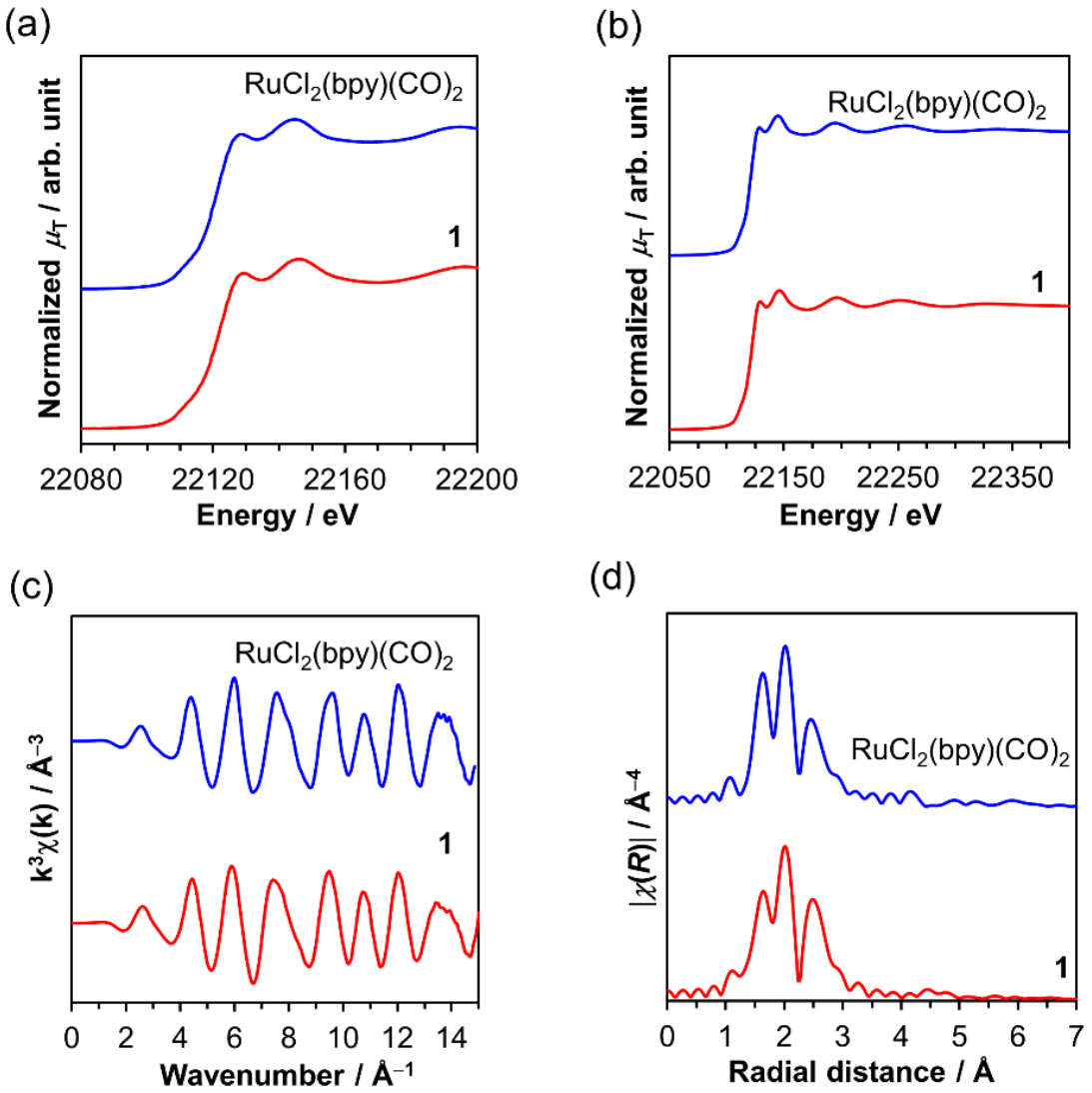

Figure 2.6. (a) Ru K-edge XANES, (b) Ru K-edge EXAFS spectra, (c) EXAFS oscillation, and (d) Fourier transforms of EXAFS spectra for **1** (red) and $RuCl_2(bpy)(CO)_2$ (blue).

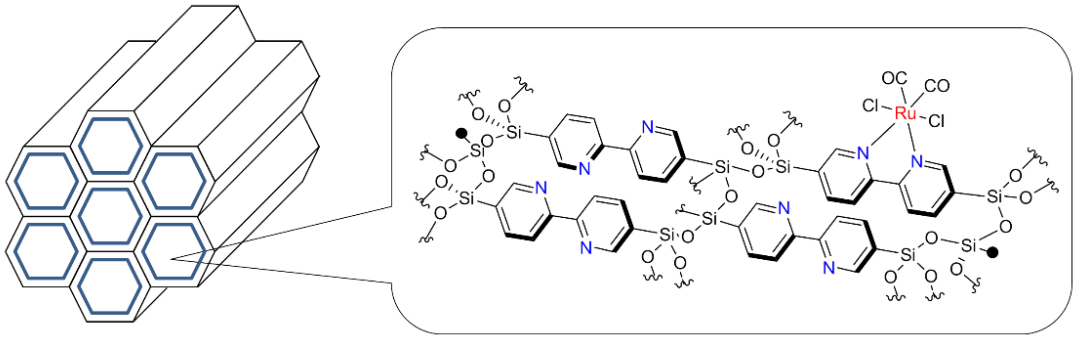

Figure 2.7. Proposed structure of **1**.

2.3.2. Oxidation reaction of alkanes

2.3.2.1. Oxidation of adamantane

Selective oxidation of alkanes is an important topic for the efficient utilization of petroleum oil and natural gas.[7-10] Adamantane was used as a model compound to evaluate the catalytic activity and selectivity for this type of oxidation (Scheme 2.3).[14] This highly symmetric alkane has four equivalent tertiary C–H and twelve equivalent secondary C–H bonds; therefore, the relative selectivity of the active species for tertiary and secondary groups (3°/2°) can be easily determined from Eq. 2.1. Furthermore, adamantane oxygenates are precursors for the production of photoresists, medicines, and engineering plastics.[14] Some homogeneous catalysts can selectively oxidize the tertiary or secondary C–H bonds of adamantine, such as $RuCl_3$ which has been commercially used for the synthesis of tertiary alcohols;[14,22-27] however, these homogeneous catalysts

have drawbacks such as complicated separation and decomposition of the catalysts. In addition, no solid catalyst has achieved good selectivity because of the presence of various catalytic active sites.[28-32] Therefore, the oxidation of adamantane was selected to evaluate the activity, selectivity, and reusability of the PMO-based catalysts.

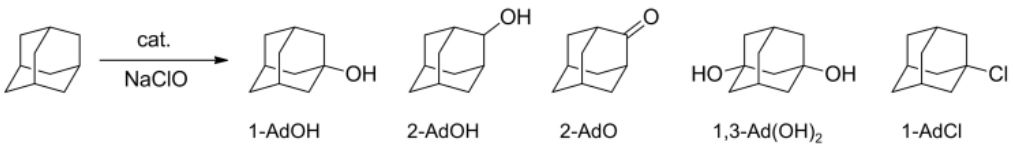

Scheme 2.3. Oxidation of adamantane with NaClO.

$$3^{\circ}/2^{\circ} = \frac{(\text{yield of 1-adamantanol})}{(\text{total yield of 2-adamantanol and 2-adamantanone})} \times \frac{12}{4} \qquad (2.1)$$

Ru-immobilized BPy-PMO catalysts were tested for the oxidation of adamantane (substrate/catalyst molar ratio S/C = 50) at 323 K with NaClO as a practical oxidant (Table 2.1). A control experiment in the absence of a catalyst gave negligible amounts of oxygenated products (entry 1). Ru-immobilized BPy-PMO **3** showed a very low adamantane conversion of 8.1%, as well as a 1-adamantanol yield of 4.3% (entry 5). **3** also afforded a significant amount of 1-chloroadamantane (1.9% yield), a typical byproduct in oxidation with NaClO. The new catalyst **1** provided a 67% conversion of

adamantane, and the major products were 1-adamantanol (44% yield), 1,3-adamantandiol (12 %; produced by successive oxidation of 1-adamantanol), and 2-adamantanone (2.3%) (entry 2). 2-Adamantanol was produced in less than 0.1% yield due to rapid consecutive oxidation to 2-adamantanone. It is notable that the amount of 1-chloroadamantane was as low as 0.2%. Ru-BPy-PMO catalyst **2**, grafting a commercial catalyst $RuCl_3$, gave a lower adamantane conversion of 43% with a 1-adamantanol yield of 31% (entry 4).[26] The author proposes that the Ru center in catalyst **1** easily forms coordination bonds with reactant molecules by releasing CO ligands, which results in high catalytic performance for the adamantine oxidation. After the reaction, the Ru centers in **1** are stabilized by the coordination of acetate in solution, and repeatedly available as active sites. In contrast, because of strong coordination of ligands with Ru center in the case of catalyst **2** and **3**, these catalysts show lower activity for the reaction than catalyst **1**. Thus, the author focused on the catalysis of **1**. For the reaction of **1** in entry 2, a turnover number of Ru for oxygenation was calculated to be 35, which indicates that **1** acts as a catalyst for the oxidation of adamantane. The 3°/2° ratio is 57, so that a tertiary C–H bond was oxidized 57 times faster than a secondary C–H bond. A time-course experiment showed that the 3°/2° ratio remained almost constant (Figure 2.8).

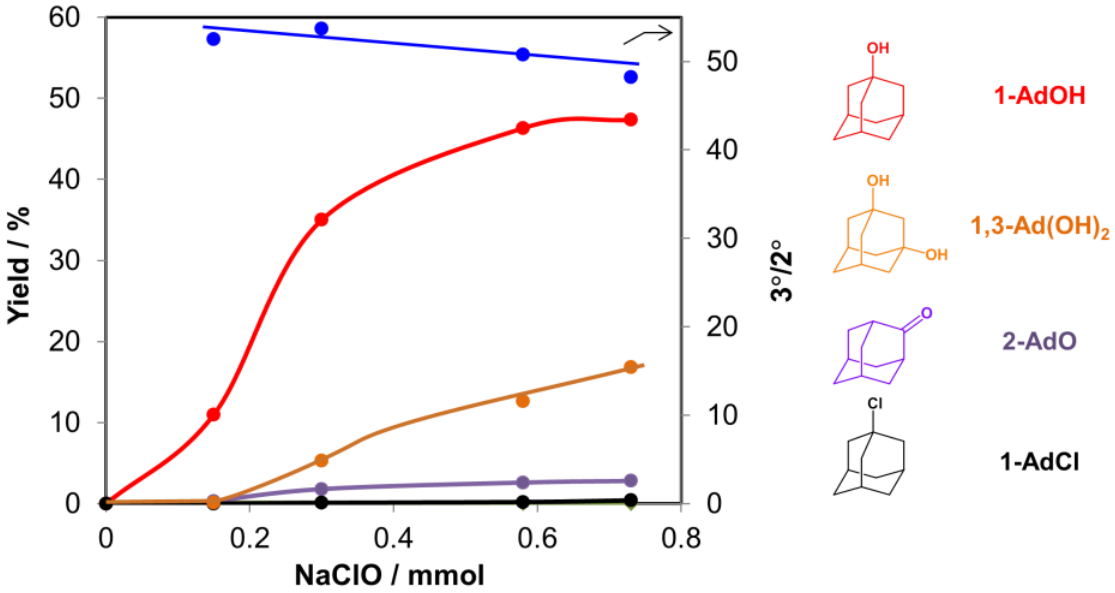

Figure 2.8. Time-course for the oxidation of adamantane over catalyst **1**.

This is the highest regioselectivity ever reported for a heterogeneous catalyst (2–20).[28-32] The result indicates that no radical chain reactions (3°/2° < 15)[33] occur and active electrophilic oxygen species are selectively formed on Ru sites.[8] Moreover, **1** maintained the catalytic activity and selectivity in a reuse experiment; the catalyst produced 1-adamantanol in 44% yield with a 3°/2° ratio of 53 (entry 3). The author has verified that the amount of Ru loading was maintained after the oxidation reaction in EDX measurements. $RuCl_2(bpy)(CO)_2$ was tested as a homogeneous model of **1**, which afforded 1-adamantanol (45% yield), 1,3-adamantandiol (12%), 2-adamantanol (0.8%), and 2-adamantanone (2.4%) (entry 6). Thus, **1** was as active as $RuCl_2(bpy)(CO)_2$, which suggests there is no diffusion limitation for **1** due to the large pores that allow quick

diffusion of the bulk substrate (adamantane, 0.7 nm diameter). The 3°/2° ratio for $RuCl_2(bpy)(CO)_2$ of 45 was slightly lower than that for **1** (57), and the homogeneous catalyst also produced a larger amount of 1-chloroadamantane (1.2%) than **1** (0.2%). Thus, **1** improved the product selectivity compared with the homogeneous counterpart, presumably due to the site-isolation of Ru species for **1**.

Table 2.1. Oxidation of adamantane by Ru catalysts with NaClO.[a]

Entry	Catalyst	Conversion (%)	Yield (%)					3°/2°[b]
			1-AdOH[c]	2-AdOH[c]	2-AdO[c]	1,3-Ad(OH)$_2$[c]	1-AdCl[c]	
1	None	0.3	0.0	0.0	0.0	0.0	0.0	-
2	1	67	44	0.0	2.3	12	0.2	57
3	1-reuse	68	44	0.0	2.5	11	0.2	53
4	2	43	31	0.0	1.7	5.9	0.1	55
5	3	8.1	4.3	0.4	1.0	0.0	1.9	9
6	$RuCl_2(bpy)(CO)_2$	77	45	0.8	2.4	12	1.2	45
7	4	41	25	0.0	1.4	4.4	1.4	54
8	4-reuse	6.1	1.9	1.2	0.1	0.0	0.0	5

[a] Reaction conditions: catalyst (10 mg), adamantane (0.23 mmol), ethylacetate (2.4 mL), and acetate buffer (0.39 mL, pH 4.4, 2 M), reaction temperature (323 K), time of aqueous solution of NaClO (19 mM) supplied at a rate of 27 μL h^{-1} (12 h). [b] 3°/2° = (yield of 1-adamantanol)/(yield of 2-adamantanol and 2-adamantanone)× 3 (see Eq. 1). [c] 1-AdOH (1-adamantanol), 2-AdOH (2-adamantanol), 2-AdO (2-adamantanone), 1,3-Ad(OH)$_2$ (1,3-adamantanediol), 1-AdCl (1-chloroadamantane).

The good durability of **1** could be ascribed to the rigid fixation of the Ru species on the pore wall. To provide evidence for this hypothesis, an analog of **1** was examined using MCM-41 bearing BPy groups via butyl group linkers (denoted **4**; Figure 2.9). MCM-41 is also an ordered mesoporous material with a similar pore diameter (3.4 nm, Figure 2.10) but consists of pure silica with an amorphous wall structure. Therefore, a linker is necessary to immobilize Ru and it provides mobile Ru sites. The immobilization of Ru complexes on MCM-41 was also confirmed by UV-vis DRS measurement (Figure 2.11).

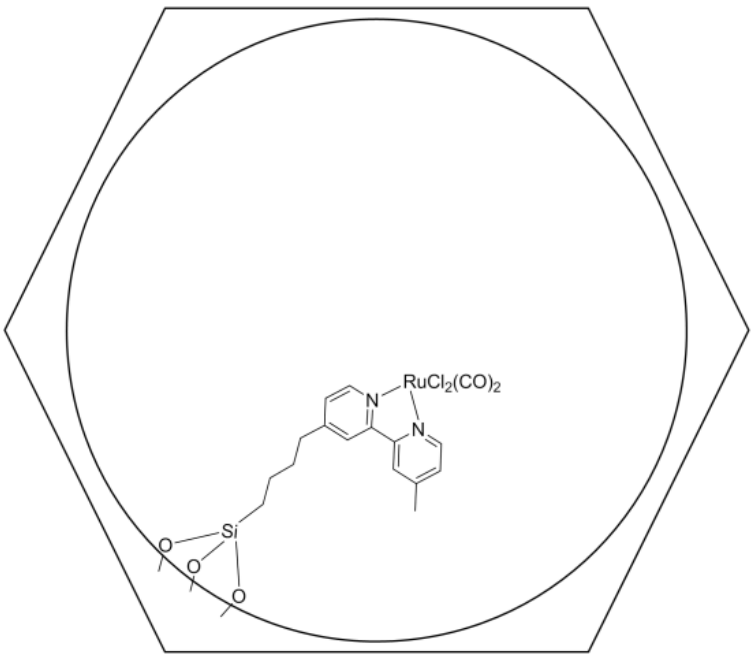

Figure 2.9. Schematic structure of **4**.

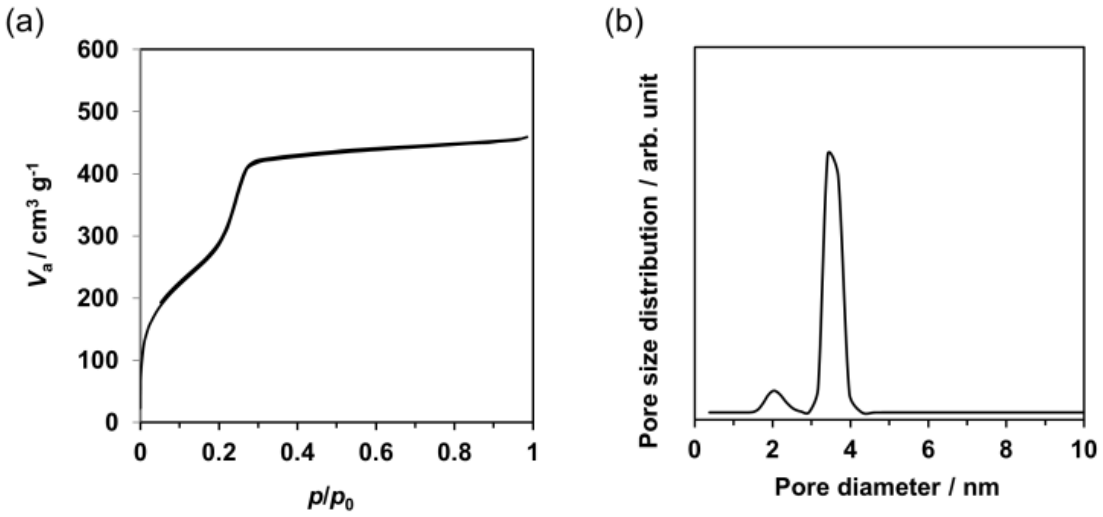

Figure 2.10. (a) N_2 adsorption isotherm and (b) NLDFT pore diameter distribution for MCM-41 bearing BPy groups at 77 K.

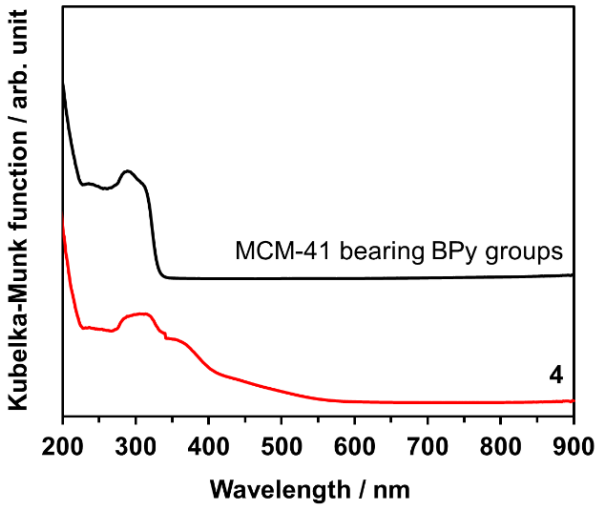

Figure 2.11. UV-vis DRS spectra of MCM-41 bearing BPy groups (black) and **4** (red).

Catalyst **4** showed a similar 3°/2° ratio (54, entry 7) to that for **1**. However, **4** had lower catalytic activity due to quick deactivation, which was clearly observed in the catalyst reuse experiment (almost no activity, entry 8). Compared the surface structure of

1 with that of 4 (Figure 2.12), the catalyst 4 was decomposed by its own active oxygen species due to high mobility of ligands (Figure 2.12(b)) and significant leaching of Ru was observed (82%). In contrast, no direct interaction among Ru complexes of Ru-BPy-PMO, due to incorporation of BPy ligands within silicate network (Figure 2.12(a)), can suppress the decomposition, thereby achieving better durability of the catalyst.

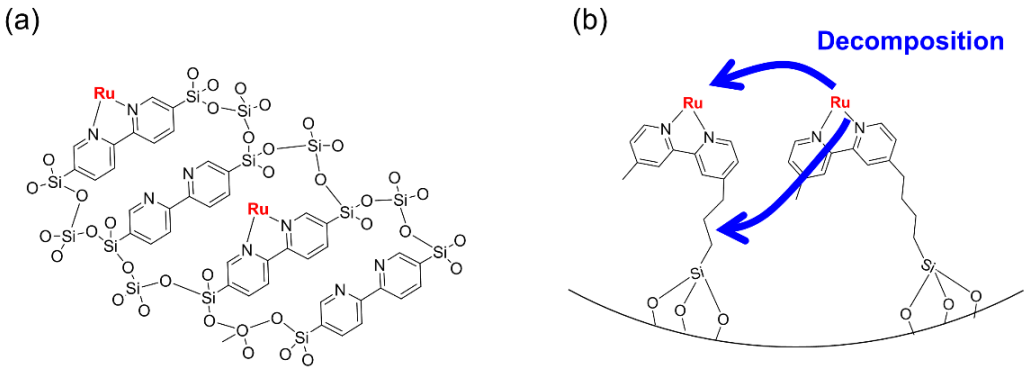

Figure 2.12. Surface structures of (a) catalyst **1** and (b) catalyst **4**.

2.3.2.2. Oxidation of *cis*-decaline

Catalyst **1** was then applied for the oxidation of *cis*-decalin to evaluate the stereospecificity of the catalytic system (Scheme 2.4), because stereospecific oxidation is important for the synthesis of fine chemicals and medicines such as steroids and terpenes.[10,17]

Scheme 2.4. Oxidation of *cis*-decalin by **1** with NaClO.

The reaction was performed under the same conditions as that for the oxidation of adamantane. **1** gave a 70% conversion of *cis*-decalin and a 63% yield of *cis*-9-decalol with complete retention of the substrate configuration (Figure 2.13). Thus, no *trans*-9-decalol was detected (<0.1%) and the only byproducts were secondary oxygenates such as *cis*-1-decalone. This result indicates that Ru catalyst **1** directly inserts an oxygen atom into a C–H bond with no free radical reaction (Scheme 2.5), which gives a mixture of *cis*-9-decalol and *trans*-9-decalol via sp^2 carbon radical intermediates.[15,34]

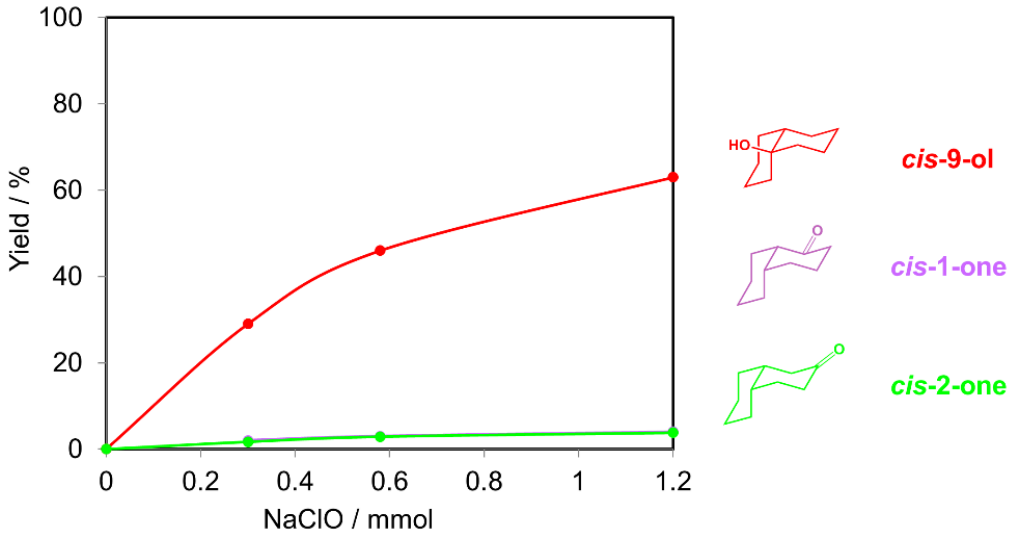

Figure 2.13. Time-course for the oxidation of *cis*-decalin over catalyst **1**.

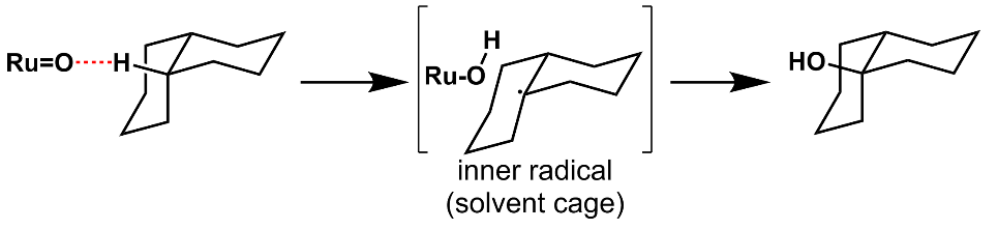

Scheme 2.5. Retention of configuration in oxidation of *cis*-decalin.

Moreover, the activity of the reuse catalyst was compared with that of the fresh catalyst at 50% conversion of *cis*-decaline (Figure 2.14). Catalyst **1** was reusable and maintained the activity and selectivity for the stereospecific oxidation of tertiary C–H bonds. The direct insertion of oxygen is also important for good durability, because free radicals would randomly attack the catalyst in addition to the substrate.

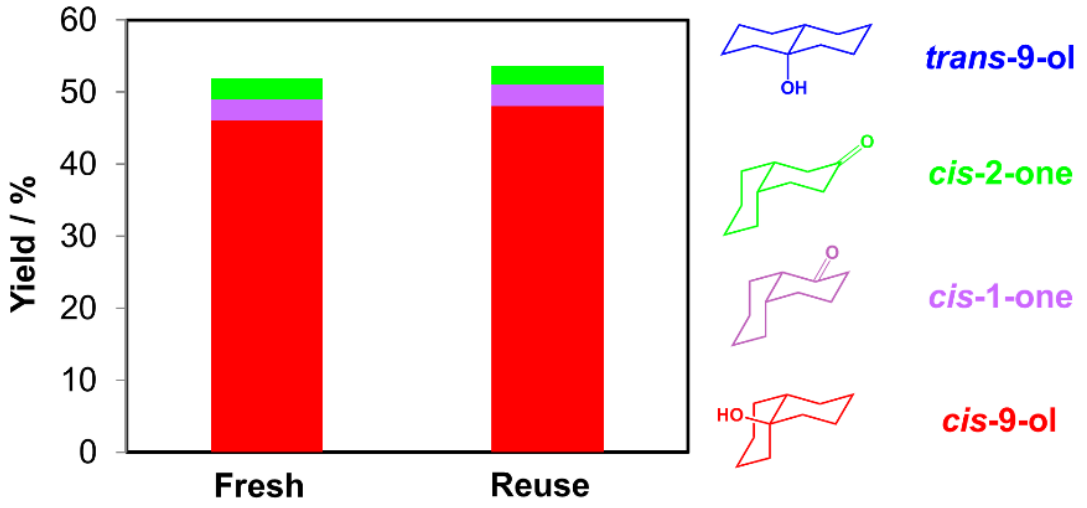

Figure 2.14. Reuse tests with catalyst **1** for the oxidation reaction of *cis*-decalin. Reaction conditions: catalyst (10 mg), adamantane (0.23 mmol), ethylacetate (2.4 mL), and acetate buffer (0.39 mL, pH 4.4, 2), reaction temperature (323 K), time of aqueous solution of NaClO (19 mM) supplied at a rate of 27 μL h^{-1} (12 h). Denotation: *cis*-9-ol (*cis*-9-decalol), *cis*-1-one (*cis*-1-decalone), *cis*-2-one (*cis*-2-decalone), *trans*-9-ol (*trans*-9-decalol).

2.3.2.3. Oxidation of tertiary C-H bonds in various alkanes

Finally, catalyst **1** was also tested in the oxidation of tertiary C-H bond in various alkanes to confirm potential applicability of the catalytic system (Table 2.2). The reaction was performed under the same conditions as that for the oxidation of adamantane. Although decalin with trans conformation has two tertiary C-H bonds with larger steric hindrance than that with cis conformation, catalyst **1** was able to oxidize one of them more preferably than secondary C-H bonds without change of its original trans configuration (Entry 1). Because of similar molecular structure to *cis*-decaline, Oxidation

of *cis*-1,2-dimethylcyclohexane was also examined. Catalyst **1** gave 60% conversion with 94% selectivity of the oxygenated compound that was formed by the oxidation of a tertiary C-H bond in *cis*-1,2-dimethylcyclohexane. In this case, substrate configuration was also preserved completely after oxidation reaction (Entry 2). Cis-1-isopropyl-4-methylcyclohexane was selected as a unique substrate to examine the effect of steric hindrance of tertiary C-H bonds (Entry 3). Despite three kinds of tertiary C-H bonds presented in this substrate, oxidation of the tertiary C_4-H bond was dominant, possibly due to small steric hindrance. Finally, catalyst **1** was applied to the oxidation of 2-methylnonane, one of a linear alkane (Entry 4). Tertiary C-H bonds in linear alkanes generally show lower reactivity to catalytic oxidation than those in cyclic alkanes. Regardless of moderate conversion (22%) in comparison with other cyclic alkanes, 2-methylnonane was also oxidized to the corresponding alcohol by oxidation of the tertiary C-H bond. Hence, this catalytic system can be applicable for wide varieties of linear and cyclic alkanes to the oxidation of their tertiary C-H bonds.

Table 2.2. Oxidation of various alkanes by catalyst **1** in the presence of NaClO.[a]

Entry	Conversion (%)	Products selectivity (%)		
1	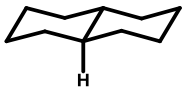	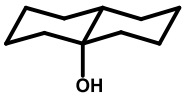	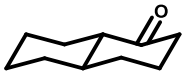	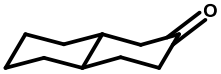
	20	31	21	25
2	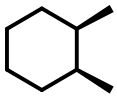	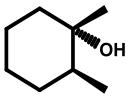	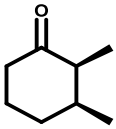	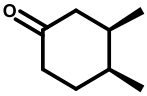
	60	94	3	3
3	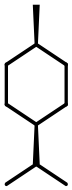	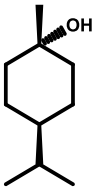	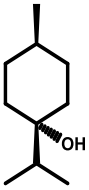	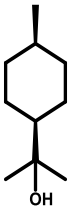
	56	67	15	16
4	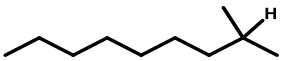	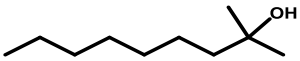		
	22	>99		

[a] Reaction conditions: catalyst (10 mg), alkanes (0.23 mmol), ethylacetate (2.4 mL), and acetate buffer (0.39 mL, pH 4.4, 2 M), reaction temperature (323 K), time of aqueous solution of NaClO (19 mM) supplied at a rate of 27 μL h^{-1} (12 h).

2.4. Conclusions

Ru species were immobilized in an isolated form directly on 2,2'-bypyridine groups in the BPy-PMO framework. The coordination structure of the immobilized Ru species was similar to that of the corresponding Ru complex, $RuCl_2(bpy)(CO)_2$. The Ru-immobilized PMO was applied for the catalytic oxidation of adamantane using NaClO as an oxidant and high selectivity toward the oxidation of tertiary C–H bonds was observed in addition to catalyst recyclability. Ru-immobilized PMO also selectively oxidized tertiary C–H bonds of *cis*-decalin with perfect retention of its configuration. From these results, the author propose that the rigid structure of Ru sites is essentially beneficial to achieve good durability. Furthermore, catalytically controlled oxidation, due to the well-designed isolated metallic sites, emphasizes the potential of the structural advantage.

References

[1] S. Inagaki, S. Guan, T. Ohsuna, O. Terasaki, *Nature* **2002**, *416*, 304-307.

[2] N. Mizoshita, T. Tani, S. Inagaki, *Chem. Soc. Rev.* **2011**, *40*, 789-800.

[3] X. Wang, D. Lu, R. Austin, A. Agarwal, L. J. Mueller, Z. Liu, J. Wu, P. Feng, *Langmuir* **2007**, *23*, 5735-5739.

[4] S. Inagaki, O. Ohtani, Y. Goto, K. Okamoto, M. Ikai, K. Yamanaka, T. Tani, T.

Okada, *Angew. Chem.* **2009**, *121*, 4102-4106; *Angew. Chem. Int. Ed.* **2009**, *48*, 4042-4046.

[5] H. Takeda, M. Ohashi, T. Tani, O. Ishitani, S. Inagaki, *Inorg. Chem.* **2010**, *49*, 4554-4559.

[6] M. Waki, Y. Maegawa, K. Hara, Y. Goto, S. Shirai, Y. Yamada, N. Mizoshita, T. Tani, W. J. Chun, S. Muratsugu, M. Tada, A. Fukuoka, S. Inagaki, *J. Am. Chem. Soc.* **2014**, *136*, 4003-4011.

[7] R. Schlögl, In *Modern Heterogeneous Oxidation Catalysis: Design, Reactions and Characterization* (Ed.: N. Mizuno), Wiley-VCH: Weinheim **2009**, pp. 1-42.

[8] A. Gunay, K. H. Theopold, *Chem. Rev.* **2010**, *110*, 1060-1081.

[9] J. Yamaguchi, K. Itami, A. D. Yamaguchi, *Angew. Chem. Int. Ed.* **2012**, *51*, 8960-9009.

[10] M. C. White, *Science* **2012**, *335*, 807-809.

[11] M. Costas, *Coord. Chem. Rev.* **2011**, *255*, 2912-2932.

[12] B. Meunier, S. P. de Visser, S. Shaik, *Chem. Rev.* **2004**, *104*, 3947-3980.

[13] A. Taguchi, F. Schüth, *Micropor. Macropor. Mater.* **2005**, *77*, 1-45.

[14] K. Chen, L. Jr. Que, *J. Am. Chem. Soc.* **2001**, *123*, 6327-6337.

[15] B. Mortini, *C. R. Phys.* **2006**, *7*, 924-930.

[16] A. A. Spasov, T. V. Khamidova, L. I. Bugaeva, I. S. Morozov, *Pharm. Chem. J.* **2000**, *34*, 1-7.

[17] K. Chen, P. S. Baran, *Nature* **2009**, *459*, 824-828.

[18] M. Haukka, J. Kiviaho, M. Ahlgrén, T. A. Pakkanen, *Organometallics* **1995**, *14*, 825-833.

[19] S. J. Carrington, I. Chakraborty, J.R. Alvarado, P. K. Mascharak, *Inorg. Chim. Acta* **2013**, *407*, 121-125.

[20] A. Gabrielsson, S. Zalis, P. Matousek, M. Towrie, A. Vlcek Jr, *Inorg. Chem*. **2004**, *43*, 7380-7388.

[21] E. Eskelinen, M. Haukka, T. Venalainen, T. A. Pakkanen, M. Wasberg, S. C.-Noblat, A. Deronzier, *Organometallics* **2000**, *19*, 163-169.

[22] I. Tabushi, A. Yazaki, *J. Am. Chem. Soc.* **1981**, *103*, 7371-7373.

[23] J. T. Groves, T. E. Nemo, *J. Am. Chem. Soc.* **1983**, *105*, 6243-6248.

[24] I. Yamanaka, T. Gomi, T. Nabeta, K. Otsuka, *Chem. Lett.* **2005**, *34*, 1486-1487.

[25] E. McNeil, J. Du Bois, *J. Am. Chem. Soc.* **2010**, *132*, 10202-10204.

[26] Y. Arai, T. Onozawa, S. Niiyama, K. Yoshida, *JP Pat.* **2008**, 4 171 879.

[27] Y. Ishii, T. Iwahama, S. Sakaguchi, K. Nakayama, Y. Nishiyama, *J. Org. Chem*. **1996**, *61*, 4520-4526.

[28] I. L. Viana Rosa, C. M. C. P. Manso, O. A. Serra, Y. Iamamoto, *J. Mol. Catal. A: Chem.* **2000**, *160*, 199-208.

[29] C. Nozaki, C. G. Lugmair, A. T. Bell, T. D. Tilley, *J. Am. Chem. Soc.* **2002**, *124*, 13194-13203.

[30] A. W. Holland, G. Li, A. M. Shahin, G. J. Long, A. T. Bell, T. D. Tilley, *J. Catal.* **2005**, *235*, 150-163.

[31] A. Dhakshinamoorthy, M. Alvaro, H. Garcia, *J. Catal.* **2009**, *267*, 1-4.

[32] S. Ikurumi, S. Okada, K. Nakatsuka, T. Kamegawa, K. Mori, H. Yamashita, *J. Phys. Chem. C* **2014**, *118*, 575-581.

[33] G. Süss-Fink, L. Gonzalez, G. B. Shul'pin, *Appl. Catal. A* **2001**, *217*, 111-117.

[34] H. Kobayashi, I. Yamanaka, *J. Mol. Catal. A: Chem.* **2008**, *294*, 37-42.

Chapter 3. Synthesis and characterization of gold nanoparticles immobilized on BPy-PMO

Abstract

Silica-supported gold nanoparticles (AuNPs) can be synthesized on a bipyridine-incorporated periodic mesoporous organosilica (BPy-PMO) as an inorganic support. Reaction of a bipyridine group in the periodic mesoporous organosilica with $HAuCl_4$ forms an $AuCl_2$-based complex, and its structure corresponds to a homogeneous complex, $[AuCl_2(bpy)]Cl$. Thermal reduction of the complex in H_2 results in the formation of small gold nanoparticles with an average size of ca. 3.8 nm. Combined with nitrogen adsorption, XRD, UV/Vis, TEM and XAFS measurements, it is demonstrated that uniform gold nanoparticles are homogeneously distributed inside mesopores. The size of gold nanoparticles is controlled by the size of mesopores. The size and distribution of gold nanoparticles is mainly controlled by strong interaction of surface metallic Au with pore walls of the periodic mesoporous organosilica. AuNPs/BPy-PMO shows higher catalytic activity than Au/MCM-41 in aerobic oxidation of benzaldehyde.

3.1. Introduction

Gold nanoparticles (AuNPs) have been widely studied as a promising material for catalysis, electronic and photonic device, and drug delivery system.[1-7] Despite bulk Au metal has no functionality for catalysis, gold particles in nanometer-scale show very unique activity for a variety of reactions, which is represented by low temperature oxidation of CO with O_2.[8,9] Because catalytic performance of AuNPs strongly depends on their particle size, Haruta et al. developed an effective technique, denoted deposition precipitation method, to form highly dispersed AuNPs on various metal oxide supports.[8,10] This method is solely based on impregnation of preformed $Au(OH)_3$ with inorganic supports, and it is able to control the size of resultant AuNPs by optimization of pH in solution containing $HAuCl_4$ precursor. In contrast, direct impregnation of ionic gold precursors on inorganic supports and subsequent reduction to form AuNPs is not simply accomplished by a conventional combination of evaporation and reduction techniques, owing to low affinity of Au with the supports resulting in the formation of large Au particles. A variety of methods were reported for the preparation of supported AuNPs catalysts such as coprecipitation,[11] photochemical synthesis,[12] solid-solid reaction of a gold complex with the supports,[13] liquid-phase reduction,[14,15] and impregnation of AuNPs stabilized with sulfur or phosphorus-containing organic

compounds and polymers.[16-18] Fe_2O_3 and TiO_2 are useful supports for the preparation of well-defined AuNPs in their sizes; however, silicas with high surface area, which are widely used as supports for organic functional groups and novel metals, are not applicable as host materials due to difficulties in controlling the size below 6 nm.

Periodic mesoporous organosilicas (PMOs) are unique mesoporous materials that consist of crystal-like ordered arrays of organic moieties bridged by siloxane bonds.[19,20] Introduction of organic groups into PMOs can lead to various chemical and physical properties.[21-23] Recently, a PMO with 2,2'-bipyridyl (BPy) groups has been synthesized from bridged precursor, 5,5'-bis(triisopropoxysilyl)-2,2'-bipyridine, in the presence of a structure-directing agent. 2,2'-Bipyridyl group incorporated into siloxane network is a versatile ligand and readily available as a chelating unit for the formation of Ir, Ru, Re, and Pd complexes.[24-26] Herein, the author reports a novel strategy for the immobilization of AuNPs on BPy-PMO through the formation of Au complex with surface BPy moiety and subsequent thermal reduction. First, an Au complex was formed by the treatment of BPy-PMO with $HAuCl_4 \cdot 4H_2O$ in ethanol. These complexes were easily transformed to AuNPs by a simple reduction with thermal treatment of the Au complex-stabilized BPy-PMO with H_2. Results of characterization and catalysis of AuNPs/BPy-PMO are also presented.

3.2. Experimental

3.2.1. Reagents

$HAuCl_4 \cdot 4H_2O$ was purchased from Wako Pure Chemical Industries, Ltd. Other reagents were obtained with the highest grade and used without further purification.

3.2.2. Synthesis of BPy-PMO supported AuNPs

BPy-PMO was synthesized using 5,5'-bis(triisopropoxysilyl)-2,2'-bipyridine as a bridged silica precursor and octadecyltrimethylammonium chloride as a surfactant.[24] An Au complex immobilized BPy-PMO, denoted $AuCl_3$-BPy-PMO, was prepared from BPy-PMO and $HAuCl_4 \cdot 4H_2O$ as follows: a 100 mg of BPy-PMO was added to a mixture of EtOH (30 mL) and $HAuCl_4 \cdot 4H_2O$ (100 mg, 0.50 mmol) under an Ar atmosphere. After stirring the mixture under reflux condition for 6 h, the resulting solid was filtered, washed with excess amounts of EtOH, and dried at 298 K in vacuo to afford $AuCl_3$-BPy-PMO (110 mg) as a pale yellow powder. The solid was conducted with thermal reduction in H_2 at 423 K for 1 h to give BPy-PMO-supported AuNPs which is denoted AuNPs/BPy-PMO. For comparison, an MCM-41-supported AuNPs was prepared by a conventional impregnation method using $HAuCl_4 \cdot 4H_2O$. After immobilization of Au species on MCM-41 by vacuum evaporation at 298 K, the dried sample was also reduced in H_2 at 423 K

for 1 h to obtain MCM-41-supported AuNPs (Au/MCM-41). A model complex for $AuCl_3$-BPy-PMO, $[AuCl_2(bpy)]Cl$, was synthesized according to a procedure in the literature[27] and purified by recrystallization.

3.2.3. Characterization of BPy-PMO supported AuNPs

The samples were characterized using UV/Vis diffuse reflectance spectroscopy (UV/Vis DRS; Jasco, V-650), X-ray fluorescence spectroscopy (XRF, Shimadzu EDX-720), nitrogen adsorption (MicrotracBEL Belsorp-mini II), X-ray diffraction (XRD, Rigaku Ultima IV, Cu Kα), transmission electron microscopy (TEM, JEOL JEM-2100F, 200 kV), and X-ray absorption fine structure (XAFS; at the BL14B2 of SPring-8).

3.2.4. Oxidation of benzaldehyde with supported AuNPs

A mixture of benzaldehyde (11 mg, 0.1 mmol), catalyst (10 mg), $NaHCO_3$ (17 mg, 0.2 mmol), and distilled water (5.0 mL) were placed into a Pyrex vial (20 mL) and stirred at 303 K for 2 h with bubbling of oxygen gas at a flow rate of 10 mL min^{-1}. After the reaction, the mixture was analyzed using gas chromatography (GC; Shimadzu GC-14B, flame ionization detector) with an HR-20m (0.25 mm diameter, 30 m long) column. Naphthalene was used as an internal standard in this experiment.

3.3. Results and discussion

3.3.1. Synthesis of Au complex on BPy-PMO

The formation of gold complexes by thermal treatment of BPy-PMO with $HAuCl_4 \cdot 4H_2O$ in ethanol (Scheme 3.1) were confirmed by Au L_3-edge XAFS measurement, which provides information on the electronic state and structure of Au species stabilized on the support. In the X-ray absorption near-edge structure (XANES) in Figure. 3.1(a), the edge energy of Au species on $AuCl_3$-BPy-PMO appeared at 11917 eV which corresponds to a trivalent Au species. Because $AuCl_3$-BPy-PMO and $[AuCl_2(bpy)]Cl$ show almost the same spectra, electronic structure of Au atoms in $AuCl_3$-BPy-PMO is the same as that of trivalent Au species in $[AuCl_2(bpy)]Cl$. This trend was also observed for extended X-ray absorption fine structure (EXAFS) oscillation (Figure 3.1(b)) and Fourier transforms of EXAFS (Figure 3.1(c)): $AuCl_3$-BPy-PMO gave almost the same spectrum as $[AuCl_2(bpy)]Cl$. These results show that a similar structure to that of the corresponding homogeneous complex, $[AuCl_2(bpy)]Cl$, is successfully formed on the surface of BPy-PMO via a BPy group as a chelating unit as shown in Figure 3.1(d).

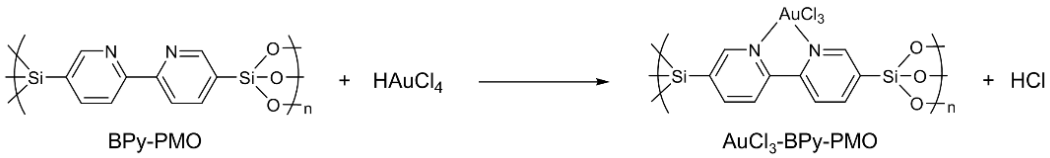

Scheme 3.1. Formation of Au complex on BPy-PMO.

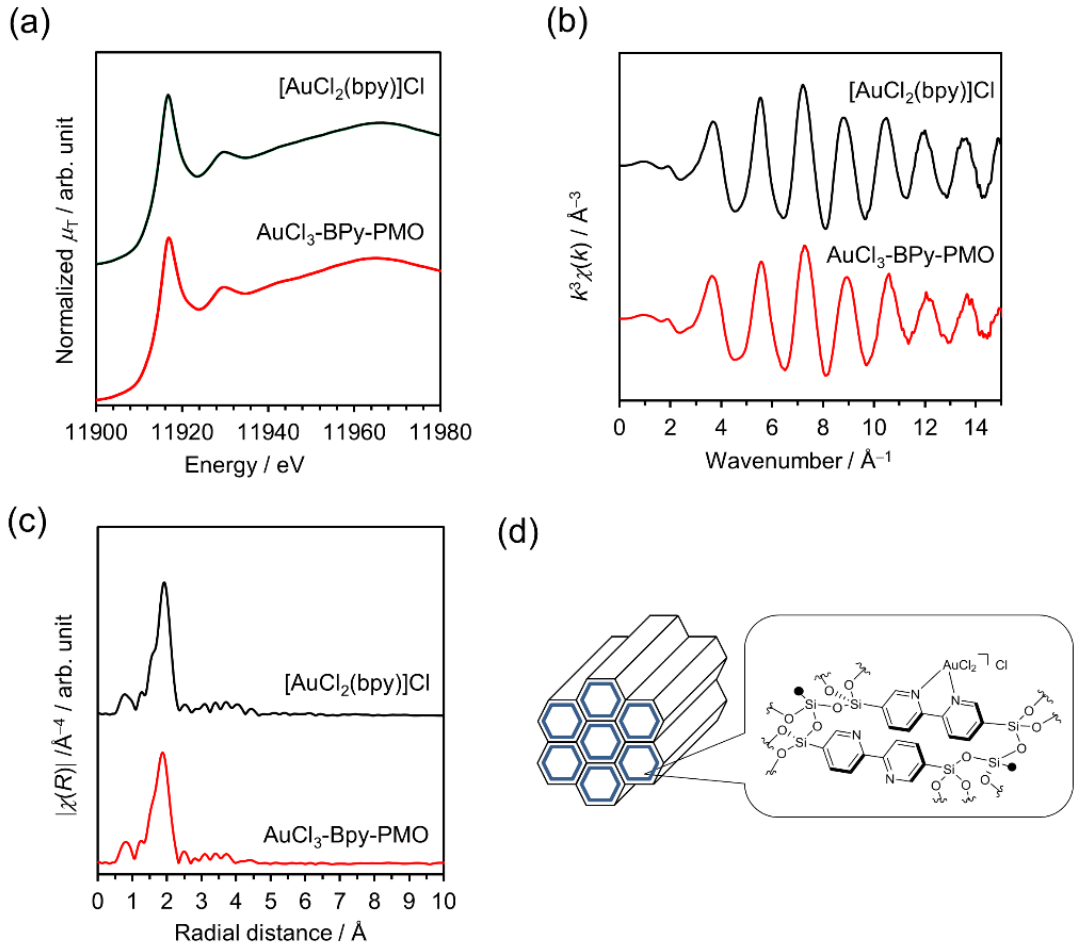

Figure 3.1. (a) Au L_3-edge XANES, (b) EXAFS oscillation, and (c) Fourier transforms of EXAFS spectra for $AuCl_3$-BPy-PMO (red line) and $[AuCl_2(bpy)]Cl$ (black line). (d) Proposed structure of $AuCl_3$-BPy-PMO.

3.3.2. Formation of Au nanoparticles on BPy-PMO

The author attempted thermal reduction of $AuCl_3$-BPy-PMO at 423 K in H_2 to obtain BPy-PMO-supported AuNPs. Figure 3.2 shows N_2 adsorption-desorption isotherms and non-linear DFT (NLDFT) pore size distribution curves of bare BPy-PMO and AuNPs/BPy-PMO. Both bare BPy-PMO and AuNPs/BPy-PMO have type-IV isotherms with no pronounced hysteresis loops, and this result is typical of mesoporous materials with small-sized mesopores (Figure 3.2(a)).[28] NLDFT calculation with the isotherms provides pore size distribution curves of these samples, which reveals the presence of uniform mesopores of about 4.4 nm in diameter (Figure 3.2(b)). While Brunauer–Emmett–Teller (BET) surface area slightly decreased from 670 to 620 m^2 g^{-1}, it is apparent that original mesoporosity of BPy-PMO retained intact after the formation of Au complex and subsequent H_2 reduction. Figure 3.3 shows XRD patterns of bare BPy-PMO and AuNPs/BPy-PMO in (a) low and (b) high-angle regions. There is one intense diffraction at $2\theta = 1.69$ that can be assigned to (100) plane of *p6mm* symmetry for mesoporous arrangement. Despite the presence of some diffractions due to periodic structure of BPy units in high-angle region, there are no signals of Au metal, suggesting the formation of small nanoparticles undetectable by XRD measurement. The amount of Au loaded on BPy-PMO was estimated to be 1.1 wt% by EDX analysis.

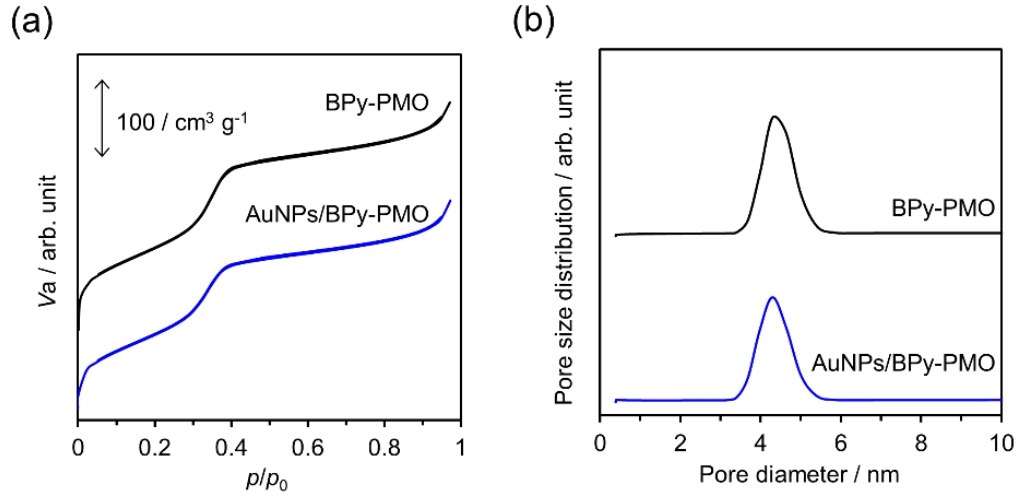

Figure 3.2. (a) N_2 adsorption isotherms and (b) NLDFT pore diameter distribution curves of BPy-PMO (black line) and AuNPs/BPy-PMO (blue line).

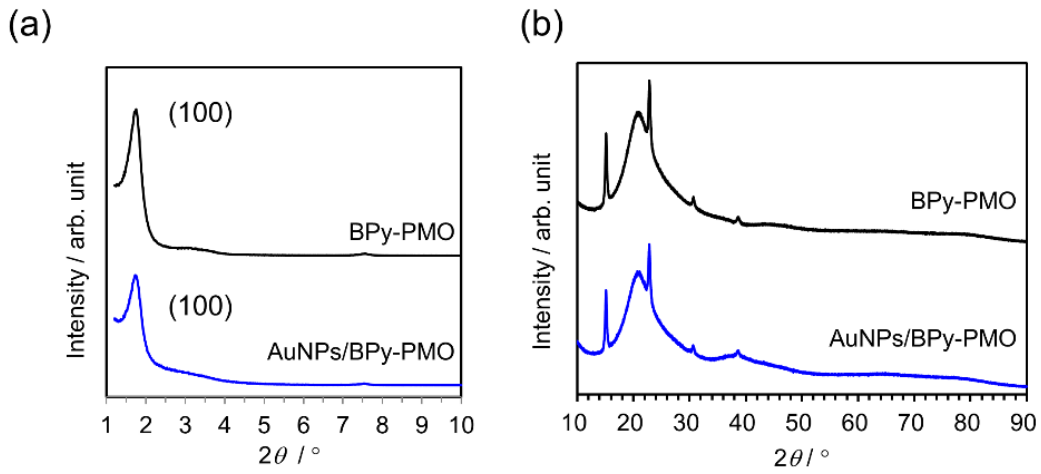

Figure 3.3. XRD patterns of BPy-PMO (black line) and AuNPs/BPy-PMO (blue line) in (a) low and (b) high-angle region.

As a control experiment, an MCM-41-supported Au particle with the same Au loading was prepared by an impregnation method. Bare and Au-loaded MCM-41s were also characterized by N_2 adsorption measurement and XRD (Figure 3.4). There is no significant difference in N_2 adsorption-desorption isotherms (Figure 3.4(a)): BET surface area and NLDFT pore diameter of bare MCM-41 are 760 m^2 g^{-1} and 4.5 nm, and those of Au-loaded MCM-41 are 750 m^2 g^{-1} and 4.3 nm. In contrast, new sharp diffractions are clearly observed in high-angle region of XRD pattern after gold metal formation (Figure 3.4(b)). They are assigned to (111), (200), (220), (311), and (222) planes on the basis of the fcc structure of gold metal. The crystallite size was determined by the Debye-Scherrer's equation for the (111) diffraction to be about 38 nm. Aggregation of small AuNPs formed inside mesopores preferably occurred to form large-sized AuNPs on the outer surface of MCM-41 particles even though Au cations were homogeneously immobilized on the silica surface before thermal reduction. This phenomenon can be induced by weak interaction of AuNPs with silica surface. It should be noted that these large Au particles are not formed on BPy-PMO.

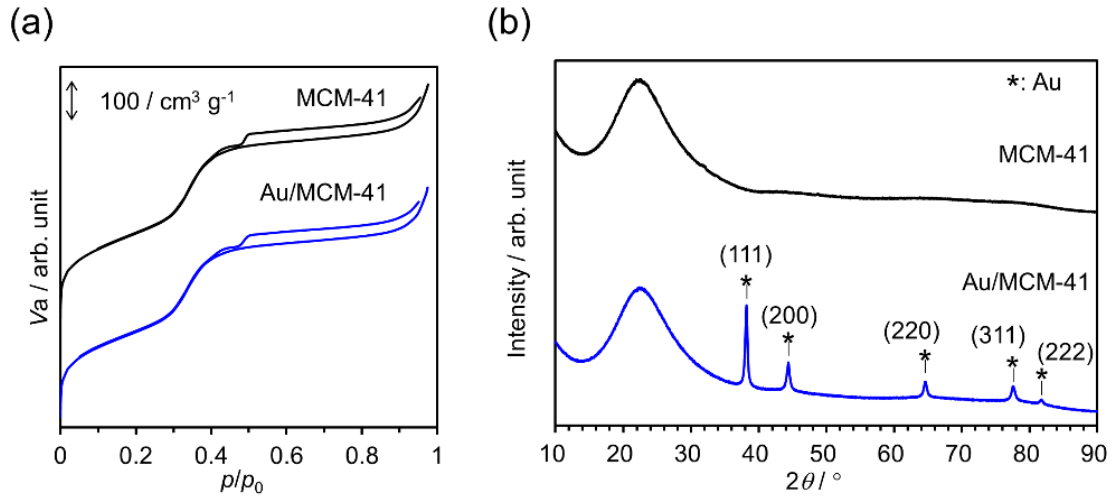

Figure 3.4. (a) N_2 adsorption isotherms and (b) XRD patterns of bare (black line) and Au-loaded MCM-41 (blue line).

The formation of AuNPs on BPy-PMO was evaluated in more details by UV/Vis DRS and TEM measurements (Figure 3.5). Plasmon absorption peak derived from AuNPs appeared around 530 nm in AuNPs/BPy-PMO (Figure 3.5(a)). A TEM image of AuNPs/BPy-PMO gives direct information for AuNPs formation with an average size of ca. 3.8 nm (Figure 3.5(b)) and their homogeneous distribution inside and outside of mesopores. Some large AuNPs in size of 6-8 nm are simultaneously observed on external surface in Figure 3.5(b). AuNPs formed inside mesopores of BPy-PMO are highly stabilized with strong interaction between metallic Au and pore wall of BPy-PMO, which restricts formation of large-sized AuNPs typically observed for MCM-41 as shown above. In addition, mesopores effectively prevent growing the size of AuNPs below the poresize

(4.4 nm). Thus, immobilization of AuNPs via the formation of gold complexes and subsequent H_2 reduction is definitely a simple and promising method to synthesize supported AuNPs on BPy-based PMO support in comparison with a conventional impregnation method.

Au L_3-edge XAFS measurement was conducted for the evaluation of Au species of AuNPs/BPy-PMO. Figures 3.6(a) and 3.6(b) show XANES and Fourier transforms of EXAFS spectra of AuNPs/BPy-PMO and Au foil. These samples give similar edge energy (11919 eV), and EXAFS spectrum of AuNPs/BPy-PMO bears a great resemblance to that of Au foil, which indicates complete reduction of Au complex on BPy-PMO and simultaneous formation of AuNPs. Weak and broad signals for metallic Au and the absence of small signals in the range of 4-7 Å can be confirmed in the EXAFS spectrum of AuNPs/BPy-PMO. These features are characteristic of small AuNPs.[29,30]

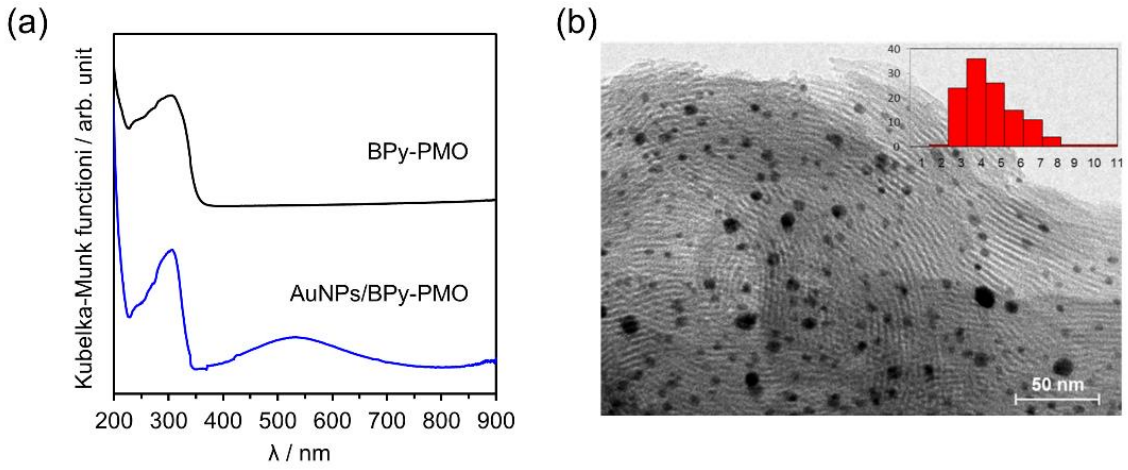

Figure 3.5. (a) UV/Vis DRS spectra of bare and AuNPs/BPy-PMO and (b) TEM image of AuNPs/BPy-PMO.

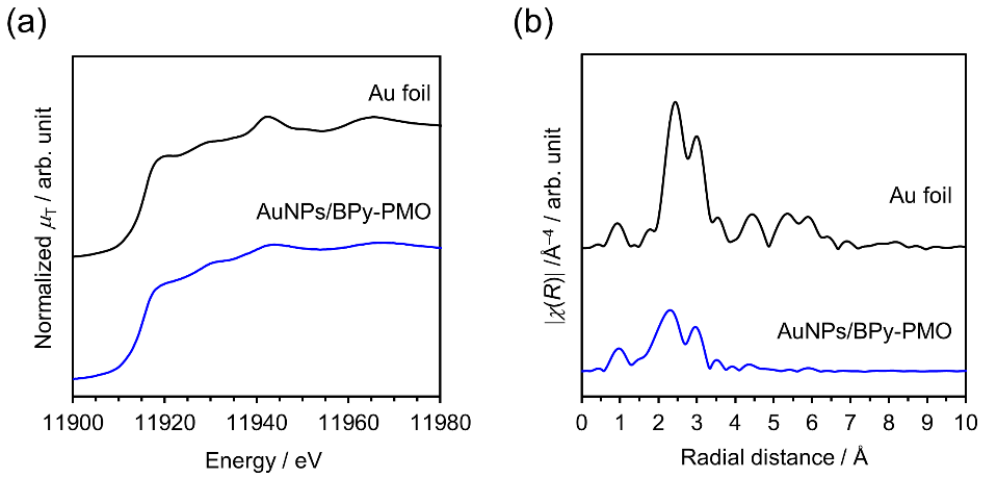

Figure 3.6. (a) Au L_3-edge XANES and (b) Fourier transforms of EXAFS spectra for AuNPs/BPy-PMO (blue line) and Au foil (black line).

Finally, catalytic activity of the supported gold catalysts was examined using a test reaction, aerobic oxidation of benzaldehyde in water at 303 K (Figure 3.7). Au/MCM-41 oxidized benzaldehyde to benzoic acid, giving 39% conversion and 22% yield toward

benzoic acid. With the same Au loading, AuNPs/BPy-PMO afforded 91% conversion and 87% yield under the same conditions; yield of benzoic acid for AuNPs/BPy-PMO was approximately four times that for Au/MCM-41. Such a high activity can be ascribed to small Au nanoparticle on BPy-PMOs, which is frequently observed for catalytic reactions by supported Au nanoparticles.[5,8] The formation of small Au nanoparticles on BPy-PMO is potentially an effective strategy for the development of a highly active heterogeneous catalyst for various aerobic oxidation reactions.

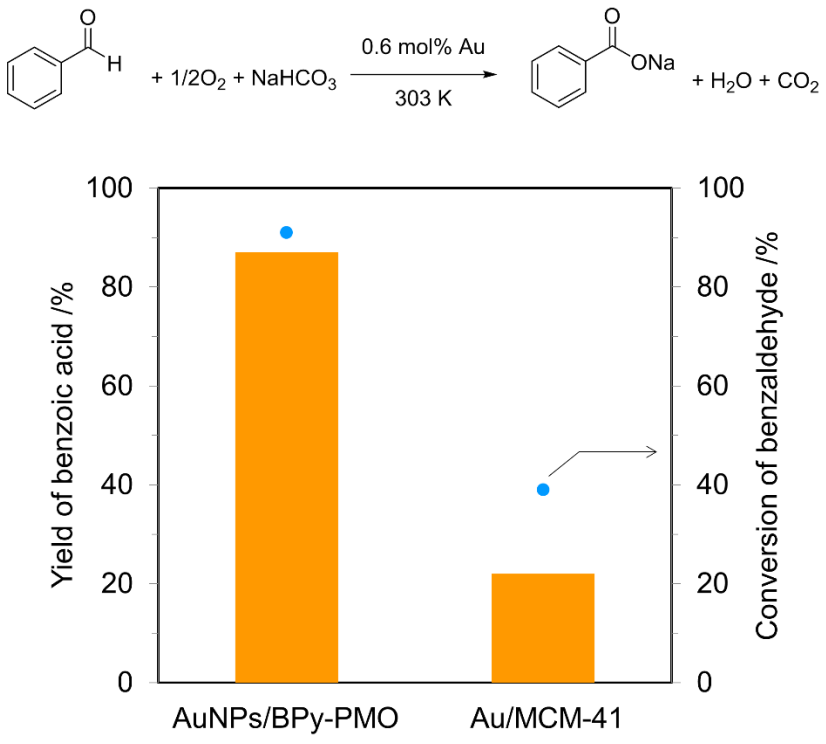

Figure 3.7. Aerobic oxidation of benzaldehyde in water with supported Au catalysts.

3.4. Conclusions

Complex formation and subsequent reduction is an effective method for the formation of small AuNPs with homogeneous distribution on 2,2'-bipyridine-based PMO material. Average diameter of AuNPs is estimated to be ca. 3.8 nm, which is much smaller than those formed on silica supports reported in the previous literatures. Mesoporous structure is one important factor controlling the size of AuNPs smaller than that of mesopores. AuNPs/BPy-PMO shows higher catalytic activity than Au/MCM-41 in oxidation of benzaldehyde. This methodology is believed to be useful for the synthesis of silica-supported AuNPs.

References

[1] M.-C. Daniel, D. Astruc, *Chem. Rev.* **2004**, *104*, 293-346.

[2] M. Turner, V. B. Golovko, O. P. H. Vaughan, P. Abdulkin, A. B.-Murcia1, M. S. Tikhov, B. F. G. Johnson, R. M. Lambert, *Nature* **2008**, 981-984.

[3] Y. Cheng, A. C. Samia, J. D. Meyers, I. Panagopoulos, B. Fei, C. Burda, *J. Am. Chem. Soc.* **2008**, *130*, 10643-10647.

[4] R. J. Tseng, J. Huang, J. Ouyang, R. B. Kaner, Y. Yang, *Nano Lett.* **2005**, *5*, 1077-1080.

[5] A. Corma, H. Garcia, *Chem. Soc. Rev.* **2008**, *37*, 2096-2126.

[6] M. Valden, X. Lai, D. W. Goodman, *Science* **1998**, *281*, 1647-1650.

[7] N. Ishito, K. Hara, K. Nakajima, A. Fukuoka, *J. Energy Chem.* **2016**, *25*, 306-310.

[8] M. Haruta, T. Kobayashi, H. Sano, N. Yamada, *Chem. Lett.* **1987**, 405-406.

[9] S. Panigrahi, S. Basu, S. Praharaj, S. Pande, S. Jana, A. Pal, S. K. Ghosh, T. Pal, *J. Phys. Chem. C* **2007**, *111*, 4596-4605.

[10] H. Sakurai, A. Ueda, T. Kobayashi, M. Haruta, *Chem. Commun.* **1997**, 271-272.

[11] M. Haruta, N. Yamada, T. Kobayahsi, S. Iijima, *J. Catal.*, **1989**, *115*, 301-309.

[12] M. Y. Han, C. H. Quek, *Langmuir*, **2000**, *16*, 362-367.

[13] M. Okumura, S. Tsubota, M. Haruta, *J. Mol. Catal. A Chem.* **2003**, *199*, 73-84.

[14] M. Brust, M. Walker, D. Bethell, D. J. Schiffrin, R. Whyman, *J. Chem. Soc., Chem. Commun.* **1994**, 801-802.

[15] Y. Sunagawa, K. Yamamoto, H. Takahashi, A. Muramatsu, *Catal. Today* **2008**, *132*, 81-87.

[16] P. D. Jadzinsky, G. Calero, C. J. Ackerson, D. A. Bushnell, R. D. Kornberg, *Science* **2007**, *318*, 430-433.

[17] W. W. Weare, S. M. Reed, M. G. Warner, J. E. Hutchison, *J. Am. Chem. Soc.*

2000, *122*, 12890-12891.

[18] M. K. Corbierre, N. S. Cameron, M. Sutton, S. G. J. Mochrie, L. B. Lurio, A. Rühm, R. B. Lennox, *J. Am. Chem. Soc.* **2001**, *123*, 10411-10412.

[19] S. Inagaki, S. Guan, T. Ohsuna, O. Terasaki, *Nature* **2002**, *416*, 304-307.

[20] N. Mizoshita, T. Tani, S. Inagaki, *Chem. Soc. Rev.* **2011**, *40*, 789-800.

[21] S. Inagaki, O. Ohtani, Y. Goto, K. Okamoto, M. Ikai, K. Yamanaka, T. Tani, T. Okada, *Angew. Chem. Int. Ed.* **2009**, *48*, 4042-4046.

[22] M. Waki, N. Mizoshita, Y. Maegawa, T. Hasegawa, T. Tani, T. Shimada, S. Inagaki, *Chem. Eur. J.* **2012**, *18*, 1992-1998.

[23] M. Ohashi, M. Aoki, K. Yamanaka, K. Nakajima, T. Ohsuna, T. Tani, S. Inagaki, *Chem. Eur. J.* **2009**, *15*, 13041-13046.

[24] M. Waki, Y. Maegawa, K. Hara, Y. Goto, S. Shirai, Y. Yamada, N. Mizoshita, T. Tani, W. J. Chun, S. Muratsugu, M. Tada, A. Fukuoka, S. Inagaki, *J. Am. Chem. Soc.* **2014**, *136*, 4003-4011.

[25] Y. Maegawa, S. Inagaki, *Dalton Trans.* **2015**, *44*, 13007-13016.

[26] N. Ishito, H. Kobayashi, K. Nakajima, Y. Maegawa, S. Inagaki, K. Hara, A. Fukuoka, *Chem. Eur. J.* **2015**, *21*, 15564-15569.

[27] V. Amani, A. Abedi, S. Ghabeshi, H. R. Khavasi, S. M. Hosseini, N. Safari,

Polyhedron **2014**, *79*, 104-115.

[28] M. Thommes, K. Kaneko, A.V. Neimark, J.P. Olivier, F. R.-Reinoso, J. Rouquerol, K.S.W. Sing, *Pure Appl. Chem.* **2015**, *87*, 1051-1069.

[29] H. Ikemoto, T. Miyanaga, *Phys. Rev. Lett.* **2007**, *99*, 165503.

[30] L. X. Chen, T. Rajh, Z. Wang, M. C. Thurnauer, *J. Phys. Chem. B* **1997**, *101*, 10688-10697.

Chapter 4. Selective reduction of carbon dioxide to carbon monoxide on alumina-supported gold catalyst

Abstract

Thermal decomposition of formic acid on SiO_2, CeO_2 and γ-Al_2O_3 was studied as an elementary step of reverse water-gas shift reaction (RWGS) over supported Au catalysts. γ-Al_2O_3 showed the highest CO selectivity among the tested oxides in the decomposition of formic acid. The formation of four formate species on γ-Al_2O_3 was confirmed by Infrared spectroscopy: three η^1–type and one μ^2-type species, and these formates decomposed to CO at 473 K or higher. Au-loaded γ-Al_2O_3 samples were prepared by a deposition-precipitation method and used as catalysts for RWGS. The supported Au catalyst gave CO with high selectivity over 99% from CO_2 and H_2, which is attributed to the formation of formates on Au and subsequent decomposition to CO on γ-Al_2O_3.

4.1. Introduction

Carbon dioxide (CO_2) has been recognized as an abundant and inexpensive carbon resource for chemical industry.[1-4] Reverse water-gas shift reaction (RWGS, equation 4.1) is one of the most important reactions in C1 chemistry, because the resulting carbon monoxide (CO)[5-9] can be utilized as feedstock for the production of valuable compounds such as methanol, dimethyl ether and hydrocarbons.[5,8] $Cu/ZnO/Al_2O_3$ is known as an active catalyst for RWGS and methanol synthesis from syngas (CO/H_2), and methanol can be directly obtained from CO_2 and H_2.[5,10-12] Methanol synthesis from CO_2 and H_2 has been currently tested in a pilot plant with a cupper-based catalyst.[13] In contrast to the direct synthesis of methanol, the production of syngas from CO_2 is one of the key technologies for sustainable chemical production, because syngas can be converted to a variety of useful hydrocarbons in the Fischer-Tropsch synthesis.[5,8,14,15]

$$CO_2 + H_2 \rightleftarrows CO + H_2O \qquad (4.1)$$

Gold (Au) nanoparticles supported on various oxides have been investigated by Haruta *et al*. for the hydrogenation of CO_2.[16] CO is a main product in this system, because the Au catalysts cannot catalyze CO hydrogenation to CH_4 or CH_3OH. Moreover,

CO_2 conversion and product selectivity greatly depend on the acid-base property of the oxide supports. Au catalysts on acidic supports produce CO and a small amount of CH_4. On the other hand, Au catalysts on basic supports give low CO_2 conversion due to a strong interaction of CO_2 with basic sites.

It is known that formate species are formed as a key intermediate in the CO_2 hydrogenation over Au catalysts.[5,17-20] Since Au nanoparticles do not decompose the formate species,[20,21] the decomposition of formate species is strongly influenced by the property of supports. In this work, the author studied the decomposition of formate species on oxide supports such as SiO_2, γ-Al_2O_3 (hereafter Al_2O_3) and CeO_2 as an elementary step in RWGS over Au catalysts. Amphoteric Al_2O_3 converted formate species into CO with higher selectivity than SiO_2 and CeO_2. Thermal decomposition of formates on Al_2O_3 was evaluated by diffusive reflectance infrared Fourier transform spectroscopy (DRIFT). Then, Au-loaded Al_2O_3 samples were prepared and their catalytic activity was tested in RWGS.

4.2. Experimental

4.2.1. Reagents

Al_2O_3 was purchased from Tokyo Chemical Industry Company (Japan). Formic acid, $HAuCl_4 \cdot 3H_2O$ and diethyl ether with highest grade were obtained from Wako Pure Chemical Industries (Japan) and used without any purification treatment.

4.2.2. Decomposition of formic acid on metal oxides

Formic acid was immobilized on metal oxides (CeO_2, SiO_2, and Al_2O_3) by simple adsorption treatment. Each metal oxide (1.0 g) was added to a mixture of formic acid (1 mL) and diethyl ether (25 mL), and the solution was stirred at room temperature for 6 h under air. After filtration, the resulting materials were washed repeatedly with diethyl ether, and then dried under vacuum for 12 h. The amount of formic acid on each metal oxide was estimated by a total organic carbon analyzer (TOC, Shimadzu SSM-5000A). The samples were heated in an IR cell from 298 to 773 K with a heating rate of 2 K min^{-1} under a mixed gas flow of Ar (2 mL min^{-1}) and He (18 mL min^{-1}). The outlet gas was analyzed by gas chromatography (Shimadzu GC 8A, thermal conductivity detector, active carbon column (2 m), temperature 383 K) to monitor the evolved CO and CO_2. FT-IR spectra were obtained at a resolution of 1 cm^{-1} using a spectrometer (Spectrum 100,

PerkinElmer) equipped with a mercury cadmium telluride (MCT) detector. A total of 16 scans were averaged for each spectrum. Deconvolution of peaks was performed by assuming Gaussian profiles of the peaks.

4.2.3. Reduction reaction of CO_2 to CO

4.2.3.1. Preparation of Au catalysts

An Au-loaded Al_2O_3 sample was prepared by a deposition-precipitation (DP) method.[22] Al_2O_3 was immersed in an aqueous solution of $HAuCl_4$ (pH 8), which was aged for 1 h. The resulting solid was filtered, washed with H_2O, dried at 383 K and reduced in H_2 at 573 K for 3 h to afford Al_2O_3-supported Au catalyst (denoted Au-DP). For comparison, an Al_2O_3-supported Au catalyst (Au 5 wt%) was prepared by a conventional impregnation method using $HAuCl_4 \cdot 3H_2O$ (99.9%, Wako). After immobilization of Au species on Al_2O_3 by vacuum evaporation and drying at 298 K, the sample was reduced in H_2 at 573 K for 3 h to obtain Al_2O_3-supported Au catalyst (denoted Au-Imp).

4.2.3.2. Characterization of Au catalysts

Structural characterization of the catalysts was performed by X-ray fluorescence spectroscopy (XRF, EDX-720, Shimadzu), nitrogen adsorption (Belsorp-mini II, MicrotracBEL), X-ray diffraction (XRD, Rigaku, Ultima IV, Cu Kα) and transmission electron microscopy (TEM, JEM-2100F, JEOL, 200 kV).

4.2.3.3. CO_2 reduction with fixed-bed flow reactor

Hydrogenation of CO_2 was conducted in a fixed-bed flow reactor (inner diameter 9.5 mm) made of SUS316 (Figure 4.1). Mass flows of CO_2 (99.95%), H_2 (99.999%), He (99.999%), and Ar (99.999 %, internal standard) were regulated by mass flow controllers (HORIBA STEC). The catalyst (0.3 g) was diluted with glass beads (diameter 0.2 mm, 1 g) and charged in the reactor. After reduction of the catalyst in H_2 flow (20 mL min^{-1}) at 673 K for 1 h and subsequent treatment in He flow (20 mL min^{-1}) at 673 K for 15 min, a gas mixture (CO_2 15 %, H_2 75%, Ar 10 %, flow rate 20 mL min^{-1}, gas hourly space velocity (GHSV) 4,000 mL g^{-1} h^{-1}, 0.1 MPa) was fed into the reactor. Products in the liquid phase collected by a water-trap were analyzed by high-performance liquid chromatography (HPLC, Shimadzu LC10ATVP, UV detector) with a Shodex Sugar SH-1011 column (ø8×300 mm, eluent: water 0.5 mL min^{-1}, 323 K). The outlet gas was

analyzed by gas chromatography (Shimadzu GC 8A, thermal conductivity detector, active carbon column (2 m), temperature 383 K).

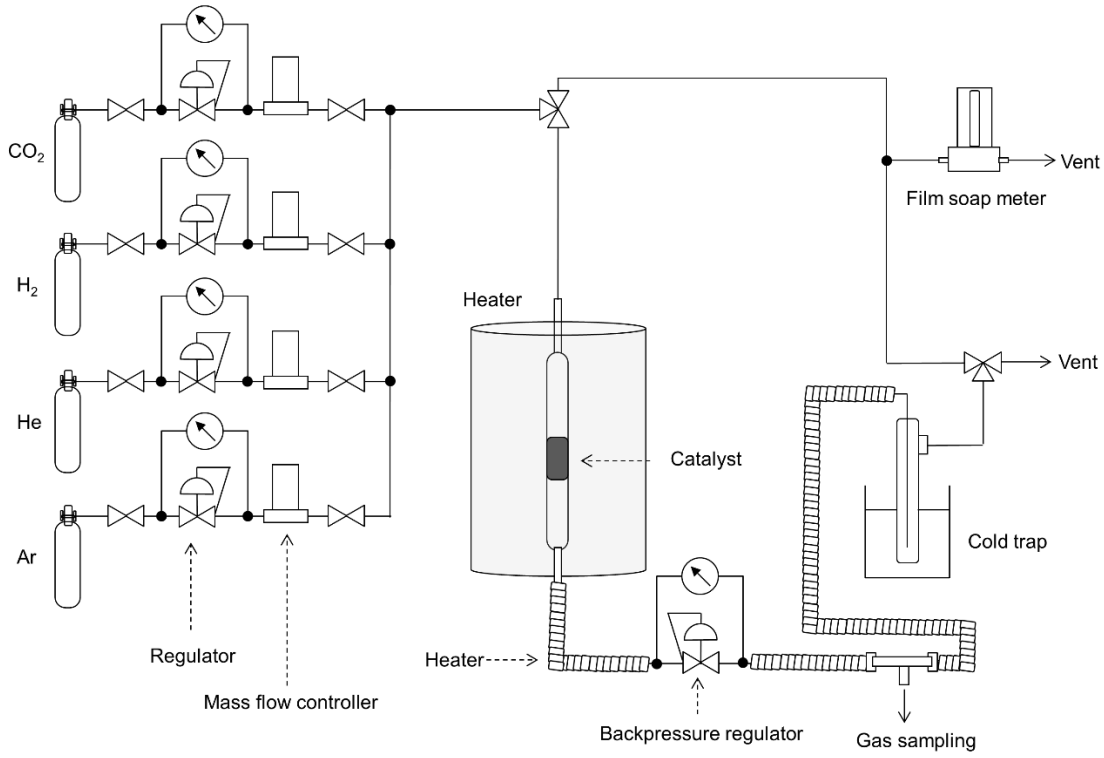

Figure 4.1. Fixed bed-flow reactor for hydrogenation of CO_2.

4.3. Results and discussion

4.3.1. Decomposition of formic acid on metal oxides

Thermal decomposition of formic acid produces CO_2+H_2 or CO+H_2O (equation 4.2). In the reaction from the left to the right (RWGS), formic acid (HCOOH) is assumed to be an intermediate and selective decomposition of HCOOH to CO is important. Hence, the effect of supports on the decomposition of HCOOH was studied.

$$CO_2 + H_2 \rightleftarrows HCOOH \rightleftarrows CO + H_2O \qquad (4.2)$$

Here the author used three metal oxides for the decomposition of HCOOH into CO to find the most appropriate support of Au for RWGS. Table 4.1 compares the amount of adsorbed HCOOH and CO/CO_2 ratio in the decomposition of HCOOH. Similar amounts of HCOOH adsorbed on metal oxides estimated by TOC. However, the densities of immobilized HCOOH for Al_2O_3 and CeO_2 are larger than that for SiO_2. This difference is attributed to weakly basic property of Al_2O_3 and CeO_2 to stabilize HCOOH by the formation of formate. Decomposition of adsorbed species was examined by heating these oxides from room temperature to 773 K under inert gas atmosphere. SiO_2 decomposed HCOOH into CO and CO_2 equally ($CO/CO_2 = 1$). CeO_2 and Al_2O_3 produced CO more

favorably than CO_2, and Al_2O_3 gave the highest CO/CO_2 ratio among the three oxides. Figure 4.2 shows dependence of CO and CO_2 formation on reaction temperature over Al_2O_3. CO evolution starts at 473 K and rapidly increases up to 543 K. On the basis of CO evolution, decomposition is completed below 673 K.

Table 4.1. Adsorption and thermal decomposition of formic acid on Al_2O_3, CeO_2, and SiO_2.

Oxide	Amount of adsorbed formic acid (mmol g^{-1})[a]	Surface area (m^2 g^{-1})	Density of adsorbed formic acid (nm^{-2})	CO / CO_2 ratio[b]
Al_2O_3	1.3	160	4.9	50
CeO_2	1.0	130	4.6	3
SiO_2	0.8	290	1.7	1

[a] Determined by TOC analysis, [b] CO and CO_2 were analyzed by GC-TCD.

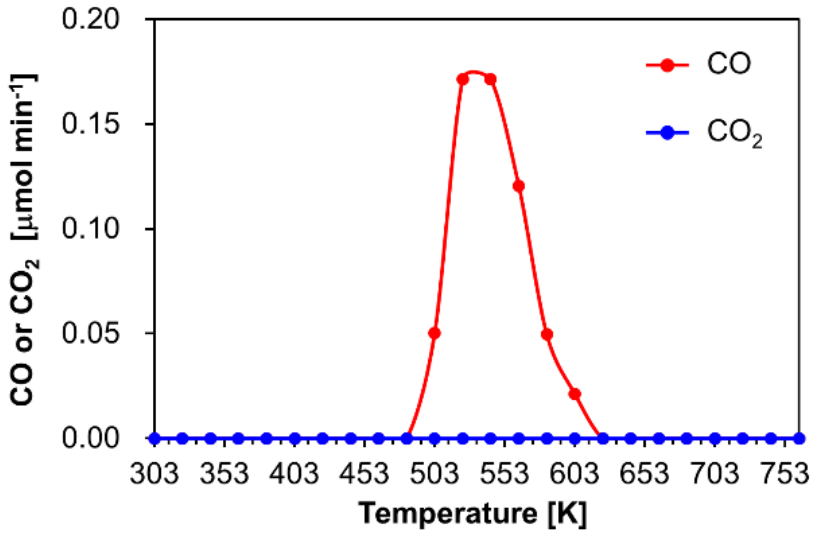

Figure 4.2. Dependence of CO (red) and CO_2 (blue) formation on reaction temperature over Al_2O_3.

4.3.2. In-situ DRIFT measurement of thermal decomposition of formic acid on alumina

From these results, decomposition of HCOOH on Al_2O_3 was monitored by IR at 483-683 K. Figure 4.3 shows a DRIFT spectrum of HCOOH-adsorbed Al_2O_3 at 483 K under inert gas atmosphere. Broad bands at 3000-2800 cm^{-1}, 1800-1400 cm^{-1} and 1400-1200 cm^{-1} are assignable to C-H stretching, C-O stretching and C-H bending modes of adsorbed formic acid, respectively. Tamaru *et al.* reported that a formate species with η^1-type structure is an intermediate in the thermal decomposition of HCOOH on γ-Al_2O_3 (Figure 4.4(a)).[23] Hence, the bands at 2892, 1678, 1323 cm^{-1} in Figure 4.3 are assignable to $\nu_{(C-H)}$, $\nu_{(C=O)}$ and $\delta_{(C-H)}$ of the η^1-type formate species. He *et al.* studied stretching

vibration modes of the adsorbed formate species on Al_2O_3 by density functional theory (DFT) calculation and proposed that formate species in the form of μ^2-type structure can be stabilized (Figure 4.4(c)).[24] Formation of the μ^2-type formate on Al_2O_3 was also confirmed from the IR bands at 2905 cm^{-1} ($\nu_{(C\text{-}H)}$), 1597 cm^{-1} ($\nu_{as(O\text{-}C\text{-}O)}$) and 1388 cm^{-1} ($\nu_{s(O\text{-}C\text{-}O)}$) in Figure 4.3. In addition to the bands for the typical η^1- and μ^2-type formates, four IR bands at 2858, 1645, 1618 and 1365 cm^{-1} are observed in Figure 2. The presence of two bands at 1645 and 1618 in the region of C=O stretching suggests that two different formate species other than η^1- and μ^2-type species are formed on Al_2O_3. Because the coordination of carbonyl group with Lewis acid sites results in red shift of original C=O stretching frequency, these bands are ascribed to η^1-type formates with carbonyl groups weakly interacting with an adjacent Lewis acid site (Figure 4.4(b)). It was reported that Al_2O_3 has three Lewis acid sites in terms of acid strength: strong, medium and weak Lewis acid sites.[25] The μ^2 species could be formed on the two strong Lewis acid sites, so that the bands at 1645 and 1618 cm^{-1} can be reasonably assigned to η^1 species interacting with weak and medium Lewis acid sites. The bands at 2858 and 1365 cm^{-1} in Figure 4.3 are assignable to $\nu_{(C\text{-}H)}$ and $\delta_{(C\text{-}H)}$ of these formate species. These three η^1 type formates are denoted η^1(1678 cm^{-1}), η^1(1645 cm^{-1}) and η^1(1618 cm^{-1}).

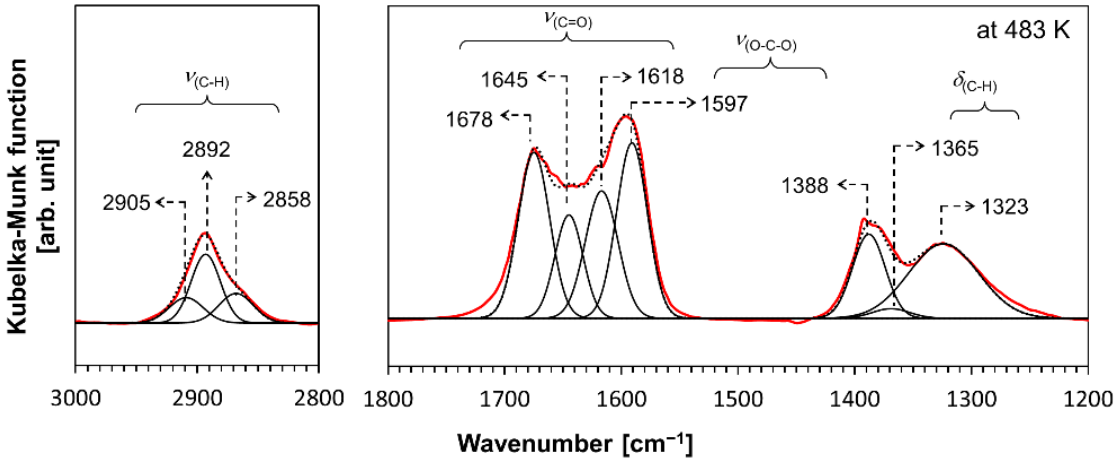

Figure 4.3. DRIFT spectrum of HCOOH-adsorbed Al_2O_3 at 483 K under inert gas atmosphere. Red line: raw spectrum, black dot line: combined spectrum of deconvoluted peaks.

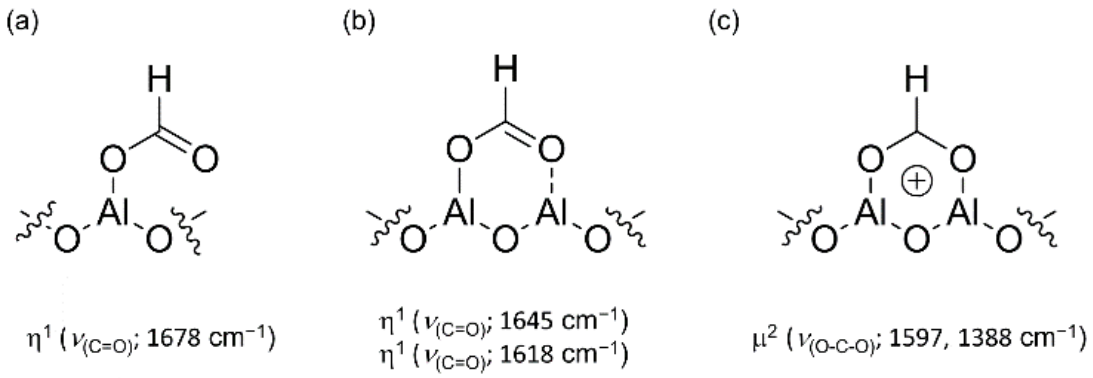

Figure 4.4. Proposed structures of adsorbed formate species on Al_2O_3: (a) typical η^1–type species, (b) two η^1–type species interacting with weak and medium Lewis acid sites and (c) typical μ^2–type species.

Decomposition of these formate species was evaluated by temperature-programmed DRIFT measurement (Figure 4.5). The band intensities of the four formate species decreased during heating.

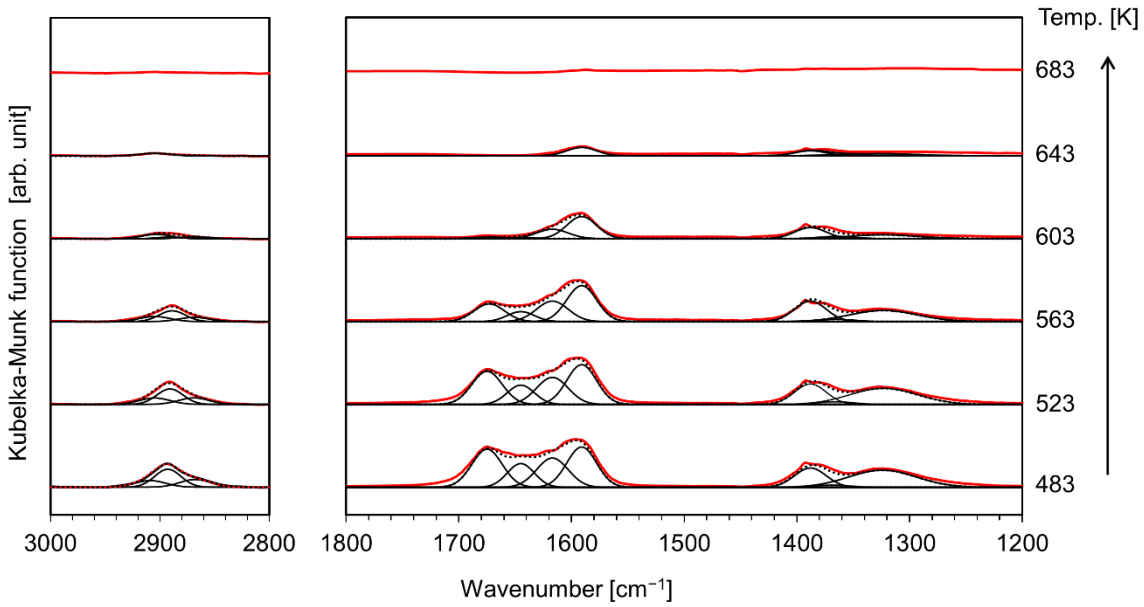

Figure 4.5. DRIFT spectra of thermal decomposition of formic acid on Al_2O_3 under inert gas atmosphere. Red line: raw spectrum, Black dot line: combined spectrum of deconvoluted peaks.

Figure 4.6(a) shows DRIFT spectra of HCOOH-adsorbed Al_2O_3 heated at different temperatures in a region of C-O stretching band. Specific bands for η^1(1678 cm^{-1}), η^1(1645 cm^{-1}), η^1(1618 cm^{-1}) and μ^2 species in 1800-1500 cm^{-1} changed continuously during the thermal treatment. The band intensities of the four formate species were plotted

against each temperature (Figure 4.6(b)). It is clearly shown that the decrease in band intensity for the three η^1 species is well correlated with the increase in CO formation, which indicates that CO formation occurs by the decomposition of the η^1 species. In contrast, the μ^2 species shows higher thermal stability; most μ^2 species remains at ca. 573 K. Therefore, CO formation at higher temperature is mainly due to the decomposition of the μ^2 species.

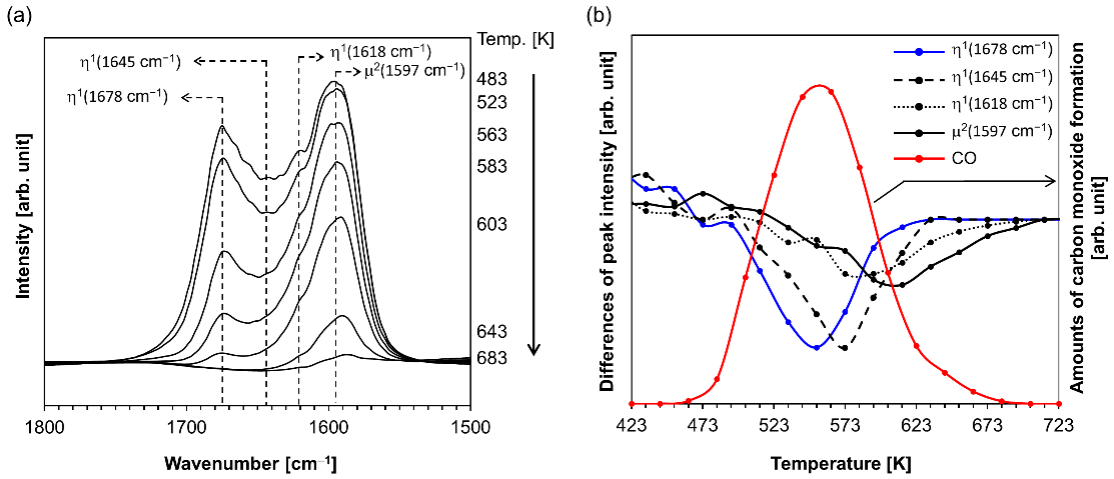

Figure 4.6. (a) DRIFT spectra of HCOOH-adsorbed Al_2O_3 at different temperatures and (b) temperature dependence of CO formation and band intensities for four formates.

4.3.3. Reduction of CO_2 to CO

As described in the previous section, formate species formed in adsorption of HCOOH on Al_2O_3 are readily decomposed to CO at above 483 K; therefore, it is expected that the introduction of Au nanoparticles on Al_2O_3 gives CO via HCOOH from CO_2 and H_2.[16] Al_2O_3-supported Au catalysts were prepared by a deposition-precipitation (DP) method and an impregnation method (Imp). Figure 4.7 shows XRD patterns of the resulting catalysts. Several sharp or broad diffractions are observed for Al_2O_3, and all the diffractions are assignable to γ-phase of crystalline Al_2O_3. In addition to the peaks, Au-Imp showed five sharp diffractions at 2θ = 38°, 44°, 65°, 78°, and 82° due to (111), (200), (220), (311) and (222) planes for face-centered cubic (fcc) lattice structure of Au metal.[26] An average size of Au particles in Au-Imp was estimated to be 38 nm by the Scherrer equation. In contrast, Au-DP represented no diffractions of Au metal, which implies high dispersion of Au particles on the Al_2O_3 surface.

Figure 4.8 is a TEM image of Au-DP, which reveals the presence of Au nanoparticles with a mean diameter of 2.6 nm. Thus, the DP method is appropriate for the preparation of Al_2O_3-supported Au catalyst.

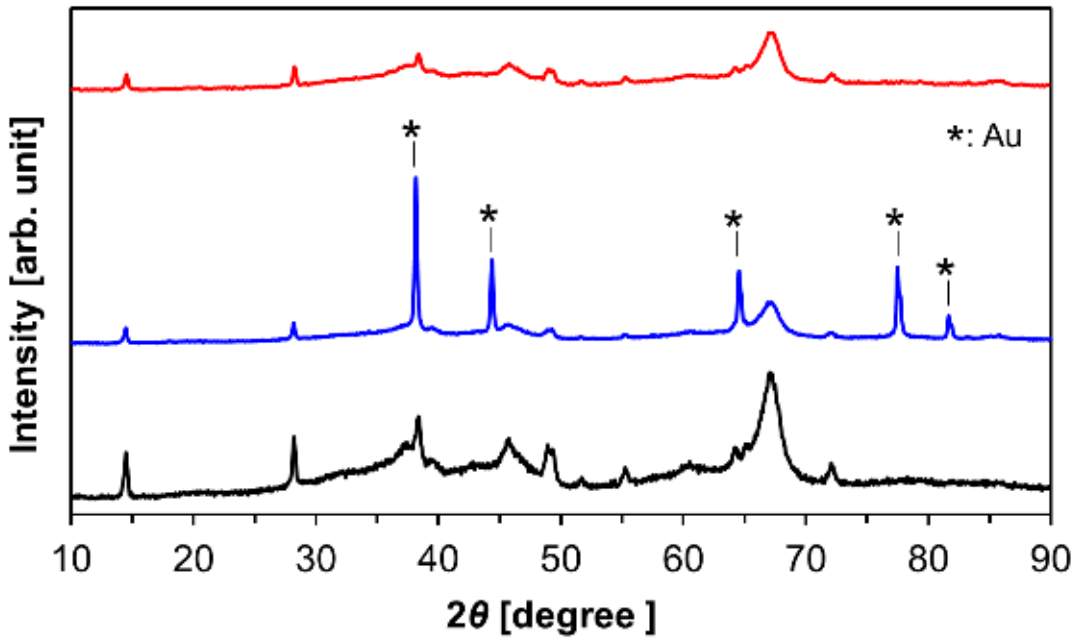

Figure 4.7. XRD patterns of γ-Al_2O_3 (black), Au-Imp (blue) and Au-DP (red).

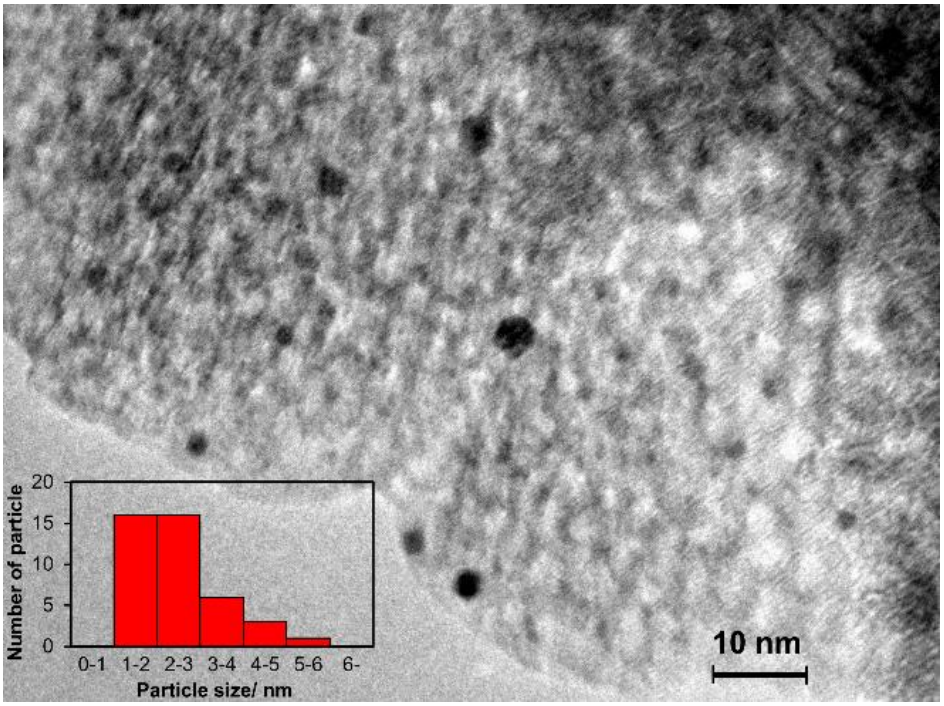

Figure 4.8. TEM image of Au-DP and size distribution of Au nanoparticles (inset).

RWGS was conducted at 623 K and 0.1 MPa with a gas hourly space velocity (GHSV) of 4000 mL g^{-1} h^{-1}. A control experiment in the absence of catalyst gave no reaction (Table 4.2, entry 1). Au-Imp showed a very low CO_2 conversion (2.0%) (entry 2), but Au-DP gave 20% CO_2 conversion with high CO selectivity over 99% (entry 3). Accordingly, Au nanoparticles on Al_2O_3 can quantitatively produce CO even under atmospheric pressure. CO_2 equilibrium conversion is estimated to be ca. 38% under the reaction conditions by chemical thermodynamic parameters.[27,28]

Table 4.2. Reverse water-gas shift reaction by Al_2O_3-supported Au catalysts[a]

Entry	Catalyst	Conversion (%)	CO yield (%)	CO selectivity (%)
1	None	0.0	0.0	0.0
2	Au-Imp	2.0	2.0	> 99
3	Au-DP	20	20	> 99

[a] Reaction condition: catalyst (50 mg), CO_2 (15%), H_2 (75%), Ar (10%), 623 K, 1 atm. Sampling after 30 and 45 min. Steady state was confirmed after 30 min.

Probably, such a high selectivity can be derived from the formation of formate species by Au nanoparticle and the subsequent decomposition to CO by Al_2O_3. The formation of formate species on Au/Al_2O_3 catalyst was directly confirmed by DRIFT measurement. Figure 4.9 shows DRIFT spectra of Au-DP at 473 K under a flow of CO_2 and H_2. After reduction of the catalyst in H_2 flow (20 mL min^{-1}) at 673 K for 1 h and subsequent treatment in He flow (20 mL min^{-1}) at 673 K for 15 min, a gas mixture (CO_2 15 %, H_2 75%, Ar 10 %, flow rate 20 mL min^{-1} 0.1 MPa) was continuously fed into the IR cell during the measurement. One intense and asymmetric band is observed at 1592 cm^{-1}. Heat treatment at 473 K enables efficient removal of physisorbed water formed by the RWGS reaction, so that the band is regarded as a combined band for η^1(1678 cm^{-1}), η^1(1645 cm^{-1}), η^1(1618 cm^{-1}) and μ^2 (1592 cm^{-1}) species of adsorbed formate on Al_2O_3 (Figure 4.6(a)). Due to low thermal stability for η^1(1678 cm^{-1}), η^1(1645 cm^{-1}), and η^1(1618 cm^{-1}), the bands started to decrease gradually in their intensities from 473 K, while the band for μ^2 (1597 cm^{-1}) species retained intact even at 623 K. This tendency was good agreement with the result for thermal decomposition of adsorbed HCOOH on Al_2O_3 (Figure 4.6(b)). Moreover, Au nanoparticles cannot adsorb and decompose formate species,[21] which means that they are formed by Au nanoparticle and stabilized on Al_2O_3

support before subsequent decomposition into CO and H_2O. Au-DP is therefore an effective catalyst for selective formation of CO from a mixture of CO_2 and H_2.

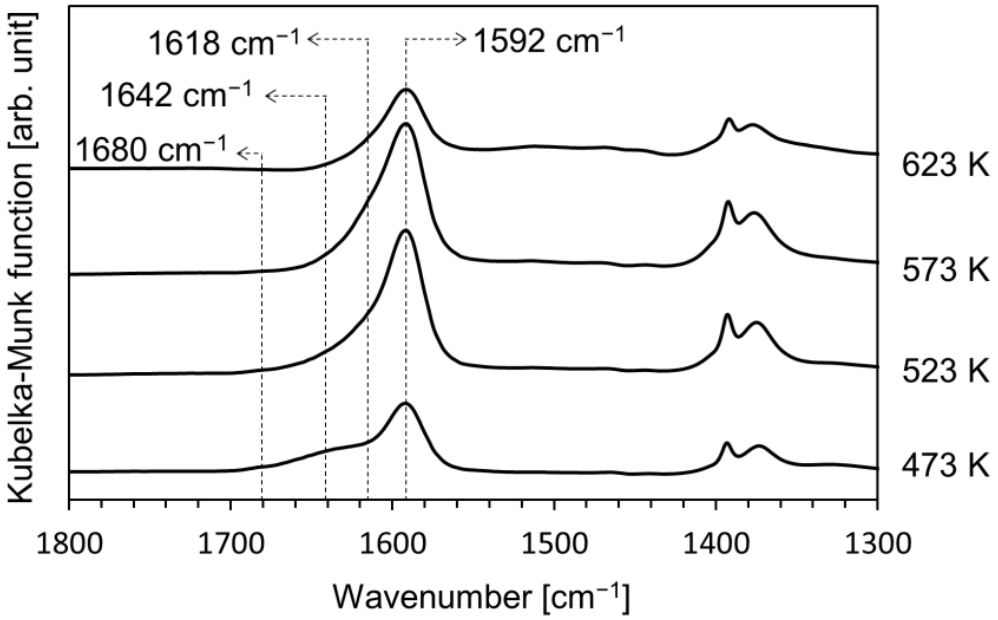

Figure 4.9. DRIFT spectra of Au-DP at different temperatures under a gas flow of H_2 and CO_2.

4.4. Conclusions

HCOOH adsorbed on Al_2O_3 selectively decomposed to CO. The decomposition pathway on Al_2O_3 was monitored by in-situ FTIR measurement, and four types of formate species were observed on Al_2O_3. Three η^1-type formates were well correlated with the formation of CO, but one μ^2-type formate was thermally stable and decomposed to CO at higher temperature. Selective decomposition of formates to CO is a great advantage of Al_2O_3 as a support of Au. Al_2O_3-supported Au catalyst was prepared by a deposition-precipitation method, and this catalyst gave CO with high selectivity (> 99%).

References

[1] G. Centi, S. Perathoner, *Catal. Today* **2009**, *148*, 191.

[2] T. Schaub, R. A. Paciello, *Angew. Chem. Int. Ed.* **2011**, *50*, 7278.

[3] S. Fukuoka, M. Kawamura, K. Komiya, M. Tojo, H. Hachiya, K. Hasegawa, M. Aminaka, H. Okamoto, I. Fukawa, S. Konno, *Green Chem.* **2003**, *5*, 497.

[4] G. W. Coates, D. R. Moore, *Angew. Chem. Int. Ed.* **2004**, *43*, 6618.

[5] W. Wang, S. Wan, X. Ma, J. Gong, *Chem. Soc. Rev.* **2011**, *40*, 3703.

[6] R. Tanaka, M. Yamashita, K. Nozaki, *J. Am. Chem. Soc.* **2009**, *131*, 14168.

[7] J. Sloczynski, R. Grabowski, A. Kozlowka, P. Olszewski, J. Stoch, J. Skrzypek, M. Lachowska, *Appl. Catal. A* **2004**, *278*, 11.

[8] R. W. Dorner, D. R. Hardy, F. W. Williams, H. D. Willauer, *Appl. Catal. A* **2010**, *373*, 112.

[9] O. S. Joo, K. D. Jung, I. Moon, A.Y. Rozovskii, G.I. Lin, S. H. Han, S. J. Uhm, *Ind. Eng. Chem. Res.* **1999**, *38*, 1808.

[10] F. S. Stone, D. Waller, *Top. catal.* **2003**, *22*, 305.

[11] Y. Zhang, Q. Sun, J. Deng, D. Wu, S. Chen, *Appl. Catal. A* **1997**, *158*, 105.

[12] M. Behrens, F. Studt, I. Kasatkin, S. Kühl, M. Hävecker, F. A.-Pedersen, S. Zander, F. Girgsdies, P. Kurr, B. L. Kniep, M. Tovar, R. W. Fischer, J. K. Nørskov, R. Schlögl, *Science* **2012**, *336*, 893.

[13] T. Matsushita, T. Haganuma, D. Fujita, US Patent 20130237618, **2013**.

[14] G. Kiss, M. G. Matturro, H. W. Deckman, F. Hershkowitz, D. R. Lumgir, G. F. Janda, D. N. King, US Patent 6049011, **2000**.

[15] P. Liu, E. N. Jacobsen, *J. Am. Chem. Soc.* **2001**, *123*, 10772.

[16] H. Sakurai, S. Tsubota, M. Haruta, *Appl. Catal. A* **1993**, *102*, 125.

[17] G. Jacobs, A. C. Crawford, B. H. Davis, *Catal. Lett.* **2005**, *100*, 147.

[18] Q. Y. Bi, X. L. Du, Y. M. Liu, Y. Cao, H. Y. He, K. N. Fan, *J. Am. Chem. Soc.* **2012**, *134*, 8926.

[19] R. A. Koeppel, A. Baiker, C. Schild, A. Wokaun, *J. Chem. Soc. Faraday Trans.* **1991**, *87*, 2821.

[20] D. Preti, C. Resta, S. Squarcialupi, G. Fachinetti, *Angew. Chem. Int. Ed.* **2011**, *50*, 12551.

[21] W. J. M. Rootsaert, W. M. H. Sachtler, *J. Phys. Chem.* **1960**, *26*, 16.

[22] M. Haruta, *Catal. Today* **1997**, *36*, 153.

[23] Y. Noto, K. Fukuda, T. Onishi, K. Tamaru, *Trans. Faraday Soc.* **1967**, *63*, 2300.

[24] H. Gao, T. Yan, C. Zhang, H. He, *THEOCHEM* **2008**, *857*, 38.

[25] X.Liu, R. E. Truitt, *J. Am. Chem. Soc.* **1997**, *119*, 9856.

[26] Y. Shao, Y. Jin, S. Dong, *Chem. Commun*. **2004**, 1104.

[27] D. D. Wagman, W. H. Evans, V. B. Parker, R. H. Schumm, I. Halow, S. M. Bailey, K. L. Churney, R. L. Nuttall, J. Phys. Chem. **1982**, Ref. Data Vol.11, supplement No.2.

[28] CO_2 equilibrium conversion at the reaction conditions was calculated as follows. ΔH_f and ΔS are given as 40.04 kJ mol^{-1} and 39.71 J K^{-1} mol^{-1} by equation 4.3 and 4.4 using the data of chemical thermodynamic properties (Table 4.3).

$$\Delta H^{\circ}(T) = \Delta H^{\circ}(298\ \mathrm{K}) + \int_{298}^{T} \Delta C_p \mathrm{d}T \tag{4.3}$$

$$\Delta S^{\circ}(T) = \Delta S^{\circ}(298\ \mathrm{K}) + \mathrm{C}_p \int_{298}^{T} \frac{\mathrm{d}T}{T} = \Delta S^{\circ}(298\ \mathrm{K}) + \mathrm{C}_p \ln \frac{T}{298} \tag{4.4}$$

Table 4.3. Chemical thermodynamic properties at 298 K in RWGS reaction.[27]

	ΔH_f° /kJ mol^{-1}	S° /J K^{-1} mol^{-1}	C_p /J K^{-1} mol^{-1}
CO_2	−393.51	213.74	37.11
H_2	0	130.68	28.82
CO	−110.53	197.67	29.14
H_2O	−241.82	188.83	33.58

Next, the author calculated ΔG and equilibrium constant K to be 15.29 kJ mol^{-1} and 0.05226 at 623 K using equation 4.5 and 4.6.

$$\Delta G^{\circ} = \Delta H^{\circ} - T\Delta S^{\circ} \tag{4.5}$$

$$\Delta G^{\circ} = -RT \ln K \tag{4.6}$$

Finally, equilibrium conversion of CO_2 is 39% at the reaction condition of H_2/CO_2 = 5 and 623 K.

Chapter 5. General conclusions

A heterogeneous catalyst showing extremely high selectivity and activity is inevitable to realize sustainable society. In chapter 1, the author comprehensively reviewed recent progress on immobilization of organic functional groups, homogeneous complexes, and novel metal nanoparticles on solid supports for the development of heterogeneous catalysts with high activity and reusability. In this work, the author has focused special attention on periodic mesoporous organosilica (PMO) as a versatile support that has a well-defined mesoporous structure and crystal-like arrangement of organic moiety inside the silica wall. Because bi-pyridine functions as a coordination site for metals, bi-pyridine-containing PMO can be utilized as a solid ligand for various homogenerous complexes with unique catalysis.

In chapter 2, the author successfully developed well-designed isolated ruthenium sites formed directly on 2,2'-bypyridine groups in the bipyridine bridged-PMO (BPy-PMO) framework. Coordination structure of the immobilized Ru complexes is similar to that of corresponding Ru complex, $RuCl_2(bpy)(CO)_2$. The Ru-immobilized BPy-PMO is applied as a heterogeneous catalyst for the oxidation of various alkanes using NaClO as an oxidant, showing high selectivity toward the oxidation of tertiary C–H bonds more

preferably than that of secondary and primary C-H bonds (Figure 5.1). The catalyst can be separated by simple filtration and reused without loss of original activity and selectivity for oxidation reactions. No interaction among Ru active sites, due to rigid structure of bipyridine ligands, is essentially beneficial to prevent oxidative decomposition and show good durability. The Ru-immobilized PMO catalyst reported in this chapter will contribute to practical application of inductrial synthesis of fine chemicals.

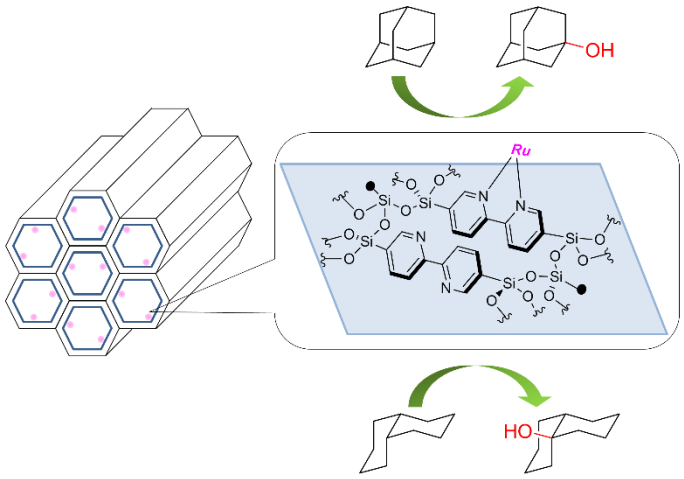

Figure 5.1. Selective oxidation of tertiary C-H bonds in cyclic alkanes over Ru-immobilized BPy-PMO.

In chapter 3, BPy-PMO was also utilized as a support for the formation of gold nanoparticles (AuNPs). A novel strategy was developed through the formation of Au

complex with surface BPy moiety and subsequent thermal reduction with H_2 (Figure 5.2). Average diameter of the resulting AuNPs was ca. 3.8 nm, much smaller than those formed on silica supports reported in the previous literatures. Mesopore diameter is one important factor controlling the size of AuNPs formed inside mesopores (4.2 nm) of BPy-PMO. This methodology is believed to be useful for the formation of small AuNPs with homogeneous distribution on silica supports.

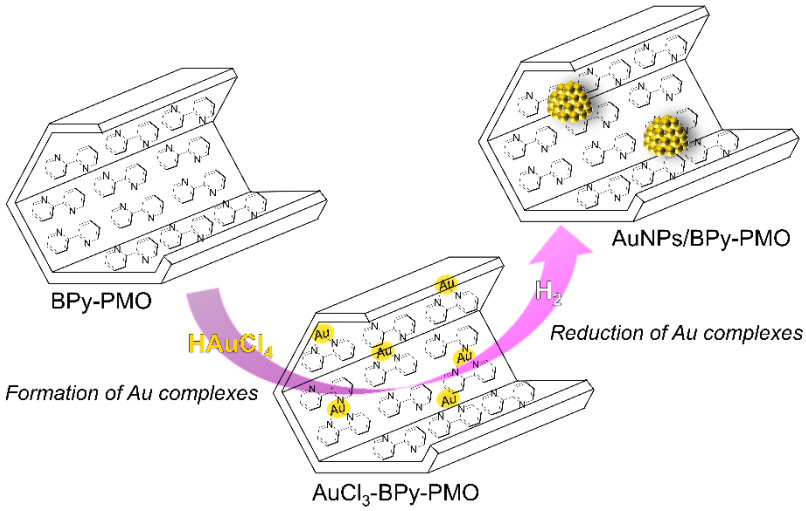

Figure 5.2. Synthesis of AuNPs-supported BPy-PMO by a sequential method.

In chapter 4, the author studied the decomposition of formate species on Al_2O_3 as an elementary step in reverse water-gas shit reaction over Au-loaded Al_2O_3. FT-IR measurement revealed the formation of four formate species on Al_2O_3: three η^1–type and one μ^2-type species, which decomposed to CO at 473 K or higher. It was confirmed that

AuNPs-supported Al_2O_3 catalyst gives CO with high selectivity over 99% from CO_2 and H_2 under the similar reaction condition. High catalytic performance is attributed to the formation of formates on AuNPs and subsequent decomposition to CO on Al_2O_3 support as shown in Figure 5.3.

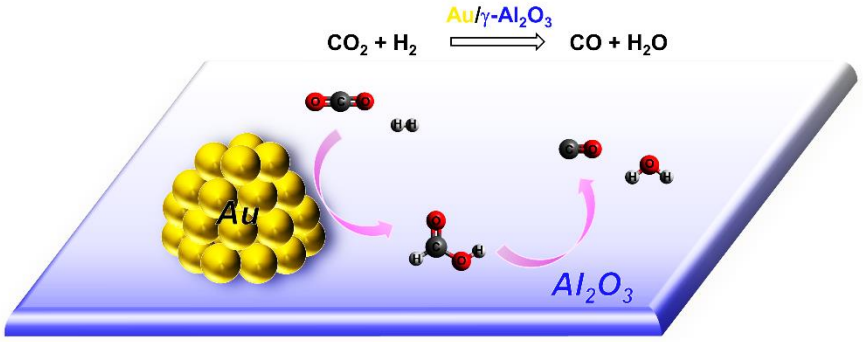

Figure 5.3. Reduction of CO_2 to CO over Al_2O_3-supported Au catalyst.

In conclusion, BPy units in PMO are useful to accumulate and stabilize various metal complexes. Resulting complexes can be used as catalytically active sites as well as precursors for corresponding nanoparticles. Combination of mesoporous structure and organic functionality on the basis of PMOs is useful to design a well-defined catalyst in the molecular level.

List of Publications

1. Papers (related to this thesis)
    1. Nobuhiro Ishito, Hirokazu Kobayashi, Kiyotaka Nakajima, Yoshifumi Maegawa, Shinji Inagaki, Kenji Hara, Atsushi Fukuoka, "Ruthenium-Immobilized Periodic Mesoporous Organosilica: Synthesis, Characterization, and Catalytic Application for Selective Oxidation of Alkanes" *Chem. Eur. J.* **2015**, *21*, 15564-15569.

    2. Nobuhiro Ishito, Kenji Hara, Kiyotaka Nakajima, Atsushi Fukuoka, "Selective synthesis of carbon monoxide via formates in reverse water-gas shift reaction over alumina-supported gold catalyst" *J. Energy Chem.* **2016**, *25*, 306-310.

    3. Nobuhiro Ishito, Kiyotaka Nakajima, Yoshifumi Maegawa, Shinji Inagaki, Atsushi Fukuoka, "Synthesis and characterization of gold nanoparticles immobilized on BPy-PMO" *Catal. Today* **2016**, *submitted*.

2. Other papers (not related to this thesis)
    1. Kenji Hara, Saeko. Akahane, J. W. Wiench, B. R Burgin, Nobuhiro Ishito, V. S.-Y. Lin, A. Fukuoka, M. Pruski, "Selective and Efficient Silylation of Mesoporous Silica: A Quantitative Assessment of Synthetic Strategies by Solid-State NMR" *J. Phys. Chem. C* **2012**, *116*, 7083-7090.

3. International conferences
    3.1. Oral presentations
    1. Nobuhiro Ishito, Kenji Hara, Wang Jae Chun, Yoshifumi Maegawa, Shinji Inagaki, Atsushi Fukuoka, "Immobilization of metal complexes on organic ligands in periodic mesoporous organosilicas", *International Symposium on Catalysis for Renewable Chemicals, TOCAT7 Pre-symposium*, Oral, OL1, May 30, 2014, Shari, Japan.

2. Nobuhiro Ishito, Kenji Hara, Wang Jae Chun, Yoshifumi Maegawa, Shinji Inagaki, Atsushi Fukuoka, "Immobilization of metal complexes on periodic mesoporous organosilicas", *France-Japan IAL International Workshop CATP4Bi*o, Oral, 19, June 7, 2014, Kyoto, Japan.

3. Nobuhiro Ishito, Hirokazu Kobayashi, Kiyotaka Nakajima, Yoshifumi Maegawa, Shinji Inagaki, Kenji Hara, Atsushi Fukuoka, "Synthesis of Ru-immobilized periodic mesoporous organosilica and application for selective oxidation of alkanes" *6th International IUPAC Conference On Green Chemistry*, Oral, IP1, September 6, 2016, Venezia, Italy.

3.2. Poster presentations

1. Nobuhiro Ishito, Kenji Hara, Yoshifumi Maegawa, Shinji Inagaki, Atsushi Fukuoka, "Immobilization of Cu Complex to Organic Ligand in Periodic Mesoporous Silica", *8th International Mesostructured Materials Symposium*, Poster, RRR-025, May 22, 2013, Hyougo, Japan.

2. Nobuhiro Ishito, Kenji Hara, Atsushi Fukuoka, "Selective catalytic reduction of carbon dioxide via intermediacy of formic acid", *The Sixteenth International Symposium on Relations between Homogeneous and Heterogeneous Catalysis*, Poster, 1P-37, August 5, 2013, Hokkaido, Japan.

3. Nobuhiro Ishito, Kenji Hara, Wang Jae Chun, Yoshifumi Maegawa, Shinji Inagaki, Atsushi Fukuoka, "Immobilization of Cu and Ru complexes on organic ligands in periodic mesoporous organosilicas", *The Seventh Tokyo Conference on Advanced Catalytic Science and Technology*, Poster, GP2078, June 3, 2014, Kyoto, Japan.

4. Nobuhiro Ishito, Kenji Hara, Wang Jae Chun, Yoshifumi Maegawa, Shinji Inagaki, Atsushi Fukuoka, "High-Density Immobilization of Metal Complexes on Organic Ligands in Periodic Mesoporous Organosilicas", *The 3rd Frontier Chemistry Center International Symposium*, Poster, P-16, June 13, 2014, Hokkaido, Japan.

5. Nobuhiro Ishito, Kenji Hara, Yoshifumi Maegawa, Shinji Inagaki, Atsushi Fukuoka, "Immobilization of metal complexes on organic ligands in periodic mesoporous organosilicas", *CRC International Symposium: Synthesis and Applications of Functional Molecules and Materials Utilizing Biomolecules as a Motif*, Poster, P6, September 30, 2014, Hokkaido, Japan.

6. Nobuhiro Ishito, Kenji Hara, Yoshifumi Maegawa, Shinji Inagaki, Atsushi Fukuoka, "Immobilization of metal complexes on periodic mesoporous organosilicas", *CRC International Symposium: Novel Photocatalysts for Environmental Purification and Energy Generation*, Poster, P20, October 14, 2014, Hokkaido, Japan.

7. Nobuhiro Ishito, Kenji Hara, Yoshifumi Maegawa, Shinji Inagaki, Atsushi Fukuoka, "Immobilization of Ru complexes on organic ligands in periodic mesoporous organosilicas", *International Symposium on Zeolite and Microporous Crystals 2015*, Poster, P2-060, July 1, 2015, Hokkaido, Japan.

8. Nobuhiro Ishito, Hirokazu Kobayashi, Kiyotaka Nakajima, Yoshifumi Maegawa, Shinji Inagaki, Kenji Hara, Atsushi Fukuoka, "Immobilization of Ru complexes on bipyridine containing periodic mesoporous organosilica and application for selective oxidation of alkanes", *First International Symposium of Institute for Catalysis*, Poster, P31, October 14, 2015, Hokkaido, Japan.

9. Nobuhiro Ishito, Kenji Hara, Yoshifumi Maegawa, Shinji Inagaki, Atsushi Fukuoka, "Immobilization of Ru complexes on organic ligands in periodic mesoporous organosilicas and catalytic application for selective oxidation of alkane", *The International Chemical Congress of Pacific Basin Societies 2015*, Poster, 770, December 18, 2015, Hawaii, USA.

11. Nobuhiro Ishito, Hirokazu Kobayashi, Kiyotaka Nakajima, Yoshifumi Maegawa, Shinji Inagaki, Kenji Hara, Atsushi Fukuoka, "Immobilization of Ru complexes on bipyridine containing periodic mesoporous organosilica and application for alkane oxidation", *The 5th International Conference on MEXT Project of Integrated Research on Chemical Synthesis*, Poster, P-69, January 29, 2016, Aichi, Japan.

12. Nobuhiro Ishito, Hirokazu Kobayashi, Kiyotaka Nakajima, Yoshifumi Maegawa, Shinji Inagaki, Kenji Hara, Atsushi Fukuoka, "Synthesis of Ru-immobilized Periodic Mesoporous Organosilica and Application for Selective Oxidation of Alkanes", *The 4th Frontier Chemistry Center International Symposium*, Poster, P-13, February 23, 2016, Hokkaido, Japan.

3.3. As a co-author

1. Kenji Hara, Nobuhiro Ishito, Yoshifumi Maegawa, Shinji Inagaki, Atsushi Fukuoka, "Immobilization of Ru Complexes on Periodic Mesoporous Organosilica and Catalytic Application in Selective Alkane Oxidation", *24th North American Meeting NAM of the Catalysis Society*, Oral, O-Tu-403-14, June 16, 2015, Pittsburgh, USA.

2. Kenji Hara, Nobuhiro Ishito, Yoshifumi Maegawa, Shinji Inagaki, Atsushi Fukuoka, "Ru-Immobilized Periodic Mesoporous Organosilica as Selective Catalyst in Alkane Oxidation", *International Conference on Nanospace Materials from fundamental to Advanced Applications (ICNM2015)*, Oral, A-IN-11, June 23, 2015, Taipei, Taiwan.

4. Domestic conferences

4.1. Oral presentations

1. 石戸信広, 原賢二, 田 旺帝, 前川佳史, 稲垣伸二, 福岡淳, “メソポーラス有機シリカ上への銅およびルテニウム錯体の固定化”, 第１１２回触媒討論会, Oral, 3C22, September 20, 2013, Akita, Japan.

2. 石戸信広, 原賢二, 前川佳史, 稲垣伸二, 福岡淳, “メソポーラス有機シリカ担持ルテニウム錯体の触媒反応への応用”, 第１１４回触媒討論会, Oral, 3D11, September 27, 2014, Higashihiroshima, Japan.

3. 石戸信広, 小林広和, 中島清隆, 福岡淳, “ビピリジン基含有メソポーラス有機シリカ上で形成したルテニウム錯体によるアルカン酸化反応” 統合物質創製化学推進事業、第６回若手研究会, Oral, July 4, 2015, Beppu, Japan.

4. 石戸信広, 小林広和, 中島清隆, 稲垣伸二, 原賢二, 福岡淳, “ビピリジン基含有メソポーラス有機シリカ表面上でのルテニウム錯体の形成とアルカン酸化反応への応用” 第１１６回触媒討論会, Oral, 2E09, September 17, 2015, Tsu, Japan.

5. 石戸信広, 小林広和, 中島清隆, 前川佳史, 稲垣伸二, 原賢二, 福岡淳, “ビピリジン基含有メソポーラス有機シリカ表面上で形成した Ru 錯体によるアルカン酸化反応” 第 31 回ゼオライト学会発表会, Oral, B20, November 27, 2015, Tottori, Japan.

6. 石戸信広, 原賢二, 中島清隆, 福岡淳, “アルミナ担持金触媒上での二酸化炭素から一酸化炭素への還元反応” 第１１８回触媒討論会, Oral, 2D05, September 22, 2016, Morioka, Japan.

Acknowledgements

触媒科学研究所物質変換研究部門の福岡淳教授には、６年間に渡り、多くの有益な議論をして頂き、研究への心構えについてご指導を賜りました。深く感謝申し上げます。

主査の加藤昌子教授、副査の澤村正也教授、向井紳教授には、学位論文作成にあたり多くのご貴重なご意見を賜りました。深く感謝致します。

触媒科学研究所物質変換研究部門の中島清隆准教授には、研究への多くのご助言を頂き、研究以外の面でも大変お世話になりました。深く感謝致します。

触媒科学研究所物質変換研究部門の小林助教には、実験手法の指導や有益な議論をして頂きました。深く感謝致します。

It is a great pleasure to thank assistant professor Abhijit Shrotri in Catalytic transformation research division of Institute for catalysis for helpful suggestion and discussion.

東京工科大学の原賢二教授には、昼夜を問わず長時間の議論や、XAFS 測定でお世話になりました。深く感謝致します。

研究室の皆様には、多くの議論や指導をして頂き、感謝致します。

最後に、あらゆる面で支えて下さった、家族の皆様には、心より感謝致します。

March 23, 2017

石戸 信広